POLITECNICO DI MILANO

Facoltà di Ingegneria Industriale

Dipartimento di Ingegneria Aerospaziale

Corso di Laurea Specialistica in Ingegneria Aeronautica

GASIFICATION SYSTEM FOR DEORBIT: DEVELOPMENT OF AN ANALYTICAL MODEL

Relatore: Prof. Luigi T. DE LUCA

Co-relatore: Prof. Valery I. TRUSHLYAKOV

Tesi di Laurea di:

Samuel Muriana Carmona 764218

Anno accademico 2012-2013

POLITECNICO DI MILANO

Facoltà di Ingegneria Industriale

Dipartimento di Ingegneria Aerospaziale

Corso di Laurea Specialistica in Ingegneria Aeronautica

GASIFICATION SYSTEM FOR DEORBIT: DEVELOPMENT OF AN ANALYTICAL MODEL

Relatore: Prof. Luigi T. DE LUCA

Co-relatore: Prof. Valery I. TRUSHLYAKOV

Tesi di laurea di:

Samuel Muriana Carmona Matricola 764218

Anno accademico 2012-2013

Acknowledgments

I would like to thank Prof. L. De Luca and Prof. V.I. Trushlyakov for giving me this great opportunity to spend six months in Omsk and learn so many things about engineering, space debris… and life itself. I also thank them for giving me the possibility to write an article in local and international journals as well as participate in international events. This is the best ending for my academic career and a great starting point for my upcoming working life. I will always be thankful for it.

I would also like to thank the OmSTU and all the international relationships staff. They made our stay at Omsk as comfortable as possible, helping us every time we needed it with the best attitude.

And last, but not least I have to thank my family for having me all the support and love. Thanks to my parents, Rosario and Enrique, for giving me the tools to cope with life always in a positive mood. Thanks to my brother, Raúl, for having always a right word to make me forget the problems. And thanks to my girlfriend, Cristina, for taking me by the hand and share this experience with me, and much more.

Ringraziamenti

Vorrei ringraziare il Prof. De Luca ed il Prof. V.I. Trushlyakov per darmi questa incredibile possibilità di passare sei messi ad Omsk ed imparare tante cose su ingegneria, space debris... e la vita stessa. Io anche loro ringrazio per darmi la possibilità di scrivere un articolo nei giornali internazionali così come di partecipare nei eventi internazionali. Questo e il migliore fine per la mia carriera accademica ed un grandissimo inizio per la mia imminente vita lavorale.

Vorrei anche ringraziare al OmSTU e tutti le persone di relazioni internazionali. Loro hanno fatto la nostra stanza ad Omsk il più comodo possibile, aiutandoci sempre che loro abbiamo richiesto e sempre con la migliore attitudine.

Per finire, vorrei ringraziare la mia famiglia per darmi tutto il supporto ed amore. Grazie a i miei genitori, Enrique e Rosario, per darmi gli instrumenti per gestire la vita sempre con l'anima positiva. Grazie al mio fratello, Raúl, per avere sempre una parola giusta per farmi dimenticare i problemi. E grazie alla mia ragazza, Cristina, per portarmi dalla mano in questa avventura e viverla insieme a me, e tante altre cose.

Благодарности

Я хотел бы поблагодарить профессор L. De Luca и профессор В.И. Трушляков за предоставленную мне прекрасную возможность провести шесть месяцев в Омске и узнать так много вещей, о технике, космический мусор ... и сама жизнь. Я также благодарю их за предоставленную мне возможность писать статьи в местных и международных журнала, а также участия в международных мероприятиях. Это лучший конец для моей академической карьеры и отличной отправной точкой для моей предстоящей трудовой жизни. Я всегда буду благодарен за это.

Я также хотел бы поблагодарить ОмГТУ и всех международных отношений персонала. Они сделали наше путешествие в Омске максимально комфортным, помогая нам каждый раз, когда мы нуждались в нем с лучшим отношением.

И последнее, но не в последнюю очередь я должен поблагодарить мою семью за то, что мне все поддержки и любви. Спасибо моим родителям, Rosario и Enrique, за предоставленную мне инструменты, чтобы справиться с жизнью всегда в позитивном настроении. Спасибо моему брату Raúl, за то, что всегда правильное слово, чтобы заставить меня забыть о проблемах. И благодаря моей подруге, Cristina, для взяв меня за руку и поделиться этим опытом со мной, и многое другое.

Я не говорю по России на всех, но я знаю, как использовать Google Translate

Table of contents

List of figures

List of tables

Abstract

Since human space activities began, debris generated by these activities started to accumulate orbiting around Earth. During the first 30 years, this situation was ignored, leading to a situation with hundreds of thousands dangerous pieces in orbit. At present, main space agencies and societies have started to highly concern about looking for means to reduce the amount of debris in the LEO and GEO orbits (remediation techniques, as we will see in chapter 3), as well as trying to find means to avoid the generation of new debris from future launches (remediation techniques).

This thesis will present the solution under study at Omsk State Technical University, to deorbit separating parts in an autonomous way. The procedure will use the residual energy, under the form of unused propellant on tanks. These propellant that remains after a Space Launching Vehicle places its load, will be gasified by means of feeding hot gases to the propellant tanks. These hot gases will be provided by a gas generator (solid, liquid or hybrid). As a result, gasified propellants will be used in a vortex gas engine to develop the thrust needed to deorbit the upper stage in a safe way back to Earth.

Among all the parts involved in this research, this thesis will focus in the development of an analytical model for the gasification processes inside the tank, and the extraction of results using numerical calculations (by its implementation into *MATLAB*®) , as well as the analysis of these results and future perspectives of the investigation.

Keywords: space debris, gasification system, mitigation, deorbit, upper stage, gas engine

Sommario

Da che le attività spaziali umani cominciarono, space debris generati da queste attività ha iniziato ad accumularsi in orbita attorno alla Terra. Durante i primi 30 anni, questa situazione è stato ignorata, portando ad una situazione con centinaia di migliaia di pezzi pericolose in orbita. Attualmente, i principali agenzie spaziali hanno iniziato a preoccupasi sulla ricerca di mezzi per ridurre la quantità di debris nelle orbite LEO e GEO (techniche di *remediation*, come vedremo nel capitolo 3), oltre a cercare di trovare i mezzi per evitare la generazione di nuovi debris dei lanci futuri (tecniche di mitigazione).

Questa tesi presenta la soluzione sotto studio presso l' Omsk State Technical University, per deorbitare le parti separate in un modo autonomo. La procedura utilizza l'energia residua, sotto forma di propellente inutilizzato su serbatoi. Questo propellente che rimane dopo che un veicolo spaziale lascia il suo carico in orbita, sarà gassificato per mezzo di alimentazione di gas caldi per i serbatoi di propellente. Questi gas caldi saranno forniti da un generatore di gas (solido, liquido o ibridi). Come risultato, propellenti gassificato saranno utilizzati in un motore a gas per sviluppare la spinta necessaria per deorbitare lo stadio superiore in modo sicuro verso la Terra.

Tra tutte le parti coinvolte in questa ricerca, questa tesi si concentrerà nello sviluppo di un modello analitico per i processi di gassificazione all'interno del serbatoio, e l'estrazione dei risultati utilizzando metodi di calcoli numerici (attaverso lo sviluppo di un codice MATLAB®), così come l'analisi di questi risultati e prospettive future delle investigazioni.

Parole chiave: *space debris, gasification system, mitigation, deorbit, upper stage, gas engine*

Chapter 1: Introduction

Since the launch of Sputnik in 1957 human activities into space have led to produce or release thousands of objects of various sizes, from particles smaller than 1 mm to inoperative satellites. Many of these objects keep orbiting around Earth, neither actively nor passively controlled, constituting what is known as space debris.

During the first 20 years of space history no agency worried about the accumulation of these object and the problems that they could produce in future. After the works by Donald Kessler and his collaborators were released, in the late 70's [1], societies and scientists started to realize that debris was a major risk for space activities; so it required solutions. In the 80's several steps forward were taken, leading to the foundation of the *Inter-Agency Space Debris Coordination Committee* (IADC) in 1993.

At present, every single company and agency is concerned about the space debris problem, and huge effort and resources are dedicated to develop technologies to mitigate it, with the aim of guarantee safety in the earth orbit, now and in future.

In this work we will see the most important solutions developed, in the frame of active debris removal and mitigation techniques, by the main space agencies. After that, we will present the solution under study by the Omsk State Technical University (OmSTU) consisting on the gasification of the propellant remaining in the tanks after the last burn, and the use of its energy to provide the thrust needed for our mission.

Finally, the ultimate scope for this work is to provide an accurate analytical model for the gasification processes inside the propellant tank, and the implementation of this model into a computing language (*MATLAB*®, as announced) to obtain some numerical results. These final results will be analyzed and commented to conclude with the work.

Presentation plan:

- Chapter 2: The space debris problem. In this chapter, we will give a some notions about the space debris problem. We will start reviewing the historical evolution of the problem, from the beginning of human space activities to present and future perspectives in some scenarios. We will give some definitions that will be useful in later chapters and finally we will make a brief description of the most important regulations nowadays.
- Chapter 3: this part is about space debris removal techniques used or under study by the main space agencies in the world. We will focus in the difference between mitigation and remediation techniques, to have a global view of the problem and to correctly place the OmSTU solution.

- Chapter 4: here we will present the gasification system under development by the OmSTU. We will start with an overall description of the system to continue with a separate depiction of the most important components.
- Chapter 5: in this chapter we will explain the analytical model developed and the results obtained. Then, the chapter will be divided into two parts: the first one will be entirely theoretical, destined to detail the model and its theoretical basis; the second one will be dedicated to show and explain the results obtained.
- Chapter 6: to close the report, final comments about the results, conclusions and future studies related to this work will be presented.

Chapter 2: The space debris problem

As previously announced, space debris problem started to be on the researchers' agenda on the 80's, and it finally became a global concern in the later decade. After over 30 years of unregulated exploitation of earth orbit, the situation evolved in such condition in which all space agencies, commercial users, and military services needed to stipulate a unified regulatory about launches and launchers, with the aim to have a reduction of new debris generated by new launches, and the mitigation of pollution already present.

NASA, ESA, Roscosmos and IADC (Inter-Agency Space debris Coordination Committee, founded by NASA, ESA, Russian Aviation & Space Agency and NASDA) have been very useful and active on the promulgation of guidelines for the mitigation/reduction of space pollution. In particular each agency has worked on a modernization and development of new techniques that allow reducing the quantity of debris generated in each launch due to separation of modules, as well as systems capable to remove spent stages, moving them into a disposal orbit or by de-orbiting them to Earth. Also, every single agency has developed a set of rules and laws that must be fulfilled in order to control and reduce the amount of debris in space. By the end of this chapter, we will see some of the most accepted rules, as they share a common base and principles.

As we can see, a great effort is being dedicated to cope with the problem of space debris. This is because situation has reached its point of no return and actions are required to be taken. At present, more than 30,000 objects have been cataloged by the US Space Surveillance Network (SSN), and there is a huge amount of objects in orbit that cannot be cataloged. Space catalogues include almost no objects smaller than 5 cm due to small cross section or target orbital instability [2]. However, a piece of debris as small as 1 cm can cause significant damage to spacecraft. The amount of debris exceeding 1 cm in LEO (Low Earth Orbit, from Earth surface to 2000 km of altitude) is higher than 300,000.

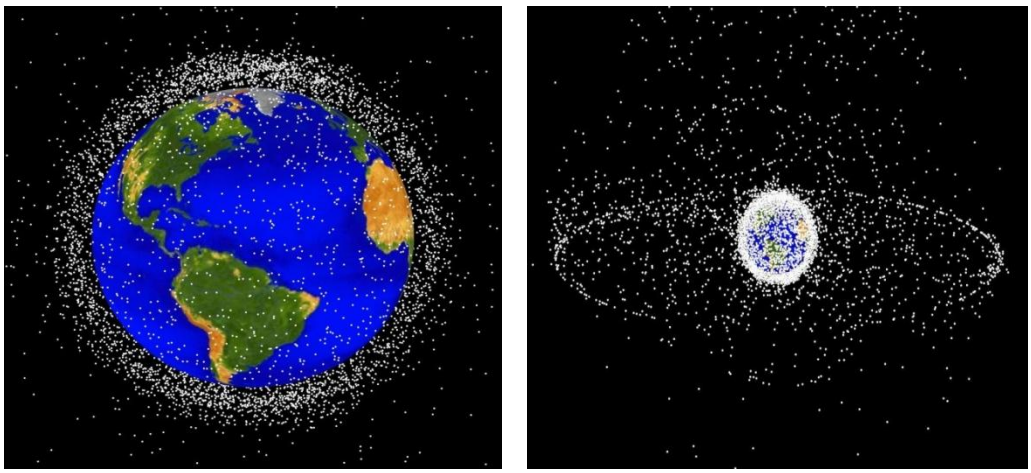

Fig. 1: Space debris distribution [3]

In the following scheme (fig 2) we can see the accumulation of debris in the LEO region from 1994 to 2009 [4]. As we can see in the figure, there is one region where the density of debris has increased in a noticeable way. This is due to two catastrophic events that took place in the last decade:

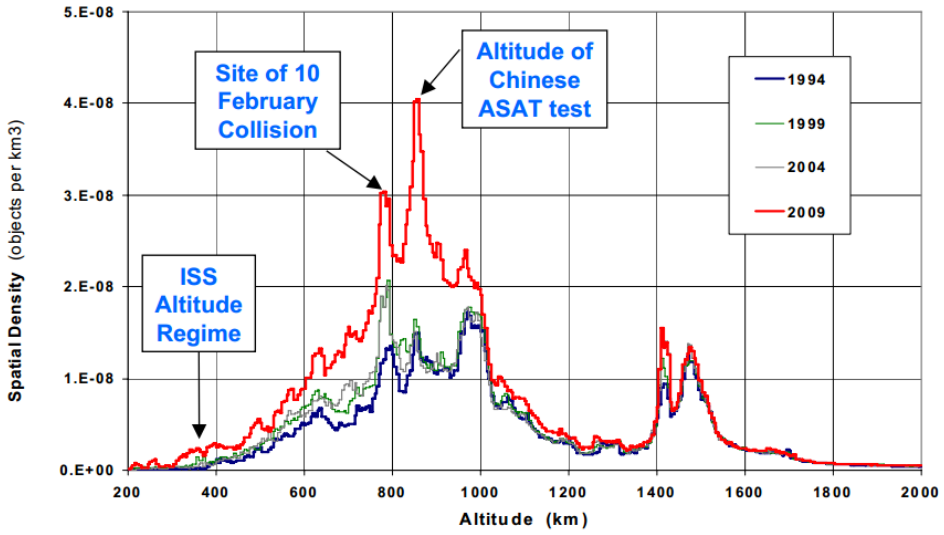

Fig. 2: Evolution of space debris between 1994 and 2009 [4]

- The China anti-satellite test (ASAT test) in 2007: conducted by China on January 11, 2007, a Chinese weather satellite was destroyed by a kinetic kill vehicle traveling with a speed of 8 km/s in the opposite direction [5]. The test released thousands of pieces, making the cloud of debris visible even amongst the rest of debris. We can see it in the following picture, with the ASAT test debris pieces marked in red, while the rest of debris is showed in green.

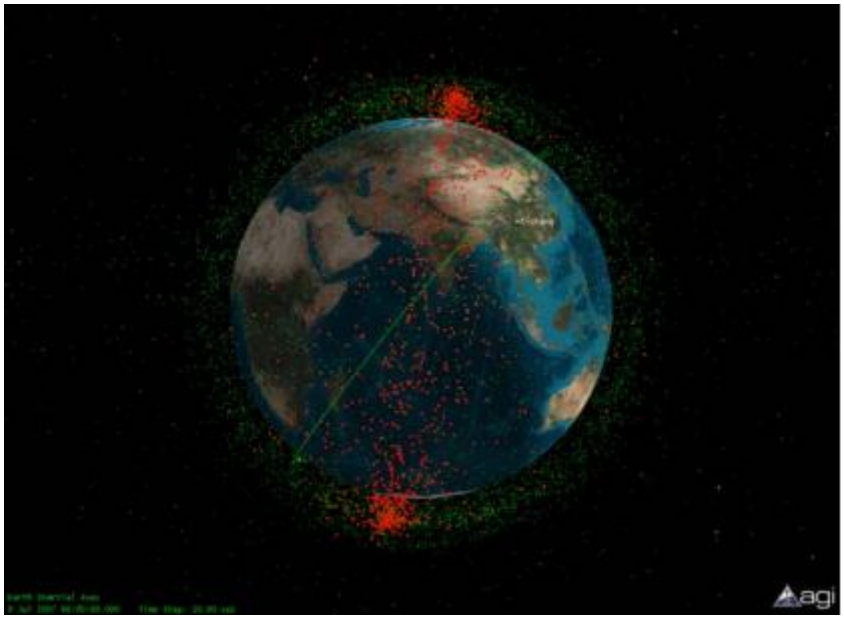

Fig. 3: ASAT test debris distribution on July 2007 [4]

- The collision between Kosmos 2251 and Iridium 33 in 2009: it was the first accidental hypervelocity collision between two intact artificial satellites in Earth orbit. The accident took place on February 10, 2009, at 789 kilometers above the Taymyr Peninsula in Siberia. The satellites collided at a speed of 42,120 km/h; both satellites were destroyed by the impact. By 2011, NASA had catalogued more than 2000 large pieces of debris produced by this unfortunate collision [6].

As we have seen in *Fig.2*, these two events turned a really worrying scenario into a critical situation, causing an increase of more than 60% to the debris population in LEO [7]. But the problem of debris was already a major threat before. From the studies by Donald Kessler [1], the current situation was explained with the following sentence: "…the debris flux will increase exponentially with time, even though a zero net input may be maintained". This is due to the creation of new debris bodies by collision between orbiting objects, debris or active spacecraft. These new fragments could collide again with other objects, generating more debris fragments. This is called the *"collision cascade"*.

The following figure shows this cascade effect due to the interaction between existing debris. This is extracted from a NASA's journal from 2010, but their calculations were made on the hypothetical scenario that no more spacecraft had been launched from 2006. We can see that, even in a no launches scenario, the number of debris will increase in more than 50% during the next two centuries.

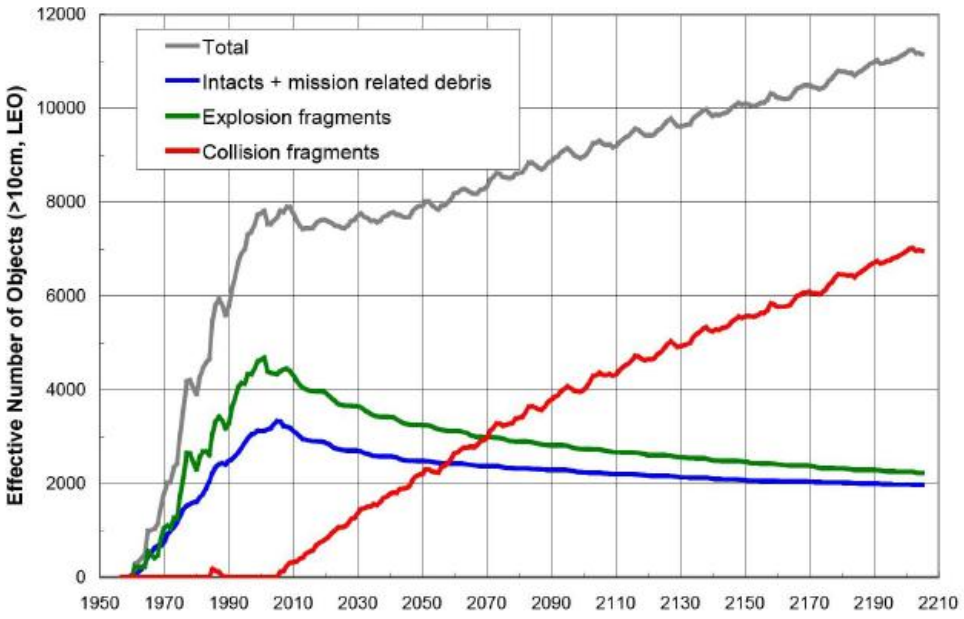

Fig. 4: Collision cascade in the "no launches after 2006" scenario [7]

2.1 Types of space debris

Space debris can divided into different groups according to its characteristics. The simplest classification could be to distinguish between natural and artificial debris: we consider natural debris the environmental products like asteroids, comets or interplanetary dust; in the other hand, we consider artificial debris those that are derived from human activities. This work is only focuses on artificial debris; natural debris is a different problem that is out of our influence.

If we consider the artificial debris, we can also do a further classification. We can differentiate between [8] nonfunctional spacecraft, rocket bodies, mission related debris and fragmentation debris.

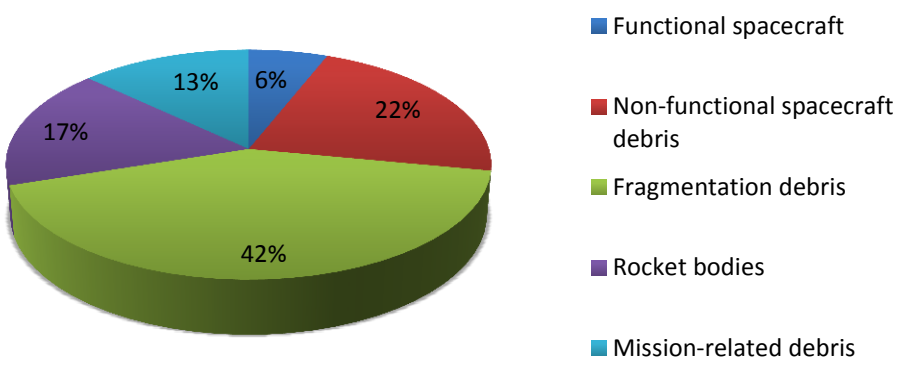

Fig. 5: Catalogued space objects by category (1994) [7]

2.1.1 Nonfunctional spacecraft

Functional spacecraft represent only about one-fifth of the spacecraft population in Earth orbit, the majority are nonfunctional. Most of the spacecraft that reach their end on life (EOL) are left in their former orbit or are transferred to slightly higher or lower altitude orbits. Typically, these EOL reorbiting maneuvers are performed only by geosynchronous or semisynchronous spacecraft and by LEO spacecraft carrying nuclear materials. Historically, these maneuvers have almost always resulted in longer orbital lifetimes. Only crewed vehicles and a few other spacecraft in very low orbits are normally returned to Earth at the conclusion of their missions.

2.1.2 Rocket Bodies

Most of functional spacecraft are placed into orbit using one or more stages (or "rocket bodies"). Usually one rocket body is left in orbit for missions to LEO, but the launch vehicle of a high-altitude spacecraft such as GOES (Geostationary Operational Environmental Satellite) may release up to three separate rocket bodies in different orbits along the way to its destination. Few spacecraft types are designed to retain their orbital insertion stages and leave no independent rocket bodies.

The presence of rocket bodies in orbit is of particular importance due to their large dimensions and the potentially explosive residual propellants and other energy sources they may contain. Nowadays, rocket bodies in modern launchers use to be passivated (the residual energy sources are depleted) before leaving them in orbit. When we talk about actual regulation, later in this chapter, we will go deeper into the passivation concept.

Larger stages –generally used to deliver spacecraft and additional stages into LEO- usually reenter the atmosphere rapidly. On the contrary, smaller stages used to transfer spacecraft into higher orbits and insert them into those orbits may remain in orbit for long periods of time. Many of these objects are in orbits that intersect those used by functional spacecraft. As we have previously explained, this thesis deals with this problem: returning upper stages to Earth after its mission to avoid them to remain on orbit that can cause damage to other spacecraft.

2.1.3 Mission-related debris

Other space objects may be released as a result of a spacecraft's deployment, activation and operation. Parts of explosive bolts, spring release mechanisms, or spin-up devices may be ejected during the staging and spacecraft separation process. Shortly after entering orbit, the spacecraft may release cords securing solar panels or eject protective coverings from payload and attitude control sensors. The amount of debris released can be quite large. A large number of debris can also be generated during a spacecraft's operational life.

Another type of mission-related debris comes from the operation of solid rocket engines normally used as final stage transfers, particularly on GEO missions. Current solid rocket fuel usually employs significant quantities of aluminum mixed with the propellant. During the combustion process, a large number of aluminum oxide (Al_2O_3) particles are formed and ejected. These particles are believed to be no larger than 10 microns in diameter, but as many as 10^{20} may be created during the firing of a single solid rocket engine.

2.1.4 Fragmentation debris

Fragmentation debris –the most numerous group of the cataloged orbital debris objects- consists of space objects created during breakups and the products of deterioration. Breakups are typically destructive events that generate numerous small objects with a wide range of initial velocities. Breakups may be accidental (e.g., due to a malfunction) or the result of intentional actions (e.g., a space weapons test). They can be caused by internal explosions or by a collision with another orbiting object. The fragmentation debris due to breakups is ejected at a variety of initial velocities, spreading out into a toroidal cloud that will expand until it is bounded only by the limits of the maximum inclinations and altitudes of the debris.

In the other hand, debris fragments that are product of deterioration usually separate at low relative velocity from a spacecraft or rocket that remains essentially intact. Products of deterioration large enough to be detected from Earth are occasionally seen. Such deterioration is believed to be the result of harsh environmental factors, such atomic oxygen, radiation and thermal cycling.

2.2 Debris population distribution

2.2.1 Large debris

The cataloged large debris population (more than 10 cm in diameter) is the best-known segment of the debris population. As we have previously seen, *fig 5* shows the distribution of cataloged space debris. Clear concentrations can be seen at seen at less than 2,000 km (LEO), around 20,000 (semisynchronous orbit), and at 36,000 km (GEO). These high concentrations are due to large number of objects in near-circular orbits at or near these altitudes.

Except for those in GEO, most cataloged objects are in orbits with high inclinations. This means that relative collision velocities for these objects will be generally higher than orbital velocity. Most spacecraft in GEO actively maintain inclinations close to zero degrees and remain stationary above a given longitude .However, the orbital planes of nonfunctional spacecraft and other debris, will oscillate due to Earth's oblateness and gravitational perturbations of the Sun and Moon.

The difference between cataloged and uncataloged debris is more a matter of of sensor capabilities than of any inherent property of the object. A fragment 30 cm in diameter could almost certainly be cataloged in LEO but not in GEO. However, due to the fact that spacecraft and rocket bodies are usually large enough to be tracked, uncataloged large debris population is mainly composed of mission-related and fragmentation debris.

2.2.2 Medium-sized debris

The population of medium-size (approximately from 1 mm to 10 cm in diameter) debris is not nearly as well known as the population of large debris. The only measurements of the medium-sized debris population come from sampling of lower altitude, higher inclination LEO orbital regions with ground-based sensors. All other estimations are based only on extrapolations.

To a first approximation, it might be expected to find medium-sized debris in about the same orbit as large debris is, because most medium-sized debris is originated from large objects. However, some large objects contribute more than others to the formation of medium-sized debris.

Although there are no measurement data providing its origin, the population of medium-sized objects is composed of fragmentation debris and mission-related objects.

2.2.3 Small debris

There is an extremely numerous population of small (<1 mm in diameter) debris particles in Earth orbit. Knowledge of the distribution of these particles comes

primarily from the examination of returned spacecraft material and a few space measurements.

Like medium-sized debris, small debris is all either mission related or fragmentation debris. In the first group we can name aluminum oxide, as we have discussed previously. There particles, ejected from rocket bodies at velocities typically from 1.5 to 3.5 km/s (depending on the particle size, whose maximum is 10 microns in diameter). Most of them rapidly reenter the Earth's atmosphere, while others are typically sent into elliptical orbits.

About fragmentation debris, we should talk about deterioration products like paint chips and many others. These particles are usually much larger than the aluminum oxide particles, having an average diameter of hundreds of microns. These particles are ejected with virtually no velocity so they nearly share the same orbit than the source object. In this group (fragmentation debris) we can also address the products of breakup. They cover a wide range of size and shape, as well as ejection velocities that place them in different orbits.

Orbital Debris Size Range	Number of Objects	Percentage of objects > 1mm	Percentage of Total Mass
Large (>10 cm)	>10,000	<0.5	>99.95
Medium (1 mm-10 cm	Perhaps tens of millions	>99.5	<0.05
Small (<1 mm)	Trillions	-	<0.01

Table 1: Approximate Orbital Population by Size [8]

2.3 Sources of space debris

While we have been explaining the types of debris and its distribution, we have seen many of the causes to its formation. These causes are very diverse, some of them are a product of the design (e.g. breakup debris), but in other cases debris is generated in an accidental way (e.g. explosions of tanks). Taking into consideration the reasons we have seen, and adding some more, we have the following ones:

- Design: spacecraft remaining on orbit after EOL, intermediate stages, separation products…
- Collisions with other space objects.
- Explosions due to batteries or remaining propellant. It can be solved by means of passivation.
- Design failures.
- Degradation.

2.4 Regulation

All the space agencies (NASA, ESA, Roscosmos, JAXA…) have their own mitigation rules. These standards may be slightly different, but their principles are the same:

- Preventing on-orbit break-ups
- Removing spacecraft and orbital stages that have reached the end of their mission operations from the useful densely populated orbit regions
- Limiting the objects released during normal operations.

2.4.1 The IADC Mitigation Guidelines

The Inter-Agency Space Debris Coordination Committee (IADC) is an international forum of governmental bodies –founded in 1993- for the coordination of activities related to the issues of man-made and natural debris in space. Members of the IADC are the Italian Space Agency (ASI), British National Space Centre (BNSC), Centre National d'Etudes Spatiales (CNES), China National Space Administration (CNSA), Deutsches Zentrum fuer Luft-und Raumfahrt e.V. (DLR), European Space Agency (ESA), Indian Space Research Organization (ISRO), Japan, National Aeronautics and Space Administration (NASA), the National Space Agency of Ukraine (NSAU) and Russian Aviation and Space Agency (Rosaviakosmos).

An important milestone in the space debris history was reached in 2002 when the first version of the IADC mitigation guidelines was approved. In 2007, the first and latest revision [9] was released. These guidelines try to set a common scenario and rules for all of the IADC's members. The IADC regulations are based on the same common principles we have previously seen and the have been agreed to by consensus among the IADC member agencies.

The IADC guidelines cover all the overall impact of the missions with a focus on the following points:

- Limitation of debris released during normal operations.
- Minimization of the potential for on-orbit breakups.
- Post-mission disposal.
- Prevention of no-orbit collisions.

2.4.1.1 Limitation of debris released during normal operations

In all operational orbit regimes, spacecraft and orbital stages should be designed not to release debris during normal operations. In case that this is not possible, any release of debris should be minimized in number, area and orbital lifetime.

Any project that releases objects should not be planned unless an adequate assessment is able to verify that the effect on the orbital environment, and the hazard to other operating spacecraft and orbital stages, is acceptably low in the long-term.

2.4.1.2 Minimization of the potential for on-orbit breakups

In order to limit the risk to other spacecraft and orbital stages from accidental break-ups after the completion of mission operations, all on-board sources of stored energy of a spacecraft or orbital stage should be depleted when they are no longer. Depletion should occur as soon as this operation does not pose an unacceptable risk to the payload. Mitigation measures should be carefully designed not to create other risks.

We can relate this with the definition of passivation, that is, the elimination of all stored energy on a space system to reduce the chance of break-up. Typical passivation measures include venting or burning excess propellant, discharging batteries and relieving pressure vessels.

On-orbit breakups due to stored energy

- Residual propellants and other fluids, such as pressuring, should be depleted as thoroughly as possible, either by depletion burns or venting, to prevent accidental break-ups by over-pressurization or chemical reaction.
- Batteries should be adequately designed and manufactured, both structurally and electrically, to prevent break-ups.
- High-pressure vessels should be vented to a level guaranteeing that no break-ups can occur.
- Self-destruct systems should be designed not to cause unintentional destruction due to inadvertent commands, thermal heating, or radio frequency interference.
- Power to flywheels and momentum wheels should be terminated during the disposal phase.
- Other forms of stored energy should be assessed and adequate mitigation measures should be applied

On-orbit breakups during operational phases

During the design of spacecraft or orbital stages, each program or project should demonstrate that there is no probable failure mode leading to accidental break-ups. If such failures cannot be excluded, the design or operational procedures should minimize the probability of their occurrence.

During the operational phases, a spacecraft or orbital stage should be periodically monitored to detect malfunctions that could lead to a break-up or loss of control function. In the case that a malfunction is detected, adequate recovery measures should be planned and conducted; otherwise disposal and passivation measures for the spacecraft or orbital stage should be planned and conducted.

2.4.1.3 Post mission disposal

GEO

Spacecraft that have terminated their mission should be maneuvered far enough away from GEO so as not to cause interference with spacecraft or orbital stage still in geostationary orbit. The maneuver should place the spacecraft in an orbit that remains above the GEO protected region.

LEO

Whenever possible spacecraft or orbital stages that are terminating their operational phases in orbits that pass through the LEO region, or have the potential to interfere with the LEO region, should be de-orbited (direct re-entry is preferred) or appropriate placed into an orbit with a reduced lifetime. Retrieval is also a disposal option.

A spacecraft or orbital stage should be left in an orbit in which, using an accepted nominal projection for solar activity, atmospheric drag will limit the orbital lifetime after completion of operations. A study on the effect of post-mission orbital lifetime limitation on collision rate and debris population growth has been performed by the IADC. This IADC and some other studies and a number of existing national guidelines have found 25 years to be a reasonable and appropriate lifetime limit. If any object is going to be re-entered, debris that reaches the Earth's surface should not represent any risk for people or properties.

Other orbits

Spacecraft or orbital stages that are terminating their operational phases in other orbital regions should be maneuvered to reduce their orbital lifetime, commensurate with LEO lifetime limitations, or relocated if they cause interference with highly utilized orbit regions.

2.4.1.4 Prevention of on-orbit collisions

During the design phase, the risk of accidental collision with known objects, during the spacecraft or orbital stage's lifetime, should be evaluated. If reliable orbital data is available, avoidance maneuvers and co-ordination of launch windows may be considered if the collision risk is not considered negligible. Spacecraft design should also limit the consequences of collision with small debris.

2.4.1.5 Protected regions

We have already defined the LEO and GEO; the IADC Mitigation Guidelines considers the following areas as protected regions, that is, places where we should prevent the generation of debris.

- Region A: Low Earth Orbit Region (LEO, from Earth's surface to an altitude of 2,000 km)

- Region B: The Region, a segment of the spherical shell defined by the following parameters:
    - The lower altitude is the geostationary altitude minus 200 km.
    - The upper altitude is the geostationary altitude plus 200 km.
    - The latitude is between 15 and -15 degrees.
    - The geostationary altitude is equal to 35,786 km (the altitude of the geostationary Earth orbit)

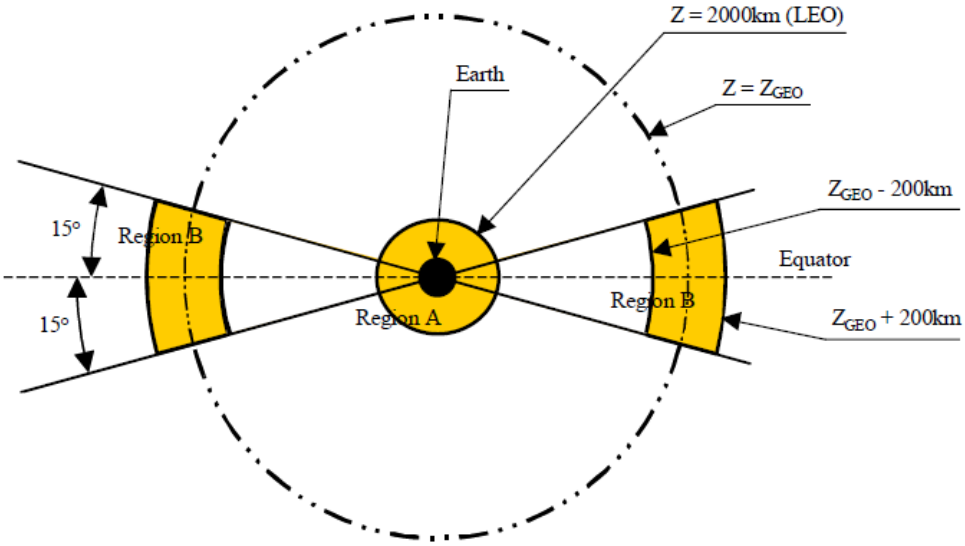

Fig.6: Protected regions

Other regulations

As we have already announced, the main agencies has their own rules and their principles are very similar. So we will not go deeper in any of them, but we will name some of them in case the reader has further curiosity.

- Technical Report on Space Debris, Text of the report adopted by the Scientific and Technical Subcommittee of the United Nations Committee on the Peaceful Uses of Outer Space, 1999
- Interagency report on Orbital Debris 1995, The National Science and Technology Council Committee on Transportation Research and Development, November 1995
- U.S. Government Orbital Debris Mitigation Standard Practices, December 2000
- CNES Standards Collection, Method and Procedure Space Debris – Safety Requirements, RNC-CNES-Q-40-512, Issue 1- Rev. 0, April 19, 1999

- Policy to Limit Orbital Debris Generation, NASA Program Directive 8710.3, May 29, 1997
- Guidelines and Assessment Procedures for Limiting Orbital Debris, NASA Safety Standard 1740.14, August 1995
- Space Technology Items. General Requirements. Mitigation of Space Debris Population. Russian Aviation & Space Agency Standard OCT 134-1023-2000
- ESA Space Debris Mitigation Handbook, Release 1.0, April 7 1999

Chapter 3: Means to deal with space debris. State-of-the-art.

As we have previously explained, the situation has become critical. Experts from both NASA and ESA predict that (even if no more launches of new spacecraft were to be performed) a cascade effect will take place and that the debris population will increase due to collisions of existing large objects with other object in the next 150 years [10]. It is therefore clear that the space debris issue is a global problem so international cooperation has been of paramour importance from the beginning.

There are two main ways to deal with the space debris problem: mitigation and remediation. "Mitigation" aims at reducing the generation of space debris through combined measures associated with the design, manufacture, operation, and disposal phases of a mission. "Remediation", on the other hand, aims at managing the existing space debris population through debris removal, principally from the low Earth and geosynchronous protected regions.

3.1 Remediation

As we already know, even in a "no more launches" scenario, the amount of debris will keep on growing exponentially. This explains the fact that only mitigation is not enough to stabilize the number of debris in the protected regions, objects need to be removed from orbit. Together with the adoption of the mitigation measures recommended by the different organizations, the active yearly removal of approximately 0.1% (around 5 to 10 large objects per year) of the abandoned intact objects would be sufficient to stabilize the cataloged debris in Low Earth Orbit [11].

In fig 7 [12], we can appreciate the effect of the application of active debris removal together with mitigation measures, using NASA's software LEGEND (a LEO-to-GEO Environment Debris model). The figure assumes three different situations: mitigation plus no active debris removal, mitigation plus removal of two heavy debris bodies per year, and mitigation plus removal of five large debris bodies per year. The third scenario proves that by removing five large debris objects per year, we could be able to stabilize the situation.

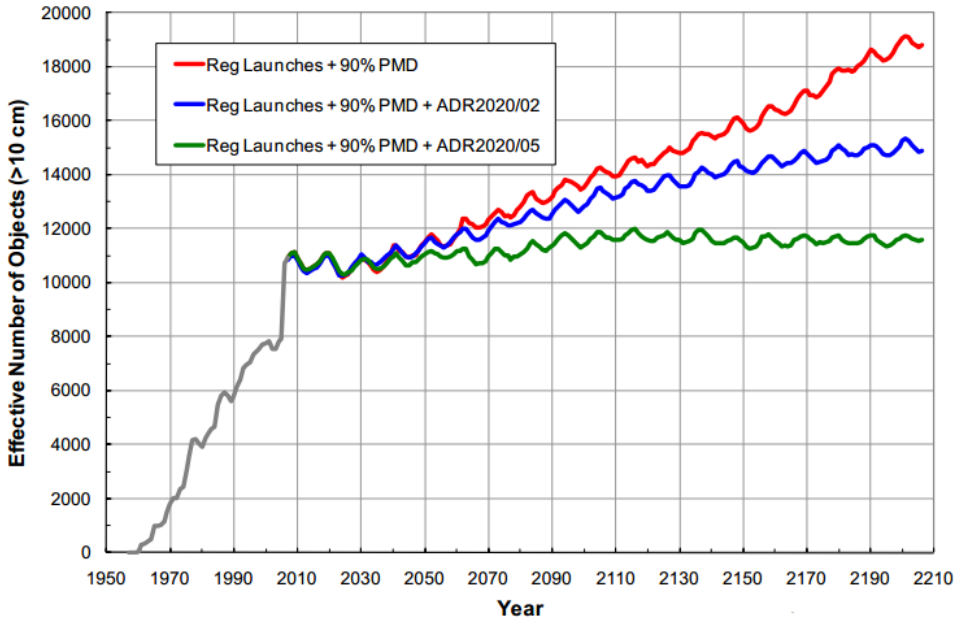

Fig 7:. Application of the effect of active debris measures [12]

Now we will introduce some of the solutions developed or under study by the main space agencies. We will not go very deep into them, as this work is related to a mitigation solution, -as we will see at the end of this chapter- but we will try to give a good view of the state-of-the-art in space debris actual solutions.

3.1.1 CNES

The CNES (Centre National d'Etudes Spatiales) is currently working in several directions [13]. The main one is using an Orbital Transfer Vehicle (OTV), to deliver small solid de-orbiting kits to target debris. This method could remove from 10 to 15 large debris objects for a year, more than enough according with what we have just explained.

This OTV is based on the experience gathered with the Automated Transfer Vehicles (ATV's) [14], specifically the Jules Verne's flight to ISS in March 2008. This ATV is able to do orbital transfer, automatic rendezvous (controlled from ground) and automatic docking operations.

Fig. 8: The Jules Verne ATV [15]

Among all the possible de-orbiting kits (drag-augmentation devices, tethers and all type of chemical propulsion systems), solid propellant engines were chosen. This system is easy to operate and need a short combustion time. On the other hand, it generates potentially high accelerations so it is restricted to robust debris, to tolerate the high loads generated. This could be a problem especially for old satellites.

In order to minimize the complexity of the system, the choice adopted is using single ignition devices with no control during the de-orbiting process.

Fig. 9: Solid de-orbiting kits [15]

The main steps of a de-orbiting mission using this method are:

- Preparatory phase: identification of targets, first evaluation of movement, manufacturing of the kit…
- Launch phase: The considered launcher is Ariane 5ME, that will be available by 2015. Classical launch profile
- Rendezvous with target 1: progressive approach, formation flying between OTV and debris
- Robotic operations: Grappling with robotic arm, movement cancellation, orientation in the direction required by de-boost, installation of the kit aligned with the debris Center of Gravity, release of the robotic arm.
- Release of the debris: Spin if the OTV+Debris, physical release of the debris and deorbiting kit, distancing of the OTV.
- Debris deorbiting: automatic ignition of the deorbiting kit.
- Preparation for the following debris.
- End of mission after N debris deorbiting.

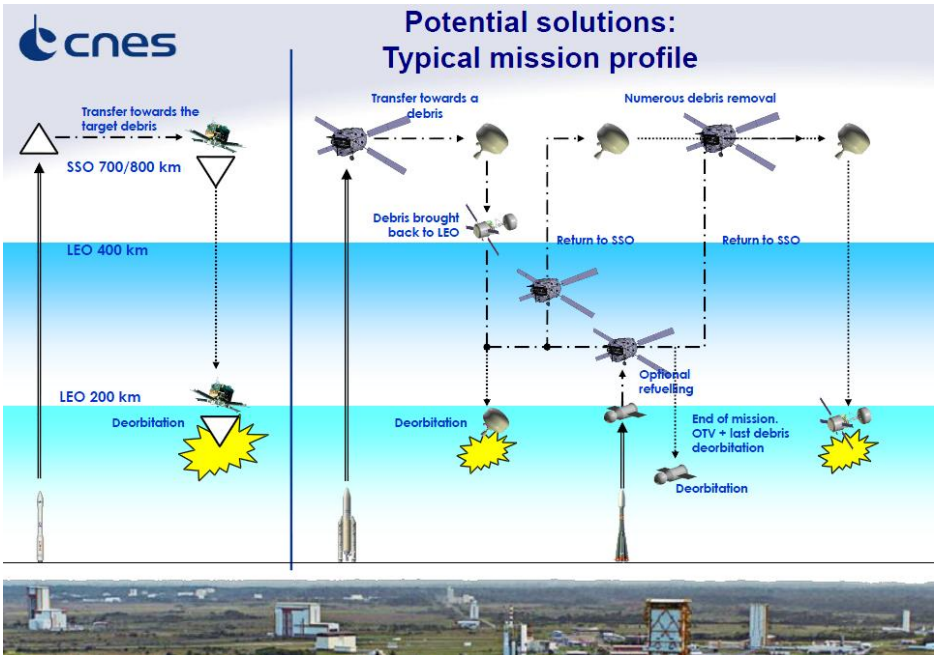

Fig. 10: Phases for a typical OTV deorbit operation

This is a conceptual study and it is not under application. The CNES roadmap expects to be able to apply this, or similar concepts, on mid 2020's.

3.1.2 ESA

ROGER – the Robotic Geostationary orbit Restorer – is a concept under study by the European Space Agency. ROGER can be tasked to approach and capture a redundant or non-operational satellite in the Geostationary (GEO) orbit and tow it into a parking or graveyard orbit. This project has been carried out under ESA contracts by two teams in competition:

- Astrium, DLR, TU Braunschweig, MD Robotics, Space Application Services, EADS-LV and SES-ASTRA.
- QinetiQ, OHB-System, ESYS and Dutch Space.

The Astrium team proposed a satellite that is a derivative of a former very detailed designed Astrium platform. It used a net to capture its targets [16]. In the other hand, the solution presented by the QinetiQ team was based on a new bus design to make easier the payload accommodation process. The principal payload element is the grappling equipment. The tradeoff for grappling equipment has led to the adoption of a novel bulk capturing device dubbed the "octopus tentacle solution" [17].

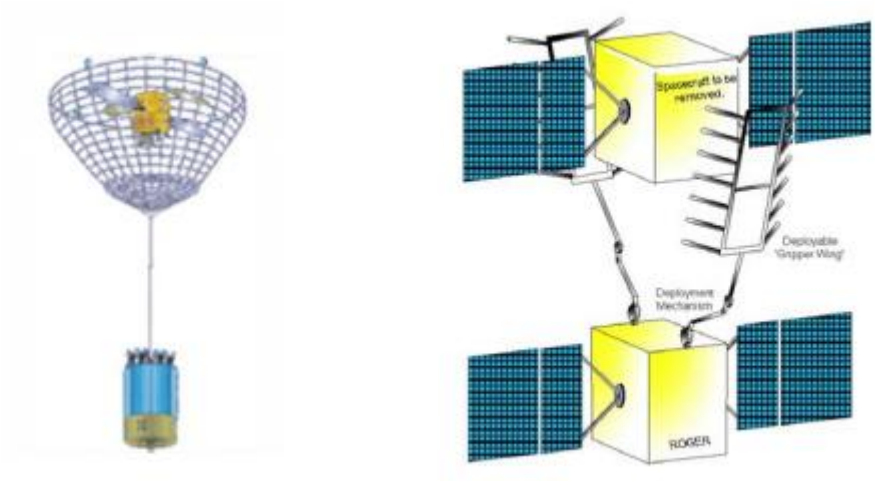

Fig.11: Astrium (left) and QuinetiQ visions for ROGER

ROGER project was proposed on 2003, and it will probably remain on a conceptual state; we should see it as a feasibility study for an active debris removal satellite.

There are other solutions in the ESA's agenda, like a drag augmentation system using expanding foam [18]. This method uses a chaser with the foam to intercept the debris target. After the interception, the debris target is covered with foam until the body is fully covered with foam. After this, the deorbit process will start and the chaser can go after another target until the end of its mission. In *Fig. 12*, we can find this process resumed:

This method is suitable for cases where no active control is required for the deorbit process. It presents some advantages, like its simplicity and reduced costs. Also, it is not affected by impacts like a solar sail can be (a strong enough impact can tear the sail, compromising the mission).

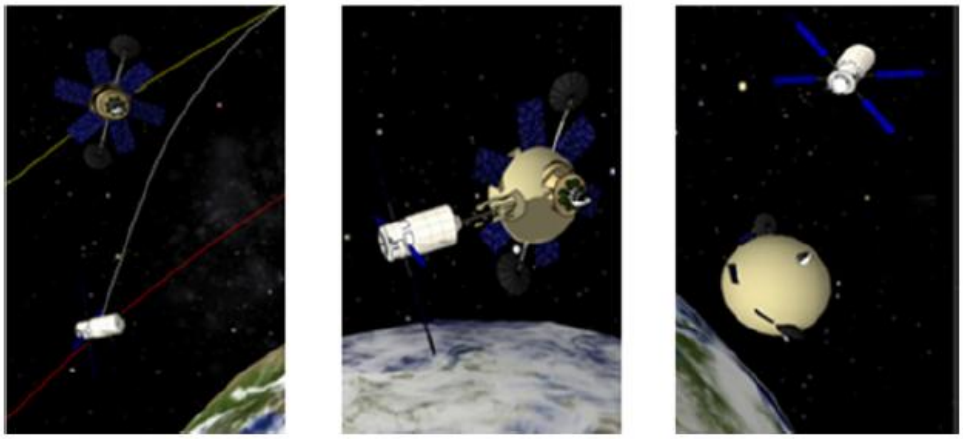

Fig. 12: Deorbit process using expanding foam [18]

3.1.3 JAXA

JAXA is studying an Active Removal System (ADR) that can rendezvous with and capture non-cooperative debris objects in crowded orbits for de-orbiting them, all within a low cost policy [19]. Although JAXA has considered the use of conventional propulsion systems, they are actually focusing on solutions using electrodynamic tether (EDT) systems. This is because, according to their own studies, EDT is the most promising method for deorbiting large debris object in LEO [20].

The principle of EDT thrust is as it follows. An electromotive force is set up within a conductive tether deployed from a space system that moves through the geomagnetic field as it orbits around the Earth. If a pair of plasma contactors at either end of the tether emits and collects electrons, the circuit is closed via the ambient plasma and an electric current flow through the tether. The tether then generates a Lorentz force which acts opposite to the direction of flight. So an EDT can provide deceleration without the need for propellant or high electrical power.

As is depicted in *Fig.13*, the steps required for the deorbit operation are:

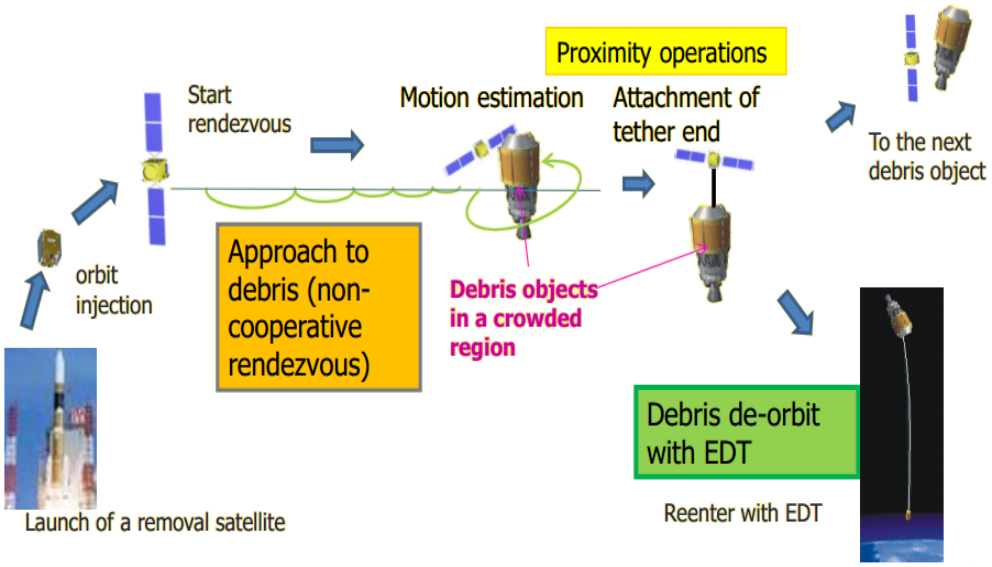

Fig. 13: Steps required for the deorbit operation using EDT [20]

1. Non cooperative rendezvous
   A rough estimate of debris position can be obtained from the observed orbits of debris objects published as Two Line Elements (TLE) by NORAD. However, these data contain observation and propagation errors, and the position accuracy is some km in LEO. A removal satellite must therefore use sensors within the vicinity the target debris to avoid colliding with it. There is much experience with cooperative rendezvous docking, but performing a rendezvous maneuver with debris is more difficult because debris objects are non-cooperative and do not possess rendezvous radar reflectors. JAXA is studying navigation using GPS and optical sensors to perform this phase at low cost.
2. Motion estimation
   Since the attitude of the debris objects are not controlled, the relative attitude as well as the relative position of the debris object should be measured in order to attach a propulsion system to de-orbit it. Since the target is assumed to be non-cooperative, it is proposed to measure or estimate these quantities using passive imaging.
3. Attachment of propulsion system
   When the motion of the target object is estimated, the removal satellite will finally approach to attach a propulsion system for de-orbit (EDT). There are two main ways under study: the first one is an extensible robot arm, or a boom, for attaching the tether end to the payload attachment fitting (PAF) of the rocket bodies; the second one is a harpoon propelled to penetrate the tank wall. We can see both methods in figures *Fig. 14* and *Fig. 15*.

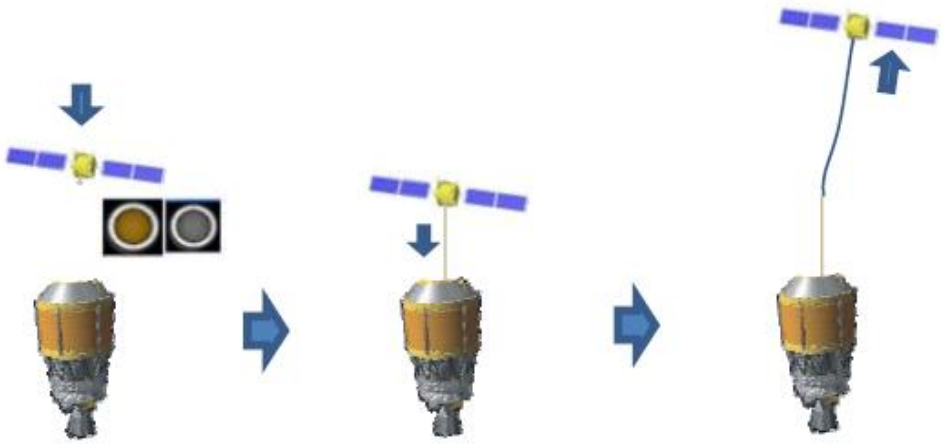

Fig. 14: Attachment to the PAF using a boom mechanism [19]

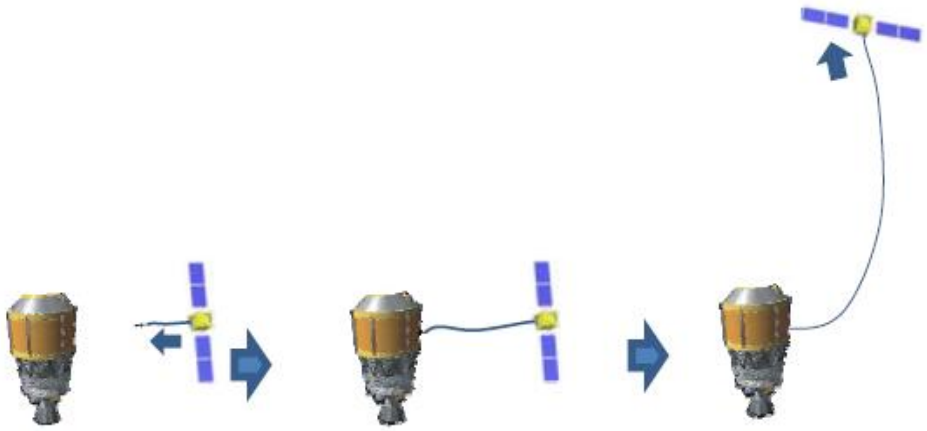

Fig. 15: Attachment using a harpoon [19]

4. De-orbit and next target: after the attachment of the EDT, the Lorentz force will decelerate the debris target and it will eventually reenter the atmosphere, the ADR will be ready to chase the next target until the end of its mission.

This solution is still on a preliminary phase and it is not under application, but preliminary numerical calculations show that an EDT would be able to de-orbit most of the large debris objects in the crowded regions described above within one year.

3.1.4 NASA

NASA is not currently focusing on any active debris removal solution. In 2010, National Space Policy for the United States of America directs NASA and the Department of Defense to "Pursue research and development of technologies and techniques… to mitigate and remove on-orbit debris…" However, since then, no U.S. government entity has been assigned the task of removing existing on-orbit debris.

Nevertheless, some solutions have been proposed from the NASA, and have been under study at different levels. NASA was the first agency –with the collaboration of the Italian Space Agency- that tested a tether system in space [21]. Also, they have also proposed a system to avoid debris-debris collisions using a laser on the debris surface to lower the perigee of its orbit [22]. Other exotic solutions have been proposed, like tugs, drag enhancement devices, and many others.

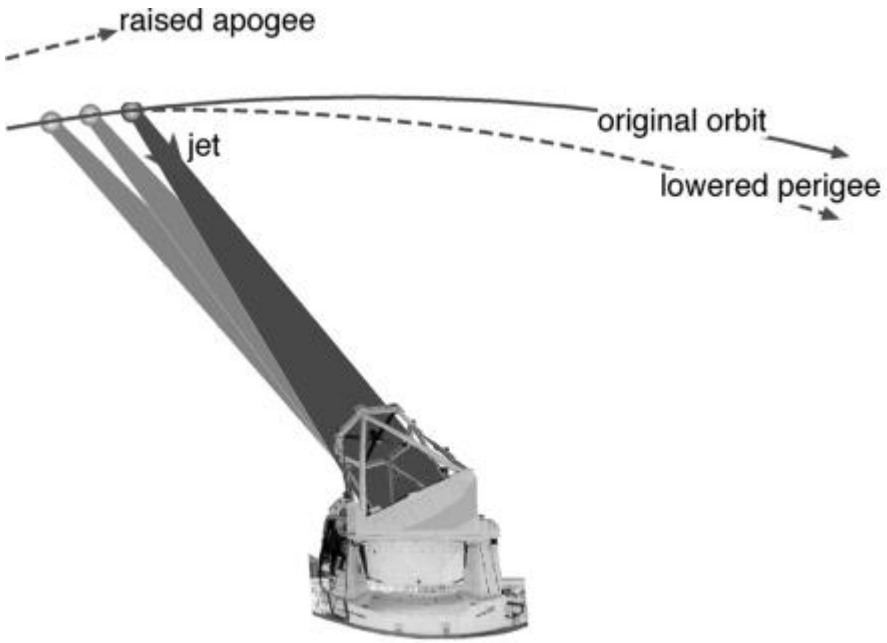

Fig. 16: NASA's laser device for deorbiting concept [22]

3.2 Mitigation

As we have explained at the beginning of this chapter, mitigation techniques are focused on reducing the amount of generated debris, through acting on the design, manufacture, operation, and disposal phases of a mission. It would have been more appropriate to start talking about mitigation and then the remediation as the further step in solutions.

But as this project is part of a mitigation solution that we will start studying on the next chapter, I have preferred to conclude this chapter seeing similar solutions to the one under study at the OmSTU.

3.2.1 Delta IV: the first controlled deorbit (NASA, 2006)

3.2.1.1 Delta IV

Delta IV is a Space Launching Vehicle from the Delta family. Delta IV uses rockets designed by Boeing's Integrated Defense Systems division and built in the United Launch Alliance (ULA) facility in Decatur, Alabama. It can be found in five different versions, Medium, Medium+ (4,2), Medium+ (5,2), Medium+ (5,4), and Heavy, tailored to suit specific payload size and weight ranges. Future upgrades are being studied including extra strap-on solid motors to boost capacity, higher-thrust main engines, and lighter materials among other modifications. These modifications could potentially increase the mass of the payload delivered to LEO to 100 tons.

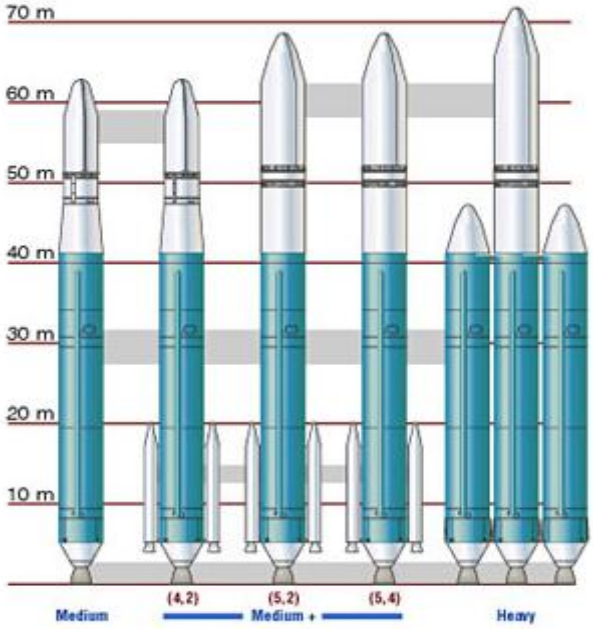

Fig. 17: Delta IV family [23]

3.2.1.2 Delta IV medium

The Delta IV Medium (Delta 9040) is the most basic Delta IV. Its first stage features a single Comon Booster Core (CBC), powrered by a Rocketdyme RS-68 engine, burning LH2 and Lox.

The upper stage is a modified Delta III second stage, with 4-meter liquid hydrogen and liquid oxygen tanks and a 4-meter payload fairing derived from the Delta III fairing. This stage is powered by a Pratt & Whitney RL10B-2 engine, also burning cryogenics.

The Delta IV Medium is capable of launching 4,210 kg (9,285 lb) to geosynchronous transfer orbit (GTO).

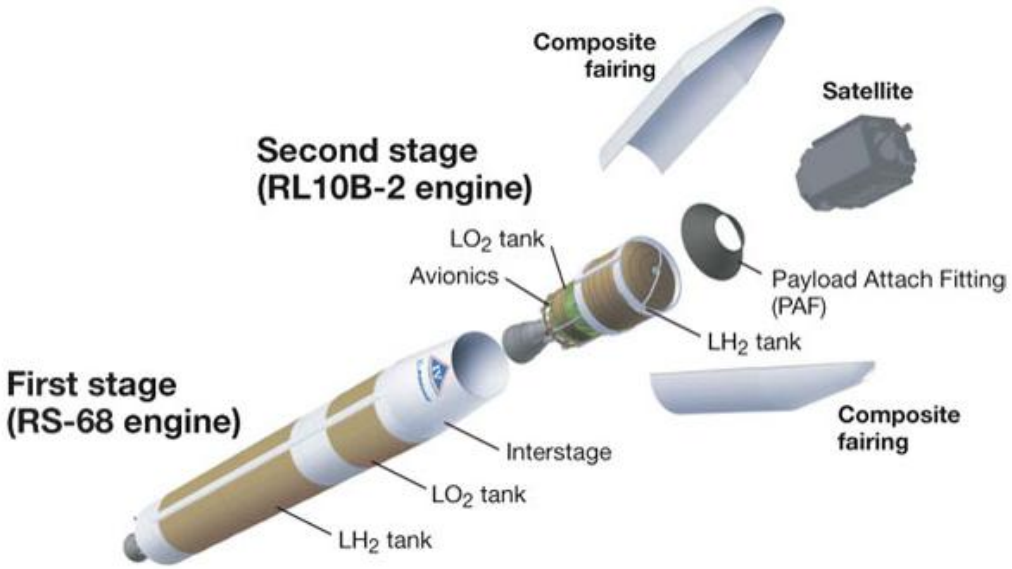

Fig. 18: Delta IV medium [24]

3.2.1.3 The RL10B-2 engine

The RL10B-2 is a rocket engine built in the United States of America by Pratt & Whitney Rocketdyne. It is an evolution of the RL-10 engine, which was first flown in 1962. Like all the RL-10 family, the RL10B-2 burns cryogenic liquid hydrogen & liquid oxygen propellants working on an expander cycle. In this cycle, the fuel is used to cool the engine's combustion chamber, picking up heat and changing phase. The gaseous fuel then powers the engine's pumps and turbine before being injected into the combustion chamber and burnt.

This variation of the classic RL-10 incorporates an extendable exit cone for increasing the specific impulse and payload capability. The basic engine and turbo pump are unchanged relative to the RL10. The engine gimbal system uses electromechanical actuators that increase reliability while reducing both cost and weight. The propulsion system and attitude control system (ACS) utilize flight-proven off-the-shelf components. The second-stage propulsion system produces a thrust of 24,750 lb (110 kN) with a total propellant load of 37,090 lb (16823 kg), providing a total burn time of approximately 700 sec. Missions requiring more than one restart are accommodated by adding an extra Helium bottle for the additional tank pressurization.

RL10B-2 characteristics	
Thrust	110 kN
Weight	299.3 kg
Fuel	Liquid Hydrogen
Oxidizer	Liquid Oxygen
Mixture ratio	5.88:1
Specific Impulse	465.5 sec
Length	2.19 m
Diameter	2.14 m

Table 2: RL10B-2 engine characteristics

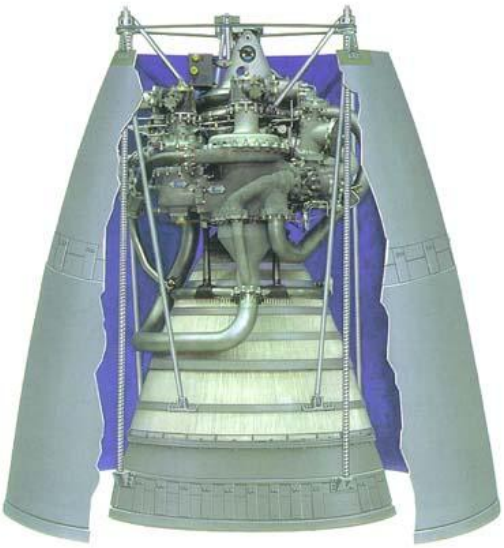

Fig. 19: The RL10B-2 engine [25]

3.2.1.4 Deorbit of Delta IV

The Delta IV Medium Upper Stage performed a controlled deorbit after delivering Defense Meteorological Satellite Program satellite 17 (or DMSP-17) to its mission orbit, on November 2006. This mission represented both the first time a Delta IV vehicle was used to launch a DMSP spacecraft, and the first time that such a deorbit maneuver was undertaken by any launch vehicle upper stage [26].

The DMSP-17 satellite was placed in a Sun Synchronous 849 km (458 nmi) circular orbit inclined at 98.7 degrees orbit. After the satellite was placed, the initial plan for the mission was to perform a perigee lowering, as the Delta upper stage usually performs, using part of the remaining propellant. This maneuver allows the upper

stage to achieve the reentry in less than 25 years, as asked by the regulations (see the previous chapter). However, this reentry would be random and a further analysis revealed that the casualty area would be very large and the casualty expectation would exceed US guidelines.

Fortunately, there was enough propellant to achieve a controlled deorbit of the upper stage. After some analysis, there was determined it was possible to perform it. The plan was the following: once the upper stage was far enough from the payload, the upper stage performed an attitude adjust maneuver in preparation for the deorbit burn. Then, after a coast period, the main engine on the upper stage was restarted and the burn continued until the propellant was depleted. The upper stage landed into the Pacific Ocean.

This maneuver was possible because the launch vehicle had a significant amount of extra performance and thanks to the restart capability of the RL10B-2 (adding additional He for the pressurization system, as explained before).

Although this was the only time NASA performed such maneuver, the starting orbit (sun synchronous) and the lack of available information, this mission have to be mentioned because it was the first time in history this kind of maneuver was performed with success.

3.2.2 Ariane 5 ES Controlled Deorbit, ESA

Ariane 5 is an expendable launch system used to deliver payloads into geostationary transfer orbit (GTO) or low Earth orbit (LEO). Ariane 5 rockets are manufactured under the authority of the European Space Agency (ESA) and the Centre National d'Etudes Spatiales (CNES). Astrium, an EADS company, is the prime contractor for the vehicles, leading a consortium of sub-contractors. Ariane 5 is launched from the Guiana Space Centre, in French Guiana.

The Ariane 5 ES version is an evolution of the Ariane 5 generic launcher vehicle. With a more powerful lower composite, identical to the one used on Ariane 5 ECA, it uses the small storable propellant upper stage (EPS: Etage à Propergols Stockables) of the generic version, which has been upgraded to allow reignition and long coast phases.

Fig. 20: The Ariane 5 ES SLV [26]

3.2.2.1 Vehicle Description

Ariane 5 is a two stage Launching Vehicle. Its lower composite comprises two solid-propellant boosters (EAP: Etage d'Accélération à Poudre) and the cryogenic main stage (EPC: Etage Principal Cryotechnique) equipped with the Vulcain 2 engine at the base.

The upper stage (EPS: Etage à propergols stockables), the one of interest for us, uses the Aestus engine, burning MMH and N2O4 to provide up to 2.7t of thrust. This stage, after placing its load in the ISS orbit, has been able to perform a deorbit burn in three different launches, as we are about to see.

3.2.2.2 The Aestus Engine

The Aestus engine was developed by Astrium in the Ottobrunn Space Propulsion Centre (Germany) during the period 1988-1995. The first operational flight of Aestus was on 30th October 1997. This engine based on the pressure fed cycle (it does not require turbopumps for its operation), it burns MMH and NON (Mixed Oxides of Nitrogen, N2O4 with a fraction of NO to lower its freezing point). As we are about to

understand, its restart capability makes possible the deorbit burn performed in the ATV missions.

The Aestus thrust chamber design is based on the regenerative cooling principle. Before combustion, MMH fuel is pressurized into a distribution manifold causing the fuel to flow through channels in the combustion chamber wall, configured to cause a highly efficient cooling. The MMH then enters the injector head.

Upon leaving the injector elements and entering the combustion chamber, the hypergolic propellants spontaneously ignite and are burned and accelerated up to sonic conditions at the throat. The combustion temperature in the combustion chamber reaches about 3000 K at a combustion pressure of 11 bar [27].

Aestus characteristics	
Vacuum thrust	30 kN
Weight	111 kG
Fuel	MMH
Oxidizer	MON
Mixture ratio	1,9
Specific Impulse	324 sec
Length	2.2 m
Nozzle diameter	1,315

Table 3: Aestus engine characteristics

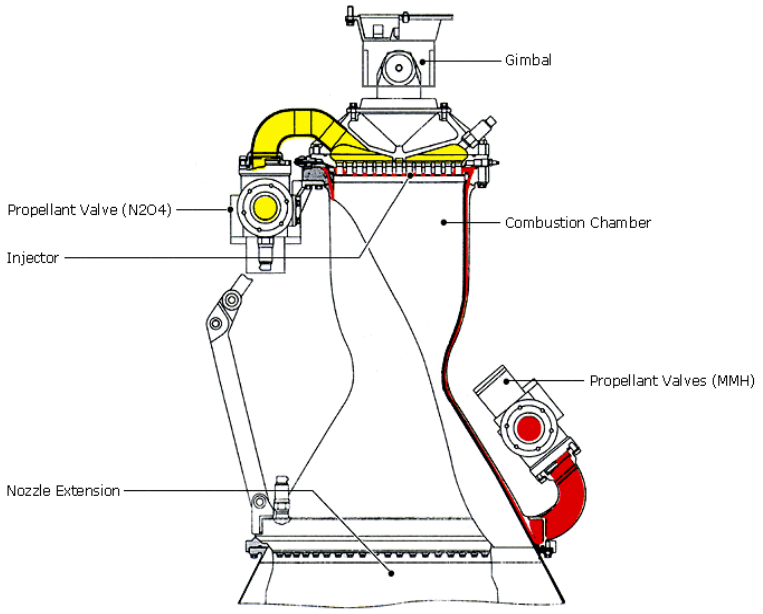

Fig. 21: Aestus engine's scheme [28]

3.2.2.3 Controlled re-entries performed

The first time the ESA developed a successful deorbit of an upper stage was in Ariane 5 flight 181 (March, 2008), after placing the ATV Jules Verne –designed to deliver supplies to the ISS [29]-. At first, ESA/CNES took into consideration a random re-entry maneuver, so a preliminary assessment of the risk was done. Once the evaluation was done, risk were judged too high- compared with the global specification for Ariane launch missions- so it was decided to accomplish a controlled re-entry, ensuring all safety objectives. In the next figure we can see the different phases of the maneuver, and the points where the orbit transfer boosts were performed.

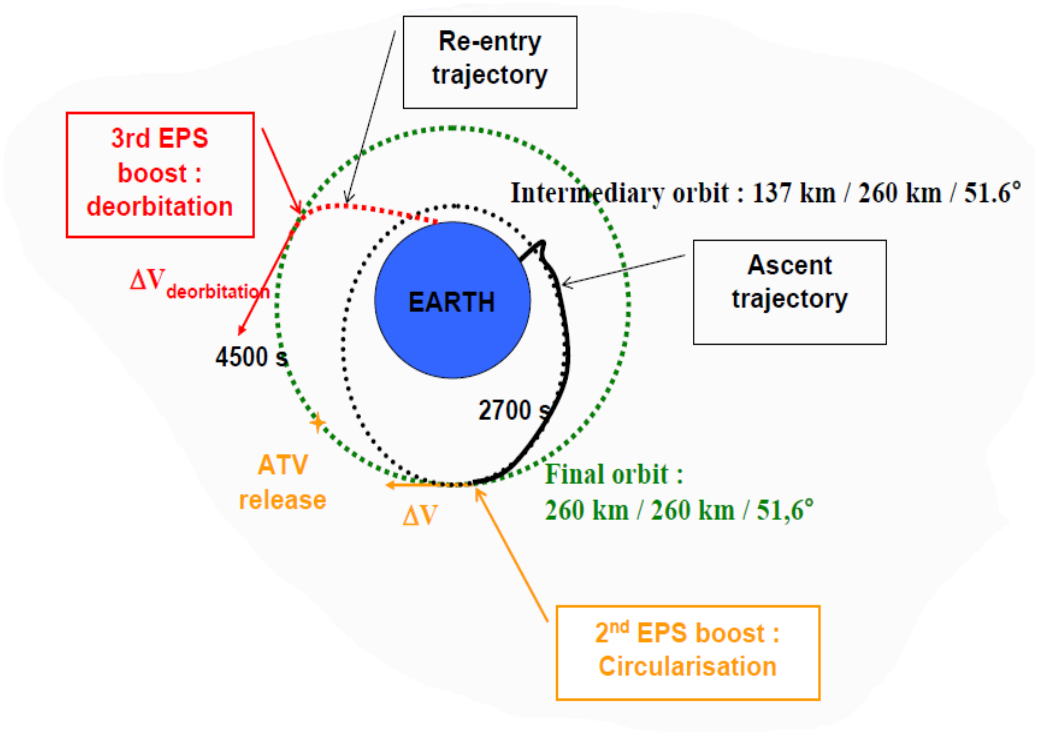

Fig. 22: Deorbit maneuver [29]

The operation achieved a great success, that lead to applying this deorbit operation to the next ATV mission flights [26][30], in flights 200 (February 2011) and 205 (March 2012). These two operations were programmed without changes.

This maneuver, as the Delta IV one, has its particularities: it was held at an altitude of 260 km, where the influence of gravity is still high (≈92% of g_0), so the engine does not operate on weightlessness conditions; the second one is the type of propellant, it uses high boiling propellant –like Soyuz, as we will see later- so the propellant could be in liquid state at the beginning of the deorbit burn; this engine operates a different

cycle without the use of turbopumps. All these conditions together can help to achieve the deorbit burn and make this case not to be a reference for the OmSTU solution. In spite of all mentioned, these actions deserve to be mentioned as they represent another step ahead in the controlled deorbit of upper stages history.

3.2.2.4 Ariane 5 ME, the next European SLV

The Ariane 5 ME (Midlife Evolution) is the next step in the Ariane 5 family. This version is currently in development, with first flight planned for 2016-2017. Ariane 5 ME will replace Ariane 5 ECA and Ariane 5 ES and will become Europe's new workhorse launcher until the arrival of the new Ariane 6 version.

The Ariane 5 ME will use the same lower composite than the Ariane 5 ECA and Ariane 5 ES. The main difference relies on a new upper stage, powered by the VINCI expander cycle engine. This engine can restart up to five times, allowing for more complex missions such as direct GEO insertion, deorbit from GEO or injection into the graveyard after payload is placed: Versatility is a key feature of this SLV.

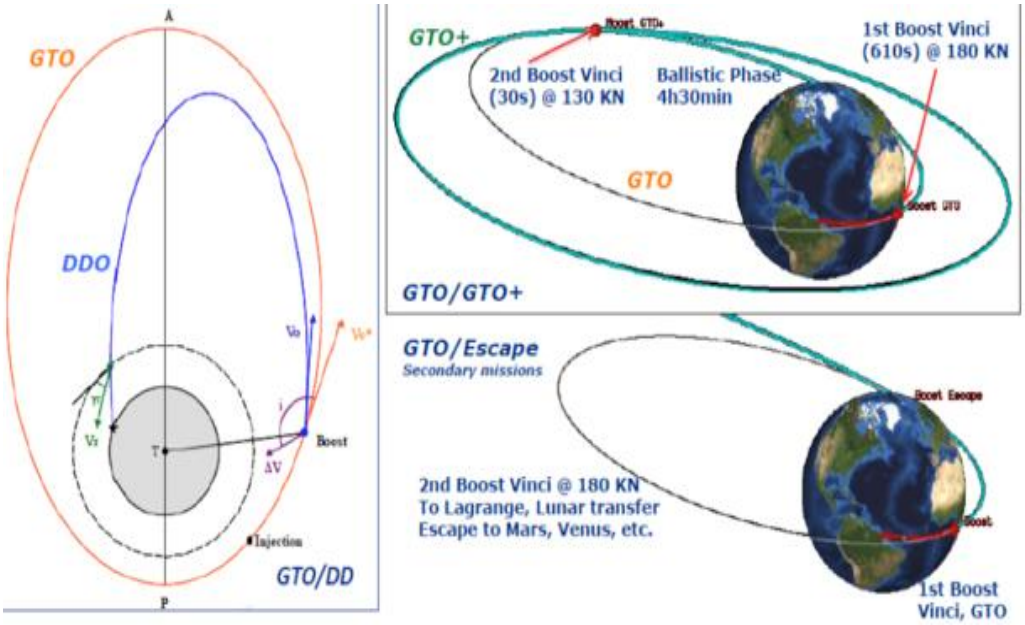

Fig. 23: Possibilities of the Ariane 5 ME [31]

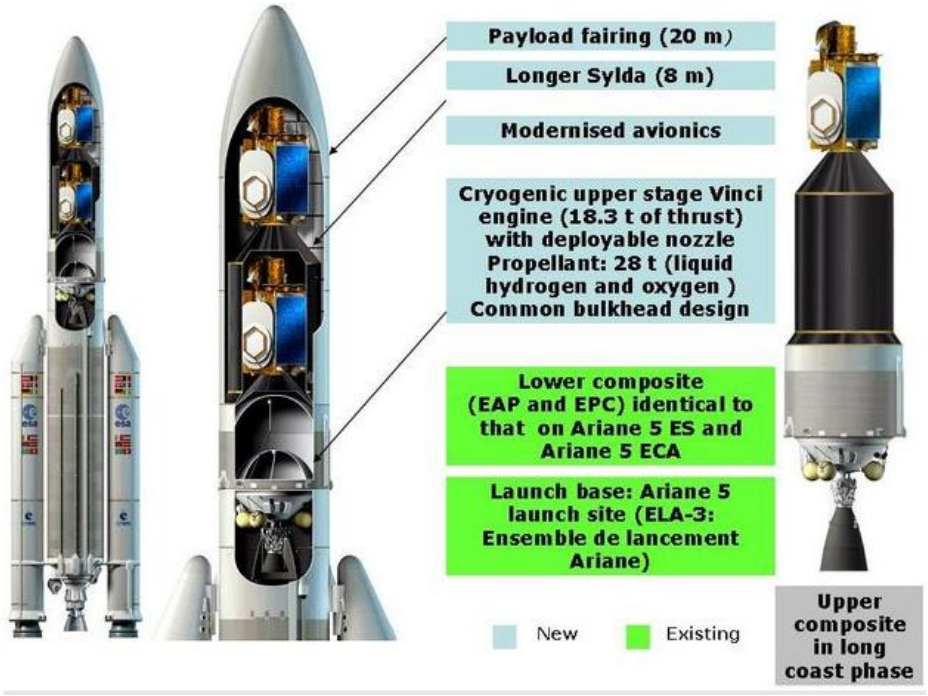

Fig. 24: Ariane 5 ME elements [31]

The VINCI engine

The VINCI engine, currently under development, will be the first re-ignitable European cryogenic engine. This engine is based on the HM7B, which powers the upper composite in the ECA version. The main differences between VINCI and its predecessor are the change of cycle –VINCI works on an expander cycle instead of a gas generator cycle- and the re-ignition capability. In the next table (*Table 4)*, we can find some of the characteristics of the VINCI upper stage [32].

VINCI characteristics	
Vacuum Thrust	180 kN
Fuel	Liquid Hydrogen
Oxidizer	Liquid Oxygen
Specific Impulse	464 sec
Length	4.2 m
Exit diameter	2.18 m

Table 4: The Vinci engine characteristics

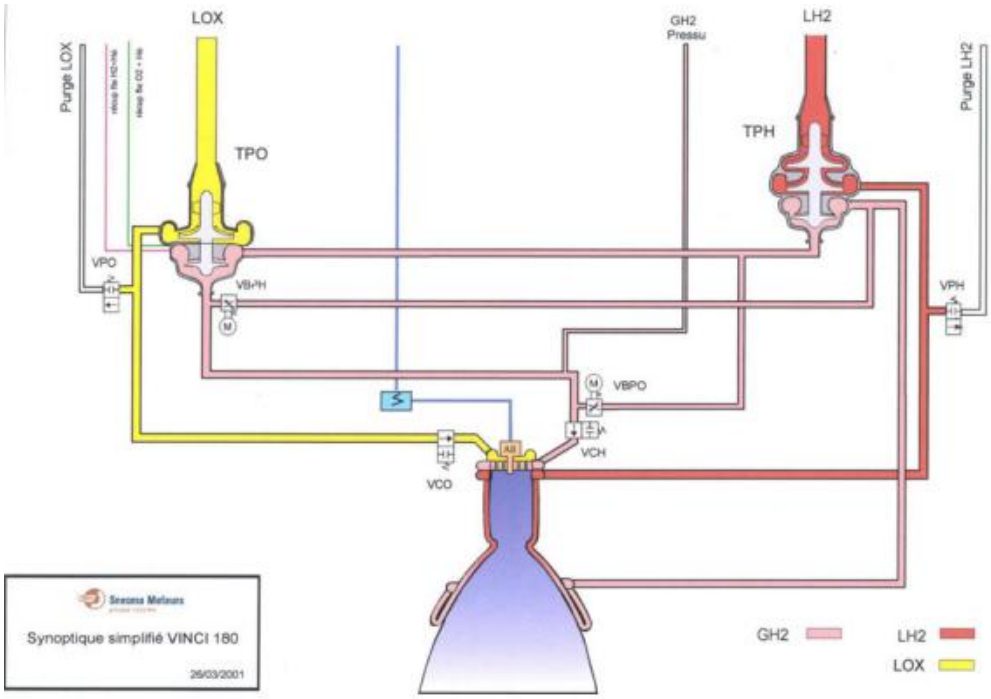

Fig. 25: VINCI's simplified flow scheme [33]

We have already explained that this engine is planned to be able to conduct a deorbit maneuver from GEO to Earth, as well as to inject the upper composite into the graveyard orbit. To accomplish this, the engine has to restart in microgravity conditions, facing several problems [34] like fluid behavior and heat transfer problems.

To cope with these problems, some operations have to be done after the first burn and the next one:

- Tanks reconditioning: the tanks are slowly depressurized to bring the propellants temperatures down. Then they are pressurized again to the nominal start pressure.
- Engine chilldown: given the very low temperatures of the propellants (around 90K for LO_2 and 20K for LH_2), propellants must be flowed through the engine in order to cool down the subsystems (lines, valves, and especially turbopumps) to their nominal operation temperature.

During these operations, some other problems can appear in microgravity:

- Propellant behavior in the tanks (sloshing, ingestion of liquid in pressurization lines).

- Fluid flows in pipes and systems with a complex geometry.
- Boiling and heat transfer during chilldown in microgravity.

The most common way to solve this is using an acceleration device –usually hydrazine thrusters- to produce a thrust. This thrust creates an artificial gravity field that will properly settle the propellant. Better knowledge about microgravity can truly explain the real usefulness of this kind of systems, so more studies are required to really understand the phenomena.

As we previously mentioned, Ariane 5 ME is currently on development and it has not been already tested in space. In the next point we will see another case of cryogenic engine: H-IIB's LE-5B; in its case, the deorbit maneuver it has been tested successfully three times.

3.2.3 The H-IIB controlled deorbit

The H-IIB is a two-stage rocket operated by the Japan Aerospace Exploration Agency (JAXA) and Mitsubishi Heavy Industries (MHI). It is derived from the earlier launchers H-II and H-IIA, expanding their launch capability so it can launch roughly 16.5 tons HTV into ISS transfer orbit. While the H-IIA has several configurations, the H-IIB SLV only flies in a single one, as we will see later.

Its developed was linked to the launch of the H-II Transfer Vehicle (HTV). The main changes introduced, relative to H-IIA, are the following [35]:

- Enhanced first stage: tank diameter extension (1.2m of diameter increase and 1m of length), cluster system for two main engines, and four solid rocket boosters (SRB-A)
- Reinforced upper stage
- 5S-H fairing, newly developed to launch the H-IIB

Its maiden flight occurred on September 10, 2009. It successfully launched the HTV-1, which was on a mission to resupply the International Space Station (ISS). Since then, it has performed two more successful missions, on January 22, 2011 and July 21, 2012. H-IIB flights are launched and directed from the Tanegashima Space Center (TSC).

Vehicle configuration

The H-IIB launch vehicle is a two-stage rocket launcher. Both stages use liquid oxygen and liquid hydrogen as propellants. The first one is powered by two Le-7A engines and has four strap-on solid rocket boosters (SRB-A3) powered by polybutadiene. In addition, the first-stage body of the H-IIB is 5.2m in diameter compared with 4m for the H-IIA. The total length of the first stage is extended by 1m from that of H-IIA. As a result the H-IIB first stage holds 1.7 times more propellant than that of the H-IIA.

The second stage is powered by a single LE-5B engine, making possible to lift payloads of up to 19,000 kilograms to Low Earth Orbit. Geostationary Transfer Orbit Capabilities are about 8,000 Kilograms.

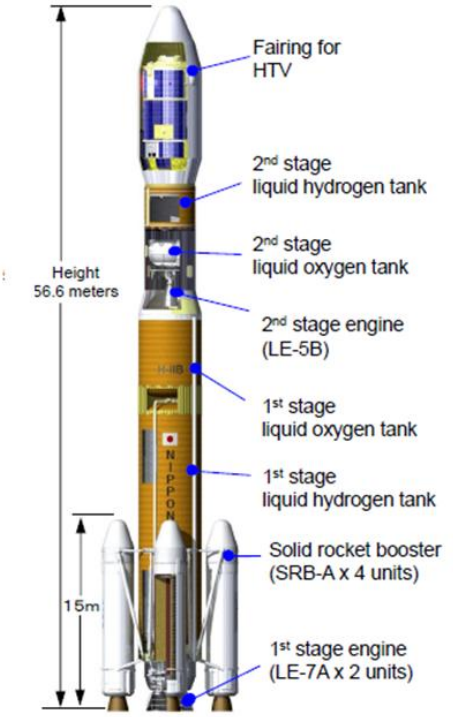

Fig. 26: The H-IIB Launching vehicle [36]

The LE-5B engine

Developed by JAXA and MHI, the LE-5B engine is the second stage engine for H-IIA and H-IIB. It is an evolution of LE-5 and LE-5B that uses the mixture LH_2/LO_2 working on an expander bleed scheme. It's interesting to mention that LE-5A and LE-5B are the only operating engines that use this cycle.

LE-5B characteristics

Vacuum Thrust	137 kN
Fuel	Liquid Hydrogen
Oxidizer	Liquid Oxygen
Specific Impulse	449 sec
Weight	269 kg

Table 5: LE-5B characteristics

This engine is able of multiple restarts, due to its spark ignition system (as opposed to the single use pyrotechnic or hypergolic igniters commonly used on some contemporary engines). It is rated for up to 16 starts and more than 40 minutes of firing time. The H-II the engine is considered expendable, being used for one flight and jettisoned.

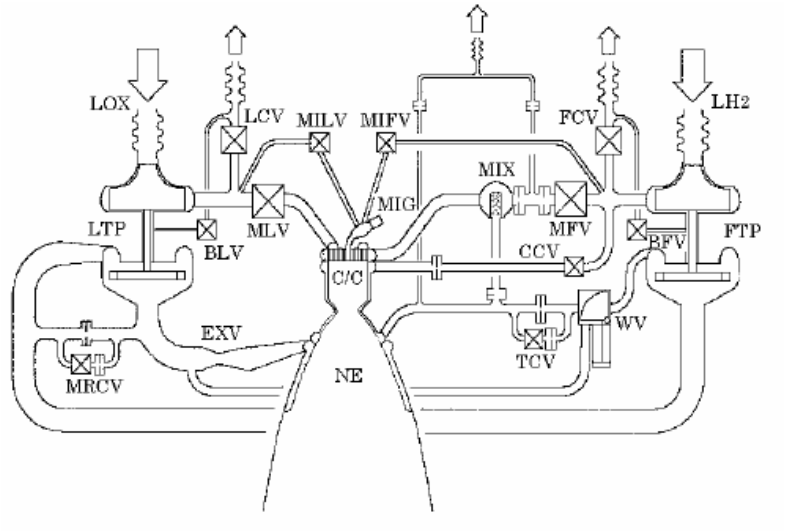

Fig. 27: LE-5B engine scheme [37]

Expander bleed cycle

The expander bleed cycle is a modification of the traditional expander cycle. Unlike the expander one, expander bleed cycle is open. In this configuration, only a small portion of the propellant is heated and used to drive the turbine and is then bled off, being vented overboard without going through the combustion chamber. Bleeding off the turbine exhaust allows for a higher turbopump output by decreasing backpressure and maximizing the pressure drop through the turbine.

As we have explained when we discussed the RL10B-2 engine, in the expander cycle fuel is used to cool the engine's combustion chamber, then powers the engine's pumps and turbine before being injected into the combustion chamber and burned. If we compare expander bleed cycle with a standard expander one, this changes lead to higher engine thrust at the cost of sacrificing some efficiency due to essentially wasting the bled propellant by not combusting it.

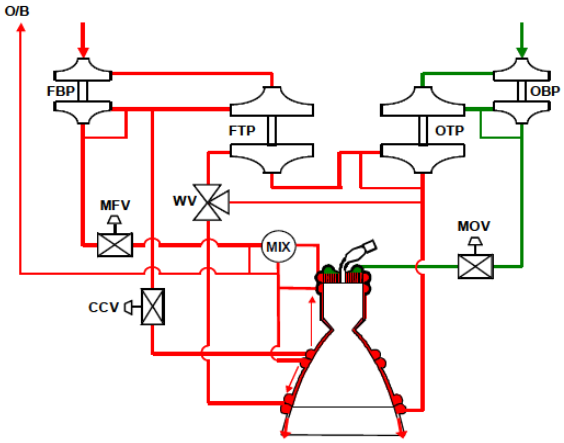

Fig. 28: Expander bleed cycle scheme [38]

Idle mode

To perform a deorbit maneuver, a unique feature of LE-5B engine called "idle-mode burn" is required. This mode consists on a low thrust level burn (4 kN compared to 137 kN of the normal thrust level). This low thrust level was chosen for the deorbit to spare enough time for guidance calculations, conducted by onboard computer. Idle mode does not use FTP/LTP (or OTP in *Fig.28*) turbopumps to feed the propellant to the main chamber; it provides propellant using a thrust of high pressure gas [36].

LE-5B has been tested on H-IIA before the first H-IIB was launched. So, idle-mode burn was used for only a short period to re-ignite the H-IIA second stage engine. Therefore, to acquire detailed performance data of idle-mode burn, additional engine qualification tests and flight experiments by the post-mission second stage of H-IIA Flight No.17 were executed [35].

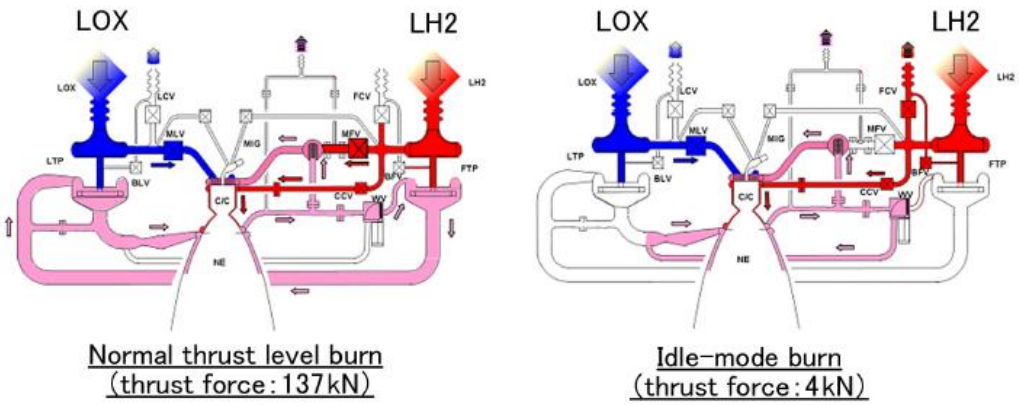

Fig. 29: Comparison between LE-5B normal and idle mode [35]

Controlled re-entry

On its first flight (September 2009), the H-IIB's upper stage performed a re-entry maneuver few days after the placement of the HTV [39]. During the atmospheric re-entry, the upper stage was disintegrated, and most of the generated fragments were burn out. However, a few fragments survived atmospheric re-entry heating environment. They might fall to the earth surface and become a risk, so JAXA decided to prepare the second flight for a controlled de-orbit on its next flight.

The changes introduced for the second flight were:

- Addition of another Bottle of Helium to pressurize the LH2 tank prior the deorbit burn.
- Application of thermal protection tape to ease the thermal effect during a long ballistic phase.
- To modify the avionics system in order to receive a deorbit approval command from ground control stations.
- To adapt the guidance control algorithm in order to issue an engine cutoff command during the deorbit burn.

Preliminary studies revealed that it was unnecessary to add more hydrazine (for the attitude control system) and batteries due to the prolonged flight time.

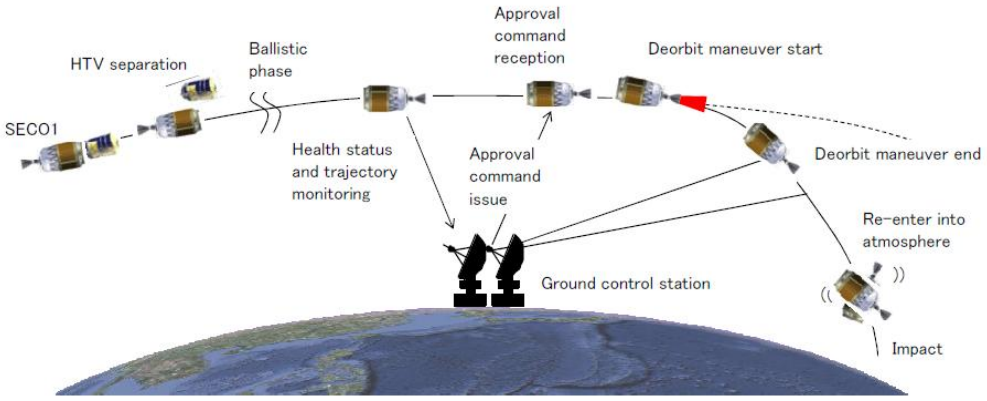

Fig. 30: Presentation of the ground control for deorbit [5]

To execute this de-orbit maneuver and controlled re-entry, the H-IIB upper stage must be re-oriented to face the opposite direction to the one in which it is moving, and an engine burn is made to decrease velocity. A high-latitude area of the South Pacific Ocean was chosen as the target impact zone since it is far from land and very few vessels pass through the area. JAXA developed a plan in which a thrust of the H-IIB upper stage engine could be made with certainty after one orbit of the Earth and while visible from the Tanegashima Ground Station.

To execute the controlled re-entry, a radio link must be established between ground control and the rocket. The horizon angle of the tracking and control antenna is less than one degree. Furthermore, since the upper stage power batteries would not maintain operable charge from the second orbit onward, it is imperative to execute a successful re-entry maneuver during the first orbit. The upper stage remains visible from the Tanegashima Ground Station for approximately 300 seconds, and once the time necessary for transmission of the reverse-thrust command is subtracted, the window for the rocket to receive radio command signals is a mere 80 seconds at the most [40].

After the HTV has been released, a contamination and collision avoidance maneuver is executed to separate the upper stage from the HTV. Once it is far enough from the HTV, the upper stage performs an attitude adjust maneuver to prepare itself for the deorbit burn. Then the upper stage starts a long ballistic phase making nearly a complete revolution around the Earth.

Approximately 100 minutes from liftoff, vehicle health status and trajectory will be evaluated at the Tanegashima ground stations for deorbit burn clearance. This clearance enables LE-5B-2 engine to reignite at low thrust level (idle mode) burn at the correct point on its orbit. The deorbit burn continued until a cutoff command is issued from onboard computer which optimizes the burn duration such that the dispersion of the impact footprint is minimized. After the deorbit maneuver, the upper stage starts to passivate the propellant tanks (LH_2 tank, LOX tank and two hydrazine tanks). The ground stations continue monitoring vehicle health status and trajectory until the telemetry loss.

To conclude with this case, we can mention that, like the Ariane 5 ECA, H-IIB performed the deorbit at very low altitude, with a non-negligible contribution of the gravity forces.

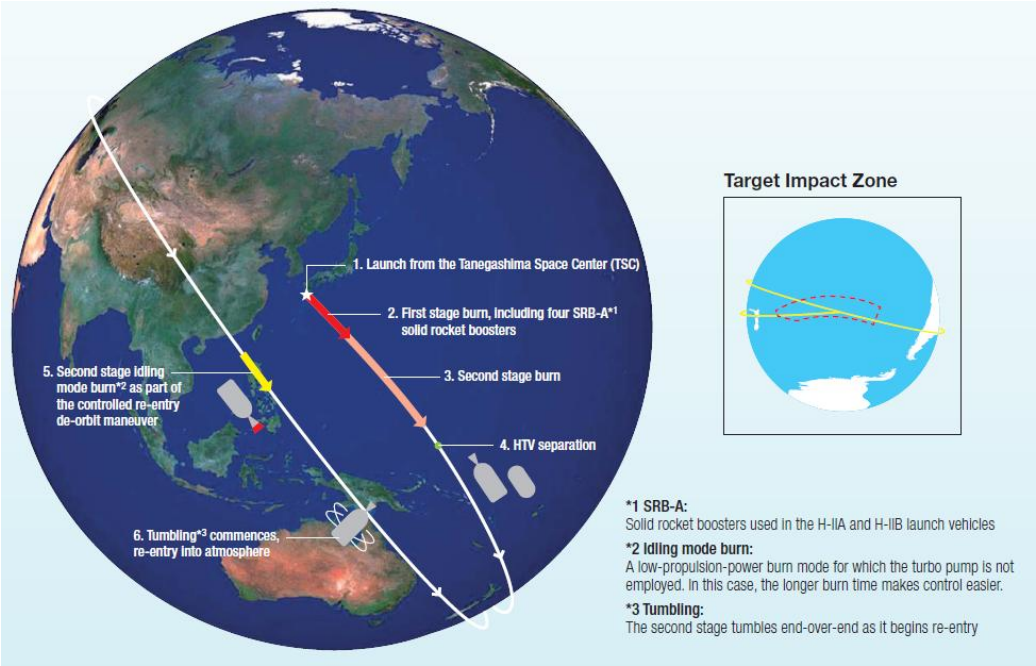

Fig. 31: Maneuver and impact zone estimation [40]

For the OmSTU, the most important aspect about this procedure is the real state of the propellants inside tanks. As H-IIB deals with cryogenics, there is a risk of gasification inside tanks, like we have explained in the Ariane 5 EM case. This information is classified and not for public knowledge, but their diagrams show that, even in idle mode, the propellant is in a liquid state at the exit of the tank. Also, the changes introduced in thermal isolation to avoid the effect of heating due to space radiation may indicate that they are working on this direction.

3.2.4 The OmSTU proposal

As we are just about to understand in the next chapter, the studies held at OmSTU show a certain similarity to the cases we have already seen in the mitigation point. The main differences lie in the fact that OmSTU's proposal is based on the implementation of an active de-orbiting system (ADS) with four independent small gas rocket engines (GRE), that is to say, it does not use the main propulsion engine –as we have seen in the previous cases-.

In addition, this study will be used on high boiling propellants (kerosene in the case of Soyuz 2.1.B) engines, to exploit its residuals remaining after mission to its depletion, via vaporization.

As a result, additional systems are required to achieve this vaporization (gasification system and feeding system) and the use of this gasified propellant (ADS with four Gas Rocket Engines). We will study all of them in the next chapters.

The OmSTU is also working on the remediation field, by the development of a chaser system to rendezvous with target debris and make it deorbit back to Earth, as well as the grabbing system required for the docking [41]. The final step, and the OmSTU target, is to combine both ways (the remediation solution here explained and the chaser), so they can use the propellant remaining in a SLV's upper stage, vaporize it and use the hot gas into a rocket engine. This stage will become the chaser that will make a rendezvous with the target debris, grab it, and make it deorbit.

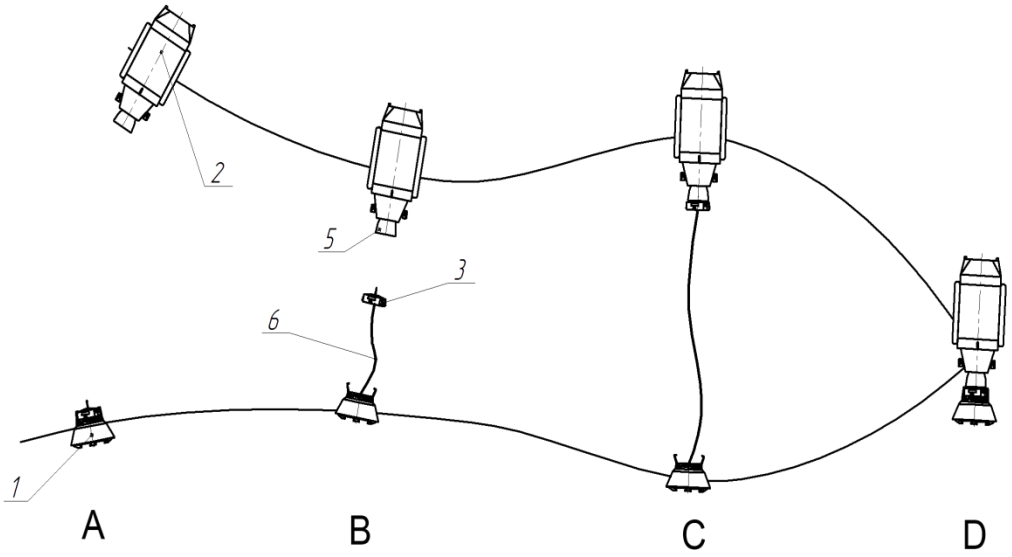

Fig. 32: OmSTU docking concept

Chapter 4: Gasification system of unused propellant

In this chapter, we will go into detail about the OmSTU system for gasification and deorbiting. As we have discussed in the precedent chapters, the objective of the OmSTU investigation is to design ADS system working on the basis of maximum exploitation of the available energy. To achieve this, the way is to use the residual propellant that remains after the end of operation, in tanks of SLV separated parts. This will provide enough energy to perform a deorbit maneuver, so we can avoid increasing the amount of space debris with another piece. It will be a mitigation technique, according to what we have seen before.

This residual part cannot be used directly, without gasification, as we need to cope with several issues: its unknown state and position inside the tank can make difficult to feed them to the combustion chamber and the use of turbopumps become impossible due to the probability of absorbing a two-phase mixture. The remaining propellant needs to be vaporized before being feed into the combustion chamber – without turbopumps- of the ADS system. In this chapter we will study this gasification system describing all the parts involved in the gasification process, and present the rest of the processes that will eventually make possible the deorbit.

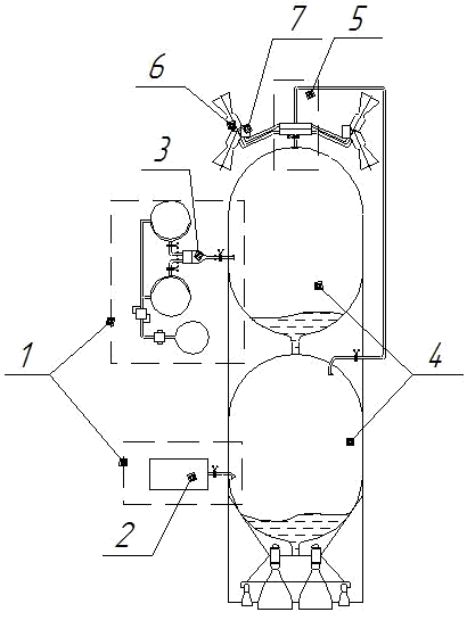

Fig. 33: Gasification system scheme [41]

For this model we have made some assumptions related to the liquid conditions inside the tanks. We assume a residual amount of propellant of around 3% of the initial mass

(3% for each propellant), and we also suppose that this propellant is placed in a simplified way (we will discuss it in *Chapter 5: Analytical model for gasification system*). The liquid conditions have a great level of uncertainness for some reasons like unsymmetrical working conditions of the fuel and oxidizer valves, weightlessness conditions or conditions that differ from the project.

4.1 Description of the components

4.1.1 Soyuz 2.1.b

This study will take Soyuz 2.1.b second stage (Block I) as its development platform, even if it can be suitable to many different international configurations [41] like Angara, Ares or Atlas Centaur among others.

More information related to Soyuz 2.1.b can be found on *Appendix 1*.

4.1.2 Propellants

As we have stated through this report, Soyuz Block I is powered by a engine burning RP-1 and LO_2, so they will be the working fluids for our gasification system. The main properties and features of RP-1 and Lox are reported in the following paragraphs.

4.1.2.1 RP-1

RP-1 (Rocket Propellant-1 or Refined Petroleum-1) is a highly refined form of kerosene similar to jet fuel, it is the standard rocket kerosene in many countries, and is frequently utilized in regeneratively-cooled liquid rocket engines. This extended use is due to the very good properties that RP-1 shows. I we compare it with Liquid Hydrogen, although having a lower specific impulse than liquid hydrogen(LH_2), RP-1 is cheaper, can be stored at room temperature, is far less of an explosive hazard and is far denser. RP-1 is significantly more powerful than LH2 by volume and LOX/RP-1 has a much better ISP-density than LOX/LH_2. RP-1 also has a fraction of the toxicity and carcinogenic hazards of hydrazine, another room-temperature liquid fuel.

RP-1 is most commonly burned with LO_2 (liquid oxygen) as the oxidizer, though other oxidizers have also been used. RP-1 is a fuel in the first-stage boosters of the Soyuz-FG, Delta I-III and Atlas rockets. It also powered the first stages of the Soyuz-FG, Titan I, Saturn I and IB, and Saturn V.

If we compare with liquid hydrogen, a hydrocarbon propellant will be less efficient chemically fuel. Hydrogen is the lightest molecule; when combusted with oxygen, the H_2O product has a low weight, and thus a high exhaust velocity. Hydrogen engines are operated fuel-rich, so some exhaust is unreacted H_2, which is even lighter. Hydrocarbons, on the other hand, produce both H_2O and CO_2. CO_2 is over 2.5 times heavier, slowing the exhaust. It can also absorb significant amounts of combustion energy by generating any of several oscillating modes between the atoms. This is

energy that could have instead gone into exhaust velocity, and thus, thrust. The heavier oxygen atoms absorb much more energy than the two hydrogen atoms of H_2O. American designed hydrocarbon engines are also run fuel-rich, which produces some CO instead of CO_2. But this also results in incomplete combustion, producing some organics of high molecular weight and numerous vibration modes. All told, kerosene engines generate an I_{sp} in the range of 270 to 360 seconds, while hydrogen engines achieve 370–465 seconds.

The low vapor pressure of kerosene gives safety for ground crews. However, in flight the kerosene tank will need a separate system of pressurization, to replace fuel volume as it drains. Generally, this is a separate tank of liquid or high-pressure inert gas, such as nitrogen or helium. This creates extra cost and weight. Cryogenic or volatile propellants generally do not need a separate pressurization gas; instead, some propellant is expanded (often with engine heat) into low-density gas, and routed back to its tank.

Any hydrocarbon-based fuel when burned produces more air pollution than hydrogen. Hydrocarbon combustion produces carbon dioxide (CO_2, a greenhouse gas), toxic carbon monoxide (CO), hydrocarbon (HC) emissions, and oxides of nitrogen (Nox), while hydrogen (H_2) reacts with oxygen (O_2) to produce only water (H_2O), with some unreacted H_2 also released.

In the next table we can find some of the main properties of RP-1:

Properties of RP-1	
Molecular mass	≈175
Melting point (K)	225
Boiling point (K)	460-540
Heat of vaporization (kJ/kg)	246
Specific heat (kcal/kg·K)	0.45
Specific gravity	0.58 (422 K)
Viscosity (centipoise)	0.75 (289 K)

Table 6: properties of RP-1 [42]

RP-1, like other distillates, can be compared to dodecane (*Fig. 34*). Dodecane (also known as Adakane 12 or Ba 51-090453, among others) is a liquid alkane hydrocarbon with the chemical formula $CH_3(CH_2)10CH_3$ (or $C_{12}H_{26}$), an oily liquid of the paraffin series. It has 355 isomers. It is used as a solvent, distillation chaser, scintillator component.

The combustion reaction for dodecane is:

$$2C_{12}H_{26(l)} + 37O_{2(g)} \rightarrow 24CO_{2(g)} + 26H_2O_{\ (g)}$$

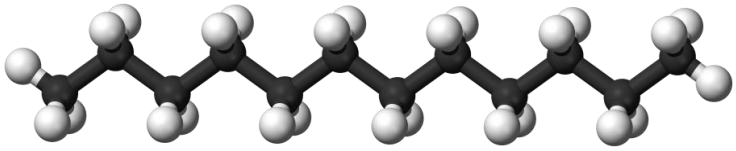

Fig. 34: n-dodecane [43]

Properties of dodecane	
Molecular mass	170.33 g
Melting point (K)	263.5
Boiling point (K)	487-491
Heat of vaporization (kJ/kg)	352
Specific heat (kcal/kg·K)	0.37
Specific gravity	0.75 (293 K)

Table 7: properties of dodecane [42]

4.1.2.2 Liquid oxygen

Liquid oxygen (often abbreviated as LOX. Lox, or LO_2), boils at 92 K at atmospheric pressure; at these conditions it has a specific gravity of 1.14 kg=m^3 and a heat of vaporization of 213 kJ/kg. It is widely used as an oxidizer and burns with a bright white-yellow flame with most hydrocarbon fuels. It has been used in combination with alcohols, jet fuels (kerosene-type), gasoline, and hydrogen.

Liquid oxygen is a desirable and commonly used propellant in large rocket engines. The following missiles and space launch vehicles use oxygen in combination with [42]:

- Jet fuel: Atlas, Thor, Jupiter, Titan I, Saturn booster
- Hydrogen: Space Shuttle and Centaur upper stage
- Alcohol: V-2 and Redstone.

Even if it usually does not burn spontaneously with organic materials at ambient pressures, combustion or explosions can occur when a confined mixture of oxygen and organic matter is suddenly pressurized. Impact tests show that mixtures of liquid oxygen with many commercial oils or organic materials will detonate, what can become a great safety risk. Nevertheless, handling and storage are safe when contact materials are clean. This is because Lox is a noncorrosive and nontoxic liquid and will not cause the deterioration of clean container walls. When in prolonged contact with human skin, the cryogenic propellant causes severe burns.

Liquid oxygen supports and accelerates the combustion of other materials. Because it evaporates rapidly, it cannot be stored readily for any great length of time. If liquid oxygen is used in large quantities, it is often produced very close to its geographical point of application. Liquid oxygen can be obtained in several ways, such as by boiling liquid nitrogen out of liquid air. It is necessary to insulate all lines, tanks, valves, and so on, that contain liquid oxygen in order to reduce the evaporation loss. Rocket propulsion systems which remain filled with liquid oxygen for several hours and liquid oxygen storage systems have to be well insulated against absorbing heat from the surroundings. External drainage provisions have to be made on all liquid oxygen tanks and lines to eliminate the water that condenses on the walls.

Properties of Liquid Oxygen	
Molecular mass	≈175
Melting point (K)	225
Boiling point (K)	460-540
Heat of vaporization (kJ/kg)	246
Specific heat (kcal/kg·K)	0.45
Specific gravity	0.58 (422 K)
Viscosity (centipoise)	0.75 (289 K)

Table 8: properties of Lox [42]

4.1.3 Gasification system

The first problem we have to face is the design of the gasification system. This gasification system must have the following properties:

- Maximum thermal capacity of the heat carrier
- Fixed mass flow rate and temperature at the inlet of the tank
- The gas generator products must not chemically react with the components of the propellant in tanks, and the resulting products of gasification form must provide the highest specific impulse.

The gasification system consists on the propellants, the tanks to store them, a small combustion chamber and the feeding system to the tanks (tubes, injectors…).

There are other investigations under study at the OmSTU to choose the best components. In this report we will only focus on the analytical model for the process of gasification. Nevertheless, we will give some hints about the subsystems here mentioned.

4.1.3.1 Propellant trade/off

First of all we have to decide what type of gas generator we are going to use in the gasification system: solid, liquid or hybrid. The type of propellant we choose will highly determine the performance and capabilities of our system.

First of all, we will do a tradeoff between advantages and disadvantages of the three types:

Solid gas generator

Advantages	Disadvantages
Simple design (few or no moving parts) Easy to operate, reliable Compact, usually higher overall density Not leaking, spilling or sloshing problems Lower cost Long term storability Solid components burn to its depletion Metal additives can be easily added	Only able to be throttled or stopped if preprogramed Explosion and fire risk is higher, failure can be catastrophic Requires an ignition system (for each restart too) Cannot be tested before operation

Table 9: Solid gas generator trade-off

Liquid gas generator

Advantages	Disadvantages
Can be randomly throttled, stopped and restarted Safety, it can be extensively checked prior to operation Typically provides higher energy	Relatively complex design, with more parts Needs pressurization and feeding system More overall weight Usually requires more volume due to average lower propellant density Spill of leaks can be dangerous Higher cost Usually some unused residual remains

Table 10: Liquid gas generator trade-off

Hybrid gas generator

The hybrid engines use one liquid and one solid propellant so it advantages and disadvantages place them it an intermediate step between the other two types, as we will see in the next table:

Advantages	Disadvantages
More simple than liquid gas generator Only requires pressurization and feeding system for one of the propellants	Higher weight and more complex than solid gas generator Oxidizer to fuel ratio shifts as the grain

Modulation, shutdown and restart regresses capability.
Higher density on the solid propellant
Metal additives can be added
Reduced explosion hazard

Table 11: Hybrid gas generator trade-off

4.1.3.2 Choice of propellants

The given criteria can give some direction, but there are more requirements that determine the final propellants used in the gas generator: budget limit, mass tradeoff or technological knowledge level, among others. As we have pointed before, one of the important requirements of the gasification system was that its products may not chemically interact with the propellant inside tanks.

Fuel tank

For the fuel tank, the option we are going to study is the use of a liquid gas generator burning RP-1 and Liquid Oxygen, so the products of the gas generator will contain non reacting species, taking into consideration the specie inside the tank. The mixture will burn taking an oxidizer to fuel ratio equal to 2.35 (a typical working condition for this kind of mixture).

Oxidizer tank

In the case of the oxidizer our choice is the hydrogen peroxide. The physical properties of hydrogen peroxide are close to those of water, with two notable differences: H_2O_2 has a significantly higher density and a much lower vapor pressure. It remains in the liquid state at ambient pressure in a wide range of temperatures and is relatively easy to handle with respect to other common liquid rocket propellant oxidizers. The propulsive performance of hydrogen peroxide monopropellant rockets is about 20% lower than hydrazine, but the volume specific impulse achievable with 90% H2O2 is higher than most other propellants due to its high density. It decomposes according to the reaction:

$$H_2O_2 \rightarrow H_2O + \frac{1}{2}O_2 + Q_{released}$$

In this case, the main limitation is the temperature of the exhaust gases. Its combustion (or –or more specifically- decomposition) temperature will be around 1000 K in the combustion chamber [44], so the heat carrier temperature we put into the tank would be even lower.

In both cases we have chosen a liquid gas generator due to its flexibility and safety cababilities.

4.1.4 ADS system engine:

The ADS system engine is the next step in the OmSTU's schedule. As we already know, it will be based on a group of four small engines, each of them working on a gas/gas scheme, with rotating combustion and counterflow vortex.

4.1.4.1 The gas engine

The gas rocket engine is a concept that has been studied and proposed for decades but never came to an end as a real SLV main engine. The first attempt was the RD-270, designed by the Russian engineer Valentin Glushko [44], during the decades of the 60's and 70's. RD-270 was to be used on the first stages of proposed heavy-lift UR-700 and UR-900 rocket families. It had the highest thrust among single chambered engines of USSR and Russia, 640 metric tons at the surface of Earth (it is still the more powerful hypergolic engine ever built). The propellants used were high- boiling propellants, specifically unsymmetrical dimethylhydrazine (UDMH) and nitrogen tetroxide (N2O4). The engine applied full flow staged combustion cycle for all the incoming mass of fuel, which was turned into a gas and passed through a couple of turbines before being burned in the combustion chamber. This allowed it to achieve a specific impulse of 301s at the Earth's surface. Unfortunately, the program was cancelled on December 1970 when the engine was being tested.

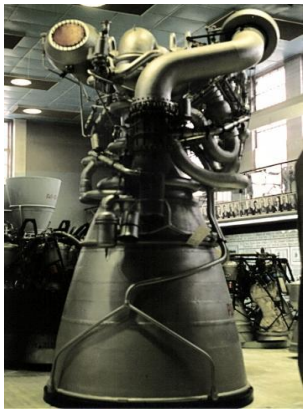

Fig. 35: The RD-270 engine [46]

The gas engine is aimed to increase the pressure inside the combustion chamber (P_{cc}), to achieve a higher impulse. To do this, both propellants are gasified in two preburners before drive them to the main combustion chamber [47].

The use of high P_{cc} involves certain engine-design difficulties. These problems include: the need for more efficient cooling, difficulties in assuring tightness of the joints, and difficulties in assuring engine unit strength and efficiency. However, these difficulties have been successfully overcome in time. Disadvantages in using high P_{cc} also include an increase in cost of the engines and a certain reduction in their reliability.

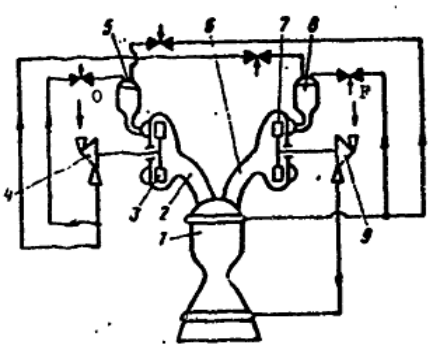

Fig. 9.6. LPRE operating on the scheme "gas-gas": 1 – afterburner section; 2, 6 – gas guides; 3 – turbine of oxidizer TPA; 4 – oxidizer pump; 5 – oxidizing liquid gasifier; 7 – turbine of fuel TPA; 8 – reducing liquid gasifier; 9 – fuel pump.

Fig. 36: LPRE operating on a "gas-gas" scheme [47]

For more than one decade, NASA has been working in a new gas engine, the IPD (Integrated Powerhead Demonstrator) [48]. The IPD also works on a full flow stage combustion cycle using the most advanced technologies, becoming the first of three phases of the Integrated High Payoff Rocket Propulsion Technology Program (IHPRPT) [49]. The IHPRPT seeks to increase the performance and capability of rocket propulsion systems while decreasing costs associated with military and commercial access to space.

On July 19, 2006 Rocketdyne announced that the demonstrator engine had been operated at full power [50]. Nevertheless, it is is still far from being a reality.

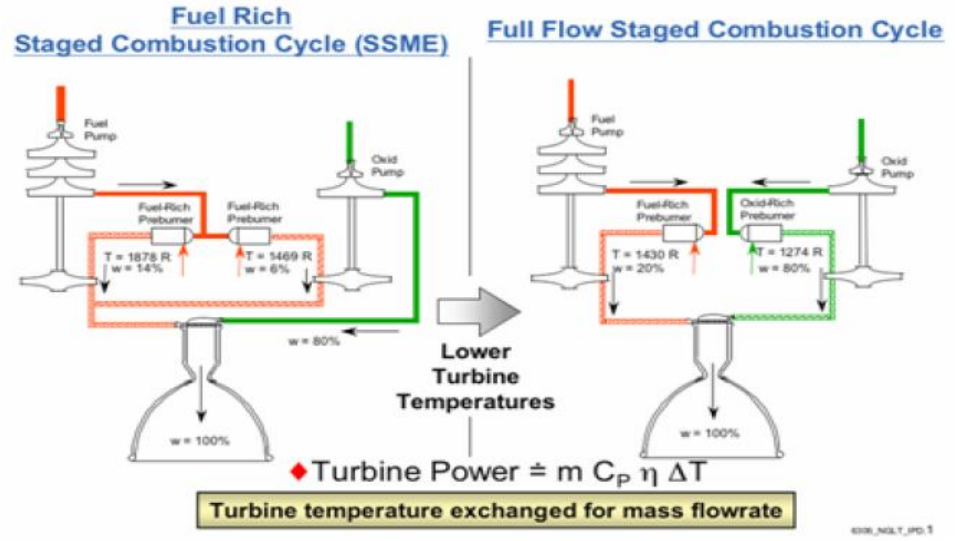

Fig. 37: Staged Combustion Cycle versus Full Flow Staged Combustion Cycle [51]

4.1.4.2 Vortex engines

In the vortex engine the reaction elements are not injected at the end of the combustion chamber as is the case with all common rocket engines but are injected tangentially to the chamber wall at the level of the nozzle throat. This process is aimed to improve the combustion efficiency as well as to reduce the length of the combustion chamber. After the elements are injected in the combustion chamber, what takes place may be described quite diagrammatically as it follows:

1. The fuel components rotate with a high revolution rate (1500 revolutions per second) on the chamber wall at the level of the nozzle throat.
2. At this point, the fuels absorb the heat flowing from the 'nozzle throat after the injection and before the combustion, whereby the problem of cooling the nozzle is solved.
3. Consequent to vortex theory and the chamber sidening conically to the rear, the reaction partners flow on spiral paths, layered alongside and over each other, as far as the rear wall of the combustion chamber.
4. In this way the fuels become mixed - pressed on to the chamber well by centrifugal acceleration - mechanically in the liquid state.
5. The gases of combustion which are created cannot force their way through the cylindrical part of the vortex owing to principles of vortex theory.
6. The gases of combustion flow in the turbulent boundary layer on the back wall of the chamber using logarithmic spiral paths to the chamber axis.
7. The gases flow along the combustion chamber axis to -the nozzle and there are accelerated to supersonic velocity in a well-known manner.

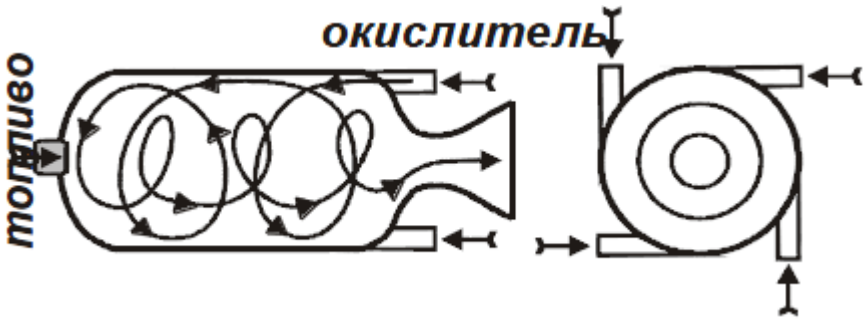

Fig. 38: Counterflow combustion chamber [52]

Chapter 5: Analytical model for gasification system

5.1 Introduction

In this chapter we will study the development of a model that allows us to understand the process of gasification. We will base this model of thermodynamics and heat transfer equations, making some justified assumptions to obtain a model simply enough to solve it in a numerical way, but also able to provide real results so we can relate them to the experimental values.

The following figure will represent a 2-D scheme of the tank of the problem under study:

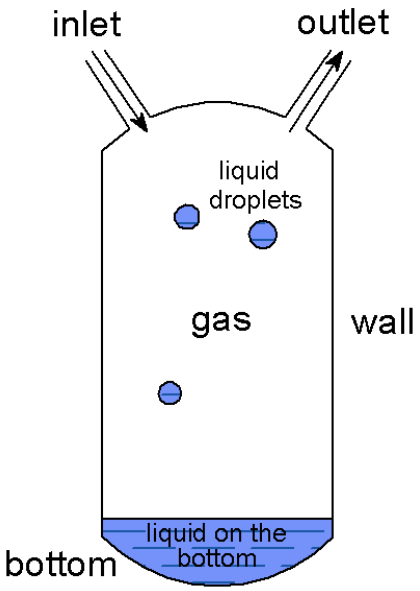

Fig. 39: Propellant tanks preview

We assume that the liquid can be in two situations:

- Liquid in the bottom of the tank
- Liquid in droplets inside the tank.

We also assume that the total amount of propellant (propellant in the bottom of the tank plus droplets) is the 3% of the initial propellant, as we have already explained. We also assume spherical symmetry for the droplets.

We will study the fluid inside the tank as three separated parts: gas, liquid in droplets and liquid in the bottom. Each part will have its own control volume. We will also

separate the wall into two parts: the part in contact with the gas, and the part in contact with the liquid in the bottom. We will consider both parts have the same temperature, what will lead to an error as we will discuss later.

5.2 Theoretical background

As we said before, we will divide the inside of the tank into three subdomains: the gaseous part, the liquid part on the bottom and nonspecific number of liquid droplets, *n*. We will consider a **zero-dimensional model** (the fluid has the same properties in all its extension) for each part of study. The equilibrium equation at the wall will finally close the problem.

The model is based on the principles of thermodynamics and heat transfer [53][54][55][56]. If we apply the first principle of thermodynamics, we can write the energy equation as:

$$\dot{E}_{st} = \dot{E}_{in} - \dot{E}_{out} + \dot{E}_g$$

where:

- $\dot{E}_{st}$ is the total energy stored in the system.
- $\dot{E}_{in}$ and $\dot{E}_{out}$ are the inflow and outflow terms, respectively.
- $\dot{E}_g$ is the term related to thermal and mechanical generation.

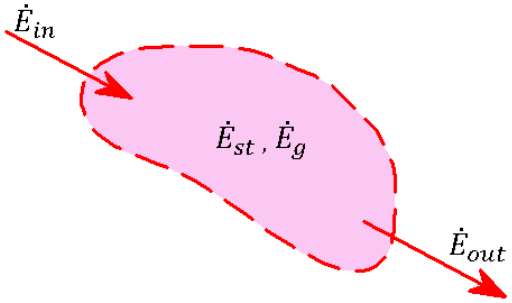

Fig. 40: Scheme of a control volume

If we develop the previous equation taking into consideration all the terms involved, including the kinetic and potential energy, we will have the following expression:

$$\dot{E}_{st} = \dot{Q} - \dot{W} + \dot{m}_i(u_i + \frac{{v_i}^2}{2} + gz_i) + \dot{m}_e(u_e + \frac{{v_e}^2}{2} + gz_e)$$

The work can be divided into two contributions: one is the work associated with the fluid pressure as mass is introduced at inlets and removed at exits. The other contribution, denoted $\dot{W}_e$, includes all other work effects.

$$\dot{W} = \dot{W}_e + \dot{m}_e(p_e v_e) - \dot{m}_i(p_i v_i)$$

where v_i and v_e are the specific volumes evaluated at the inlet and the outlet respectively.

If we don't consider the potential energy terms, and we assume that all the work in the system is the one associated with the mass fluxes, the final expression will be:

$$\dot{E}_{st} = \sum \dot{Q} + \dot{m}_i \left(u_i + \frac{{v_i}^2}{2} + p_i v_i \right) + \dot{m}_e \left(u_e + \frac{{v_e}^2}{2} + p_e v_e \right)$$
$$= \sum \dot{Q} + m_i h_{0_i} + m_e h_{0_e}$$

5.2.1Heat transfer equations

5.2.1.1 Convection

Convection heat transfer is the energy transfer process which occurs between a fluid in motion and a bounding surface when the two are at different temperatures. Convection heat transfer may be classified according to the nature of the flow. We speak of forced convection when the flow is caused by external means, such as by a fan, a pump, or atmospheric winds. In contrast, for free (or natural) convection, the flow is induced by buoyancy forces, which are due to density differences caused by temperature variations in the fluid.

Regardless of the nature of the convection heat transfer process, the appropriate rate equation is of the form:

$$q_{conv} = A \cdot h \cdot (T_s - T_\infty)$$

where A is the area of contact, h (W/m^{2}K) is the heat transfer coefficient, T_s is the temperature of the surface and T_∞ the temperature of the fluid.

The heat transfer coefficient depends on conditions in the boundary layer, which are influenced by surface geometry, the nature of the fluid motion, and an assortment of fluid thermodynamic and transport properties.

5.2.1.2 Radiation

Thermal Radiation is the energy emitted by one body when the body is at a finite temperature. The intensity of such energy depends upon the temperature of the body and the nature of its surface. Thermal radiation occurs in a range of the electromagnetic spectrum of energy emission.

In all cases, we assume that the emittance and absorbtance are diffuse, so their values do not depend on the incidence angles. Finally, we will consider that the solid and liquid parts are opaque and the gas phase does not reflect any wavelength (just absorption and transmission).

In case we cannot consider diffuse surfaces, other methods can be applied. Among them, the Monte Carlo technique is probably the most widely used. The Monte Carlo technique tracks emissions and reflections through various angles among the surfaces and estimates the probability of absorption or reflection [57].

The typical expression for the radiation balance for each subsystem will be:

$$q_{rad} = E - \alpha \cdot G$$

where E is the energy emitted by the subsystem, α the absorptivity coefficient and G the incident radiation.

Solid and liquid radiation

We will assume that the walls and liquid act as gray bodies, that is, the emissivity ε is independent of the wavelength (λ). No real body is a gray body, but many bodies can be approximated as a gray one. With gases, as we will see later, we cannot apply this because gases just participate in the radiation exchange in a very narrow specter of light.

In the case of radiation exchange between two surfaces we will have a net flux, seen from observer "1", equal to:

$$q_{net} = A_1 \cdot F_{1-2} \cdot (\varepsilon_1 \cdot {T_1}^4 - \alpha_2 \cdot {T_2}^4)$$

Gas radiation

Gas radiation is more complicated than liquid or solid ones. In the other two cases, you can model the radiation as a surface phenomenon, but in gases all the fluid can interact with photons to some extent. This effect is generally very small, especially in air and if the distance between surfaces is small (meters or less).

The scattering is usually very small (except when the gas contains foreign particles), so we will focus on absorption an emission. Molecular structure determines how a molecule absorbs and emits energy. For practical purposes, monoatomic and symmetrical diatomic molecules are transparent to thermal radiation. In the other hand, asymmetrical molecules absorb thermal radiation of certain wavelengths.

Predicting the total emittance of a gas layer can be complex. We have to take account of the gases' absorption bands as well as the layer's thickness and density. For making simples (but less accurate) estimates, correlations of ε_g have been developed [58]. A simpler but cruder method is the use of total emittance charts.

The tests developed during the preliminary simulations proved that the contribution of gas radiation was negligible (around 2% of variation of the main parameters of the system: time and energy employed). Calculations have been made using total emittance charts.

5.3 Model equations

5.3.1 Gas phase

We will study the gas phase as a mixture of non-reacting gases in a non-steady state. We have an initial amount of a mixture of gases (propellant and pressurization gas) at initial temperature T_0 and pressure P_0. Once we start the process, we add to the control volume a flux of gas coming from the gas generator and, when the vaporization begins, another flux due to the vaporization of liquid propellant; that two fluxes will change the composition of the gas inside the tank, so its properties will also change. There is also an outlet flux of gas discharging from the tank to the gas generator. To close the problem we will have the heat fluxes corresponding to the interaction between the gas phase and each subpart of the system: liquid on the bottom, liquid droplets, and tank walls.

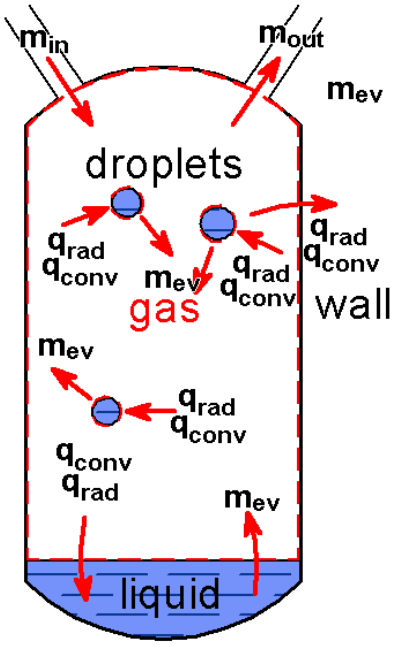

Fig. 41: Representation of the fluxes applied on the gas phase

The equation corresponding to the gas part is:

$$\frac{dE_{gas}}{dt} = \dot{H}_{0_{in}} - \dot{H}_{0_{out}} + \dot{H}_{ev} - q_{conv_{g-l}} - q_{conv_{g-w}} - \sum_{i=1}^{n} q_{conv_{g-d_i}} - q_{rad_g}$$

Where:

- E_{gas} is the energy stored in the gas phase at the instant of time under study.
- $\dot{H}_{0_{in}}$ and $\dot{H}_{0_{out}}$ are the inflow and outflow enthalpy terms.

- $\dot{H}_{ev}$ is the inflow term due to the liquid evaporation, that's it, the energy that is added by the liquid that becomes gas and enters the gas phase.
- $q_{conv_{g-l}}$ is the convection heat flux due to the interaction between the gas phase and the liquid in the bottom of the tank.

$$q_{conv_{g-l}} = h_{g-l} \cdot A_{g-l}(T_{gas} - T_{liq})$$

h_{g-l} is the heat transfer coefficient between gas and liquid (W/m^2·K), A_{g-l} is the area of the interface between gas and liquid in the bottom, T_{gas} is the temperature of the gas mixture inside the tank (K) and T_{liq} is the temperature of the liquid phase.

- $q_{conv_{g-w}}$ is the convection heat flux due to the interaction between the gas phase and the tank wall

$$q_{conv_{g-w}} = h_{g-w} \cdot A_{g-w}(T_{gas} - T_{wall})$$

being h_{g-w} the heat transfer coefficient between the gas phase and the wall, A_{g-w} is the area of contact between the gas and the wall and T_{wall} is the temperature at the surface of the wall.

- $q_{conv_{g-d_i}}$ is the convection heat flux between the gas phase and the *i* droplet of liquid

$$q_{conv_{g-d_i}} = h_{g-d} \cdot A_{d_i}(T_{gas} - T_{d_i})$$

being h_{g-d} the heat transfer coefficient between the gas phase and the droplet, A_{g-w_i} the area of contact between the gas and the *i* droplet ($A_{d_i} = 4r_i^2$ as we have assumed spherical droplets, being r_i the radius of the droplet) and T_{d_i} is the temperature of the droplet.

- q_{rad_g} is the radiation net flux due to the difference between the radiation energy emmited by the gas and the radiation absorbed coming from the liquid parts and the tank.

$$q_{rad_g} = \varepsilon_{gas} A_{gas} \sigma {T_{gas}}^4 - \alpha_{gas} \sigma ({A_{g-l}} {T_{liq}}^4 + A_{g-w} {T_{wall}}^4 + \sum A_{d_i} {T_{d_i}}^4)$$

where ε_{gas} is the emissivity of the gas, α_{gas} its absorptivity, A_{gas} the total surface of the gas and σ the Stefan-Boltzmann constant.

As we have explained before, we can consider that the gas does not participate in the process without adding a big error to the system.

5.3.2 Liquid phase

5.3.2.1 Bottom

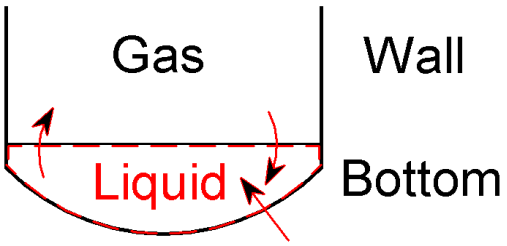

Fig. 42: Representation of the fluxes applied on the liquid phase

$$\frac{dE_{liq}}{dt} = q_{conv_{g-l}} + q_{conv_{bw-l}} - q_{rad_l} - q_{ev_l}$$

where:

- E_{liq} is the energy stored in the liquid phase.
- $q_{conv_{g-l}}$ is the convection heat flux between the gas phase and the liquid phase on the bottom of the tank.

$$q_{conv_{g-l}} = h_{g-l} A_{g-l} (T_{gas} - T_{liq})$$

- $q_{conv_{bw-l}}$ is the convection heat flux between liquid phase and the bottom of the tank:

$$q_{conv_{bw-l}} = h_{w-l} A_{l-w} (T_{wall} - T_{liq})$$

being A_{l-w} the area of contact between the liquid and the wall, that is it, the area of the bottom of the tank.

- q_{rad_l} is the net radiation heat flux exchanged between the liquid in the bottom and the rest of the system.

$$q_{rad_l} = \varepsilon_{liq} A_{liq} \sigma {T_{liq}}^4 - \alpha_{liq} \sigma ({A_{g-l}} {T_{gas}}^4 + {A_{l-w}} {T_{wall}}^4 + (1 - \alpha_{gas}) F_{l-w} A_{g-w} {T_{wall}}^4 + \sum (1 - \alpha_{gas}) F_{l-d} A_{d_i} {T_{d_i}}^4)$$

where ε_{liq} is the emissivity of the liquid, α_{liq} the absorptivity, A_{liq} the total surface of the liquid and σ the Stefan-Boltzmann constant, F_{l-w} the visibility factor between liquid and wall and F_{l-d} the visibility factor between droplets and liquid.

If we consider that the gas does not participate in the radiation exchange, the equation reads:

$$q_{rad_l} = \varepsilon_{liq} A_{liq} \sigma {T_{liq}}^4 - \alpha_{liq} \sigma \left(A_{l-w} {T_{wall}}^4 + F_{l-w} A_{g-w} {T_{wall}}^4 + \sum F_{l-d} A_{d_i} {T_{d_i}}^4 \right)$$

- q_{ev_l} is the heat flux needed to vaporize $\dot{m}_{ev_l}$ kilograms per second of liquid plus the energy lost due to the evaporation mass transfer.

$$q_{ev_l} = \dot{m}_{ev_l} \cdot (\Delta H_{vap} + c_{liq} \cdot T_{ev}) = \dot{H}_{ev}$$

being ΔH_{vap} the heat of vaporization of the liquid (kJ/kg) and $\dot{m}_{ev_l}$ the mass evaporation rate.

5.3.2.2 Liquid droplets

We will develop the mathematical formulas assuming a generic number of droplets (n).

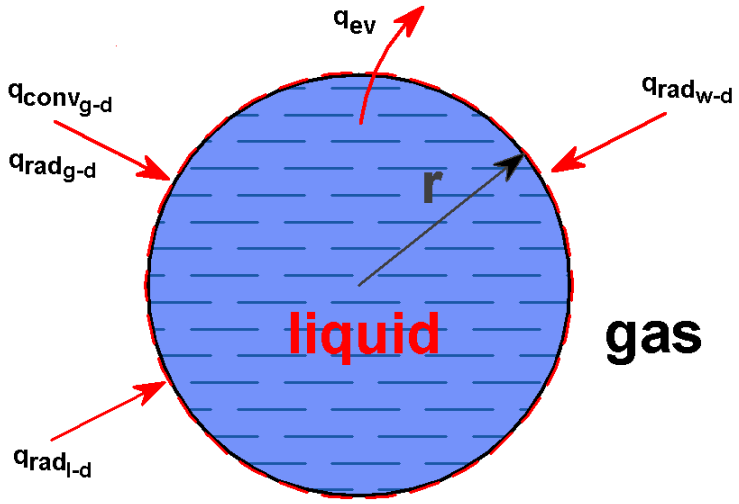

Fig. 43: Representation of the heat fluxes applied on a generic liquid droplet

Each droplet of propellant will add an energy balance equation to our system, so we will have n equations like:

$$\frac{dE_{drop_i}}{dt} = q_{conv_{g-d_i}} - q_{rad_{d_i}} - q_{ev_{d_i}}$$

Where

- E_{drop_i} is the energy stored in the *i* droplet.
- $q_{conv_{g-d_i}}$ is the convection heat flux between the gas phase and the i droplet
- $q_{rad_{d_i}}$ is the net radiation heat flux exchanged between the liquid in the bottom and the rest of the system.

$$q_{rad_{d_i}} = \varepsilon_{liq} A_{d_i} \sigma {T_{d_i}}^4 - \alpha_{liq} \sigma ({A_{d_i}} {T_{gas}}^4 + (1 - \alpha_{gas}) F_{d_i - w} A_{g-w} {T_{wall}}^4 + (1 - \alpha_{gas}) F_{d_i - l} A_{g-l} {T_{liq}}^4)$$

If we do not consider the effect of gas, the equation reads:

$$q_{rad_{d_i}} = \varepsilon_{liq} A_{d_i} \sigma {T_{d_i}}^4 - \alpha_{liq} \sigma (F_{d_i - w} A_{g-w} {T_{wall}}^4 + F_{d_i - l} A_{g-l} {T_{liq}}^4)$$

- $q_{ev_{d_i}}$ is defined like in the precedent case as the heat flux needed to vaporize $\dot{m}_{ev_{d_i}}$ kilograms per second of liquid:

$$q_{ev_{d_i}} = \dot{m}_{ev_{d_i}} \cdot \Delta H_{vap}$$

5.3.2.3 Evaporation model

We will consider two stages of the vaporization process: heating and boiling.

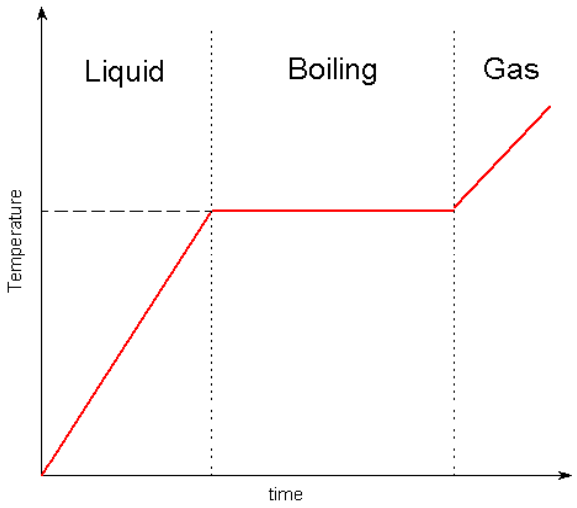

Fig. 44: Heating curve

Heating phase

This stage goes from the initial temperature to the boiling temperature. In this range, we are going to use the Hertz-Knudsen equation to evaluate the evaporation rate [59][60][61].

This model is based on a kinetic approach, assuming a free molecular flow near the droplet surface. The expression of the mass flux from the liquid surface can be written in the following way:

$$j_{lg} = \frac{\dot{m}_{ev}}{Area} = \frac{\beta}{\sqrt{2 \cdot \pi \cdot R_g}} \left(\frac{p_s}{T_s} - \frac{p_\infty}{T_\infty} \right)$$

where $\dot{m}_{ev}$ is the rate of fuel mass loss, $Area$ is the area of the surface where the mass exchange is being considered, β is the evaporation (or condensation) coefficient, R_g is gas constant, T_s is the droplet surface temperature and T_∞ is the gas temperature at large distances from the surface, p_s is the saturated fuel vapor partial pressure corresponding to T_s and p_∞ is the fuel vapor partial pressure at large distances from the liquid surface.

The evaporation coefficient β represents the portion of molecules that hit the interface and change its state. It can be obtained only experimentally.

Boiling phase

Once the liquid has reached its boiling temperature, it starts to boil. Boiling occurs in the full volume of the liquid, and during the whole process temperature keeps constant until the change of phase is finished.

So as temperature keeps constant, we can use the energy equation to evaluate the evaporation mass flux. The expression for the boiling phase will be, for the liquid in the bottom:

$$\frac{dE_{liq}}{dt} = q_{conv_{g-l}} + q_{conv_{b-l}} - q_{rad_l} - q_{ev_l}$$

as

$$\frac{d}{dt}\left(M_{liq}\right) = -\dot{m}_{ev_l}$$

we can obtain the vaporization rate:

$$\dot{m}_{ev_l} = \frac{q_{conv_{g-l}} + q_{conv_{b-l}} - q_{rad_l}}{\Delta H_{vap}}$$

We can operate in a similar way for the liquid droplets, and we will get the expression:

$$\dot{m}_{ev_{d_i}} = \frac{q_{conv_{g-d_i}} - q_{rad_{d_i}}}{\Delta H_{vap}}$$

5.3.3 Tank walls

We will divide the tank walls into two subdomains: the part in contact with the gas phase (from now, we will call it simply "*wall*") and the part on the bottom of the tank (we will call it "*bottom*")

5.3.3.1 Wall

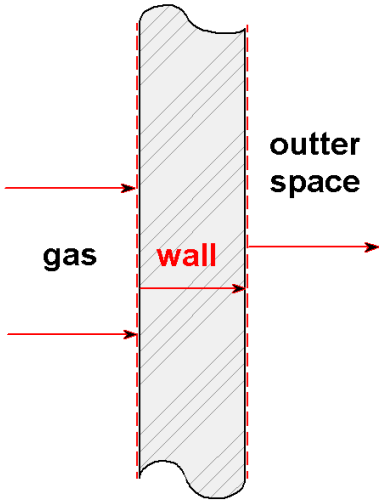

Fig. 45: Heat balance at the wall surface

5.3.3.2 Bottom of the tank

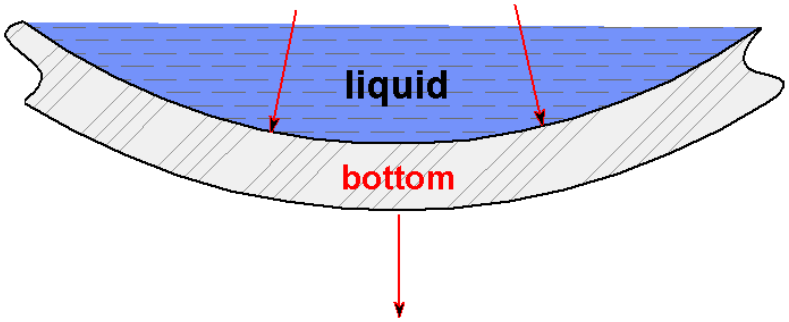

Fig. 46: Heat balance at the bottom of the tank

The problem at the wall is a transient conduction problem. In order to simplify thing, we can consider a lumped capacitance method. The essence of the lumped capacitance method is the assumption that the temperature of the solid is spatially uniform at any instant during the transient process. This assumption implies that temperature gradients within the solid are negligible.

This assumption is proved to be valid when:

$$Bi = \frac{h \cdot s}{k} \ll 1$$

Bi is the Biot number, h the heat transfer coefficient, s the thickness of the wall and k the thermal conductivity. Typically, it is assumed that the error is small if:

$$Bi < 0.1$$

Using this model, the heat balance equation on the wall can be expressed as:

$$\frac{dE_{wall}}{dt} = q_{conv_{g-w}} - q_{conv_{bw-l}} - q_{rad_w} + q_{space}$$

Where

- E_{wall} is the internal energy of the wall. Using the approach that we have used in the other parts we have:

  $$dE_{wall} = \rho_{wall} \cdot V_{wall} \cdot c_{wall} \cdot \frac{dT_{wall}}{dt}$$

  Where ρ_{wall} is the density of the material of walls, in our case it is an aluminum alloy, V_{wall} is the volume of material on the tank walls, c_{wall} is the specific heat of aluminum, and T_{wall} is the temperature at the wall.
- $q_{conv_{g-w}}$ is the convection flux between gas and wall, as it has been defined before.
- $q_{conv_{bw-l}}$ is the convection flux between liquid and wall, as it has been defined before.
- q_{rad_w} is the net radiation heat flux exchanged between the tank walls and the rest of the system.

  $$\begin{aligned} q_{rad_w} &= 2 \cdot \varepsilon_{wall} \cdot \sigma \cdot {T_{wall}}^4 - \alpha_{wall} \cdot \sigma \cdot (A_{g-w} \cdot {T_{gas}}^4 \\ &+ A_{l-w} \cdot {T_{liq}}^4 + (1 - \alpha_{gas}) F_{w-w} A_{g-w} {T_{wall}}^4 \\ &+ (1 - \alpha_{gas}) F_{l-w} A_{g-w} {T_{liq}}^4 \\ &+ \sum (1 - \alpha_{gas}) F_{w-d} A_{d-l} {T_{d_i}}^4) \end{aligned}$$

  If we consider that the gas does not participate in the radiation process, this equation leads to:

  $$\begin{aligned} q_{rad_w} &= 2 \cdot \varepsilon_{wall} \cdot \sigma \cdot {T_{wall}}^4 - \alpha_{wall} \cdot \sigma \cdot (A_{l-w} \cdot {T_{liq}}^4 \\ &+ F_{w-w} A_{g-w} {T_{wall}}^4 + F_{l-w} A_{g-w} {T_{liq}}^4 \\ &+ \sum F_{w-d} A_{d-l} {T_{d_i}}^4) \end{aligned}$$

  where ε_{wall} is the emissivity of the wall, A_{wall} the whole surface of the wall, and α_{wall} the emissivity of the wall. The two factors appear because the wall is irradiating on both surfaces (the inner and the outer). F_{w-w} is the visibility factor between a tank wall and another tank wall.

- q_{space} is the space radiation absorbed by the tanks. We can model it by using any of the available spacecraft system design handbooks. By using one of them [62] we cans split this term into other three:

$$q_{space} = q_{Sun} + q_{albedo} + q_{Earth}$$

where q_{Sun} is the radiation absorbed coming from the Sun, q_{albedo} is the radiation coming from the Sun and reflected by the Earth and q_{Earth} is the radiation coming from the Earth. These values can be calculated using the expressions:

$$q_{Sun} = \alpha_{wall} \cdot A \cdot \frac{P}{4\pi d^2}$$
$$q_{albedo} = \alpha_{wall} \cdot A \cdot J_s \cdot a \cdot F$$
$$q_{Earth} = \alpha_{wall} \cdot A \cdot J_e \frac{R_e}{R_e + R_{orbit}}$$

where A is the area of the tank that is affected by the space radiation, $P = 3.856 \cdot 10^{26}\ W$ is the total power output from the Sun, d is the distance from the Sun to the Spacecraft, J_s is the solar radiation intensity in the Earth's surface, a is the planetary albedo (the fraction of the incident radiation that is reflected), F is a visibility factor depending on the distance between the Earth and the spacecraft and the angle between the local vertical and the Sun's rays (can be found in tables), R_e is the Earth radius and R_{orbit} is the spacecraft's orbit radius. For the calculations we will assume that the spacecraft is in LEO and in the bright side between Earth and Sun.

As we pointed at the beginning of the chapter, we are considering that both parts of the wall are at the same temperature. We must know that this is just a simplification and it is not a real condition, because the different boundary conditions will create a non-uniform distribution of temperatures; this will also lead to a conduction flux from the hottest part to the coldest ones. However, for the sake of simplicity, we consider a uniform temperature at the wall as we have done with the rest of parts of the system. If we wanted to consider non-uniform temperature for the tank walls, as well as for the rest of the parts of the system, we should have used numerical methods based on finite elements, like ANSYS. This study is in the OmSTU agenda and will be performed in a not distant future.

5.4 Properties of the gas

The gas part in the tanks is a mixture of different gases (propellant, helium and products of the gasification system) with a time dependent composition. We will study the properties of the gas taking into consideration the mass fraction of the different species. That's it:

$$x_i = \frac{m_i}{m_{gas}}$$

Where

- m_i is the mass inside the tank of the i-specie.
- $m_{gas} = \sum m_i$ is total mass inside the tank.

As we have explained before, that x_i will change in time, as there is an exchange of matter in the tank (we are adding products of the gas generator and taking gas).

Using the mass fraction, the expressions for the enthalpy and specific heat will be [3]:

$$h = \sum x_i \cdot h_i$$

$$c_v = \sum x_i \cdot c_{v_i}$$

The density of the gas can be obtained as:

$$\rho_{gas} = \frac{M}{V}$$

The pressure can be obtained as the sum of the partial pressures for each species of gas:

$$p = \sum p_i$$

5.4.1 Ideal gases

We are going to assume ideal gas behavior for this study; the partial pressure can be obtained using the state equation for ideal gases, for each species:

$$p_i = \frac{m_i \cdot R_{s_i} \cdot T_{gas}}{V_{gas}}$$

Where R_{s_i} is the specific gas constant for the *i* gas:

$$R_{s_i} = \frac{R}{M_i}$$

About the energetic properties of the gas, the expressions will be:

$$U = \hat{c}_v \cdot n \cdot R \cdot T$$

$$H = \hat{c}_p \cdot n \cdot R \cdot T$$

Where $\hat{c}_v$ is the dimensionless specific heat capacity at constant volume, taking a value around 3/2 for monatomic gas, 5/2 for diatomic gas and 3 for more complex molecules; $\hat{c}_p$ is the dimensionless specific heat capacity at constant pressure.

This assumption is not always suitable. This is because at low pressures and high temperature, real fluids approximate the behavior of a classical ideal gas. However, at lower temperatures or a higher density, a real fluid deviates strongly from the behavior of an ideal gas, particularly as it condenses from a gas into a liquid or as it deposits from a gas into a solid. This deviation is expressed as a compressibility factor.

5.4.2 Real gases

We must notice that ideal the ideal gas behavior hypothesis works well under high temperatures and low pressures. In this case, we are dealing with moderate temperatures, especially at first. This will lead us to some errors.

In case we consider real gases, we will evaluate the pressure inside the tank using the compressibility factor, Z.

$$Z = \frac{V_m}{(V_m)_{ideal\ gas}}$$

so

$$p = \frac{R \cdot T}{V_m} \cdot Z$$

This compressibility factor can be obtained from charts or using the virial expression:

$$Z = 1 + \frac{B(T)}{V_m} + \frac{C(T)}{{V_m}^2} + \frac{D(T)}{{V_m}^3} + \cdots$$

For moderate pressures, the compressibility factor can be approximated as:

$$Z \approx 1 + \frac{B(T)}{V_m}$$

Where the coefficient B is:

$$B = \lim_{(\frac{1}{V} \to 0)} \left(\frac{\partial Z}{\partial \left({}^{1}/_{V}\right)}\right)$$

But can be obtained using some simple correlations.

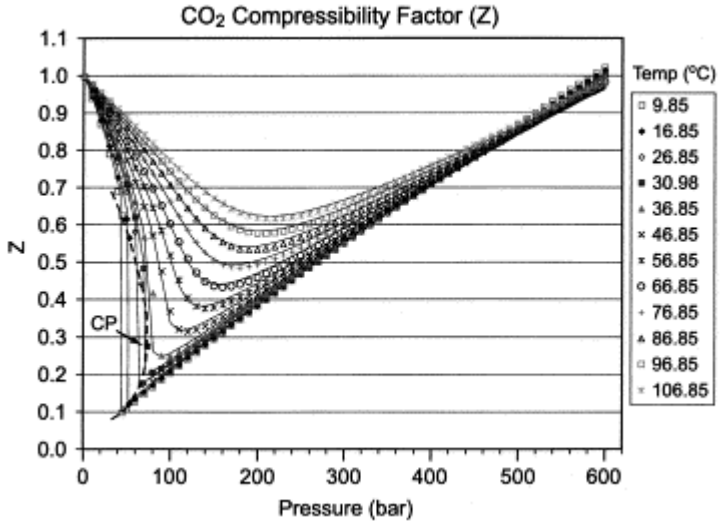

Fig. 47: Compressibility factor table for CO_2 [63]

Also the specific heat capacities must consider the new behavior. Despite all mentioned, this work is focused on the obtaining of a methodology and future modifications can easily added, so ideal gas behavior will be considered from here.

5.5 Initial and working conditions

We will consider the following conditions for the fuel and oxidizer tanks:

Fuel tank	
Initial temperature (K)	280
Initial pressure (MPa)	0.28
Initial mass of propellant (kg)	300
Initial mass of vaporized propellant (kg)	5
Combustion chamber pressure (MPa)	0.405
Relief valve pressure (MPa)	0.425

Table 12: Initial and working conditions for the fuel tank

Oxigen tank	
Initial temperature (K)	90
Initial pressure (MPa)	0.17
Initial mass of propellant (kg)	900
Initial mass of vaporized propellant (kg)	0
Combustion chamber pressure (MPa)	0.405
Relief valve pressure (MPa)	0.425

Table 13: Initial and working conditions for the oxidizer tank

With all we have presented until here, we have all the necessary data and background to develop a model and obtain some results using numerical methods. Some of the results obtained, using *MATLAB®*, will be presented in the next and last chapter. There will be a further discussion about them and a selection of the more acceptable combinations for the gasification system.

Chapter 6: Analytical Results and Conclusions

In this chapter, the final one, we will present some of the final results obtained in the simulations for the RP-1 and LO_2 tanks, taking into consideration several inlet conditions

We advance that main parameters for our study are four: time required for gasification (it should be less than 500 seconds), the energy required for total gasification (the less the better), the mass budget for the gasification system (propellant required plus the weight of its storage tank), and the volume occupied by the gasification system (we must think that this system must be integrated inside existing upper stages).

6.1 Oxidizer tank

For the oxygen tank, we are going to study three boundary conditions:

1. Liquid in the bottom of the tank with cylindrical tank: the bottom and top surfaces are considered plain surfaces. This case needed to be considered because it suits better the experimental installation (see the end of the chapter).
2. Liquid in the bottom with real surfaces: the real tank of Soyuz 2.1b (see appendix 1) is a cylindrical body with two spherical caps in both sides.
3. Liquid in one big drop in the middle of the tank

6.1.1 Liquid in the bottom of the tank with plain surface

For the oxygen tank, we use a monopropellant liquid engine, burning hydrogen peroxide. According to the calculations by *Terra*, the combustion chamber temperature for the mixture under study is 1670 K. Nevertheless, the temperature in the inlet will never achieve this value and will be lower due to losses.

	T=800 K	T=1000 K	T=1200 K	T=1400 K	T=1600 K
0.1 kg/s	2511.06	2014.46	1689.37	1459.55	1288.15
0.2 kg/s	1571.96	1258.75	1055.27	912.13	805.66
0.4 kg/s	1013.8	809.04	677.02	584.54	515.96
0.6 kg/s	796.83	633.52	528.9	455.93	402
0.8 kg/s	676.68	536.14	446.59	384.37	338.49
1 kg/s	598.79	472.93	393.1	337.81	297.17
1.2 kg/s	543.52	428.02	355.06	304.7	267.76

Table 14: Time for gasification (s) versus inlet temperature and mass flow

	T=800 K	T=1000 K	T=1200 K	T=1400 K	T=1600 K
0.1 kg/s	251.106	201.446	168.937	145.955	128.815
0.2 kg/s	314.392	251.75	211.054	182.426	161.132
0.4 kg/s	405.52	323.616	270.808	233.816	206.384
0.6 kg/s	478.098	380.112	317.34	273.558	241.2
0.8 kg/s	541.344	428.912	428.912	307.496	270.792
1 kg/s	598.79	472.93	393.1	337.81	297.17
1.2 kg/s	652.224	513.624	426.072	365.64	321.312

Table 15: Mass required for gasification (kg) versus inlet temperature and mass flow

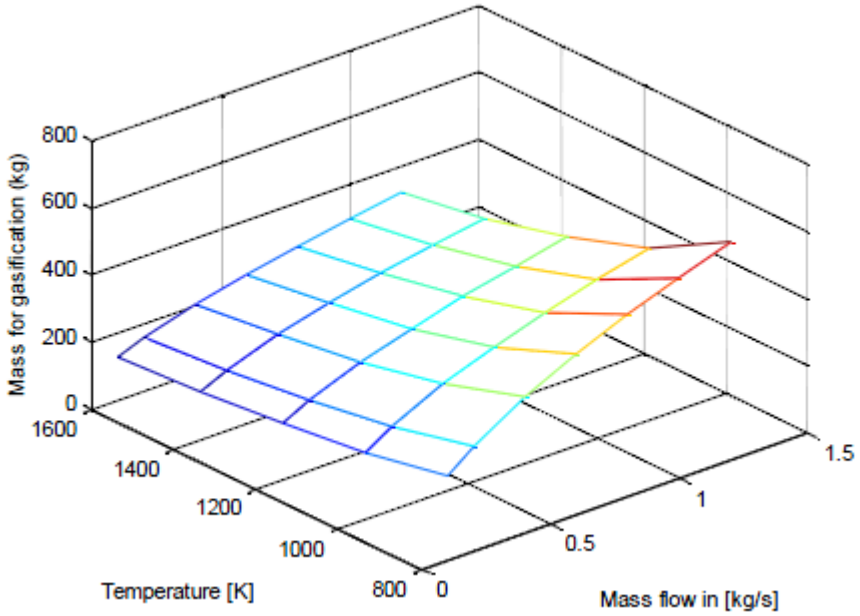

Fig 48: Mass required for gasification (kg) versus inlet temperature and mass flow

	T=800 K	T=1000 K	T=1200 K	T=1400 K	T=1600 K
0.1 kg/s	3.75E+08	3.86E+08	3.98E+08	4.10E+08	4.22E+08
0.2 kg/s	4.69E+08	4.83E+08	4.97E+08	5.13E+08	5.28E+08
0.4 kg/s	6.05E+08	6.20E+08	6.38E+08	6.57E+08	6.76E+08
0.6 kg/s	7.14E+08	7.29E+08	7.48E+08	7.69E+08	7.90E+08
0.8 kg/s	8.08E+08	8.22E+08	8.42E+08	8.64E+08	8.87E+08
1 kg/s	8.94E+08	9.06E+08	9.26E+08	9.49E+08	9.73E+08
1.2 kg/s	9.73E+08	9.84E+08	1.00E+09	1.03E+09	1.05E+09

Table 16: Total energy required (J) versus inlet temperature and mass flow

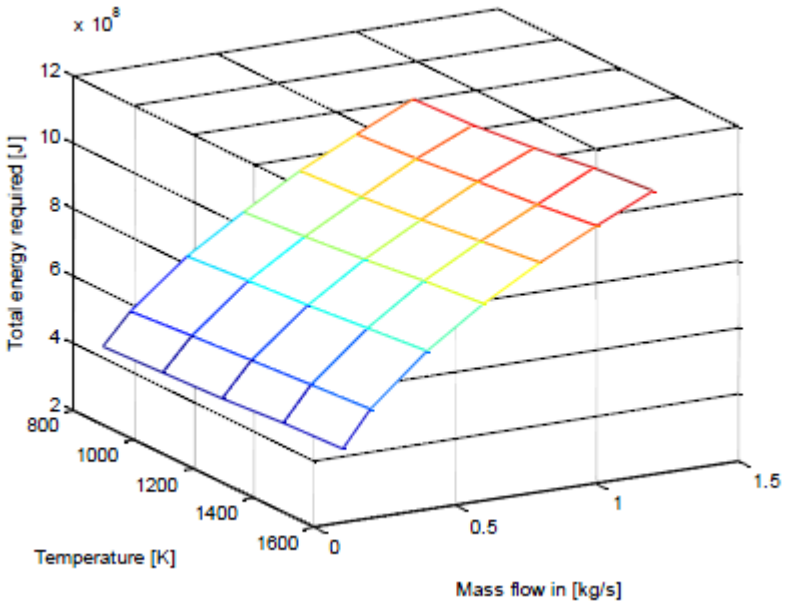

Fig. 49:Total energy required (J) versus inlet temperature and mass flow

	T=800 K	T=1000 K	T=1200 K	T=1400 K	T=1600 K
0.1 kg/s	8.77E+06	7.04E+06	5.90E+06	5.10E+06	4.50E+06
0.2 kg/s	5.49E+06	4.40E+06	3.69E+06	3.19E+06	2.81E+06
0.4 kg/s	3.54E+06	2.83E+06	2.36E+06	2.04E+06	1.80E+06
0.6 kg/s	2.78E+06	2.21E+06	1.85E+06	1.59E+06	1.40E+06
0.8 kg/s	2.36E+06	1.87E+06	1.56E+06	1.34E+06	1.18E+06
1 kg/s	2.09E+06	1.65E+06	1.37E+06	1.18E+06	1.04E+06
1.2 kg/s	1.90E+06	1.49E+06	1.24E+06	1.06E+06	9.35E+05

Table 17: Energy absorbed from space (J) versus inlet temperature and mass flow

As it is obvious, the process is very dependent of the inlet temperature and the mass flow, the bigger they are the less time is required for the process.

6.1.1.1 Influence of inlet temperature

We will start showing the role that inlet temperature plays in gas temperature, liquid temperature, wall temperature, evaporation mass rate and liquid propellant remaining mass. All this figure are the result of a set of simulations with a mass flow in equal to one kilogram per second and a temperature range from 800 K to 1600 K.

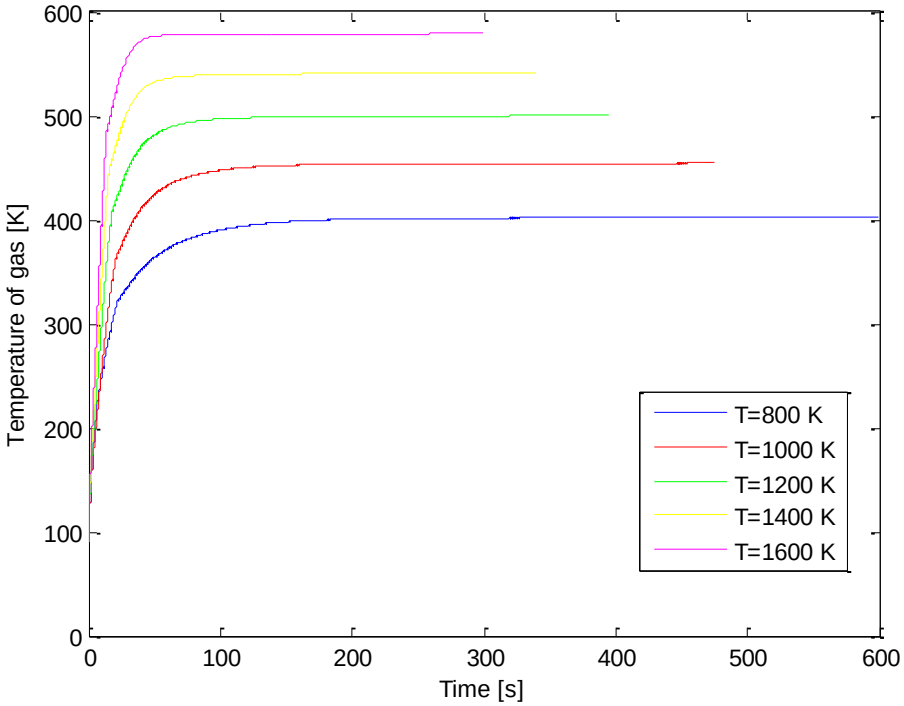

Fig. 50: Influence of the inlet temperature on the temperature of gas

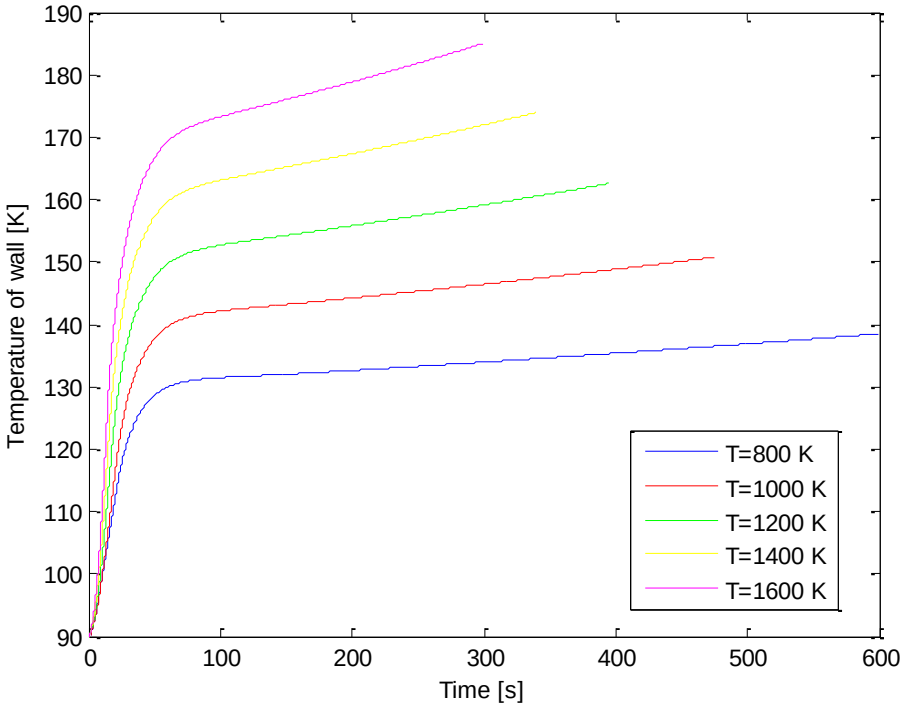

Fig. 51: Influence of the inlet temperature on the temperature of gas

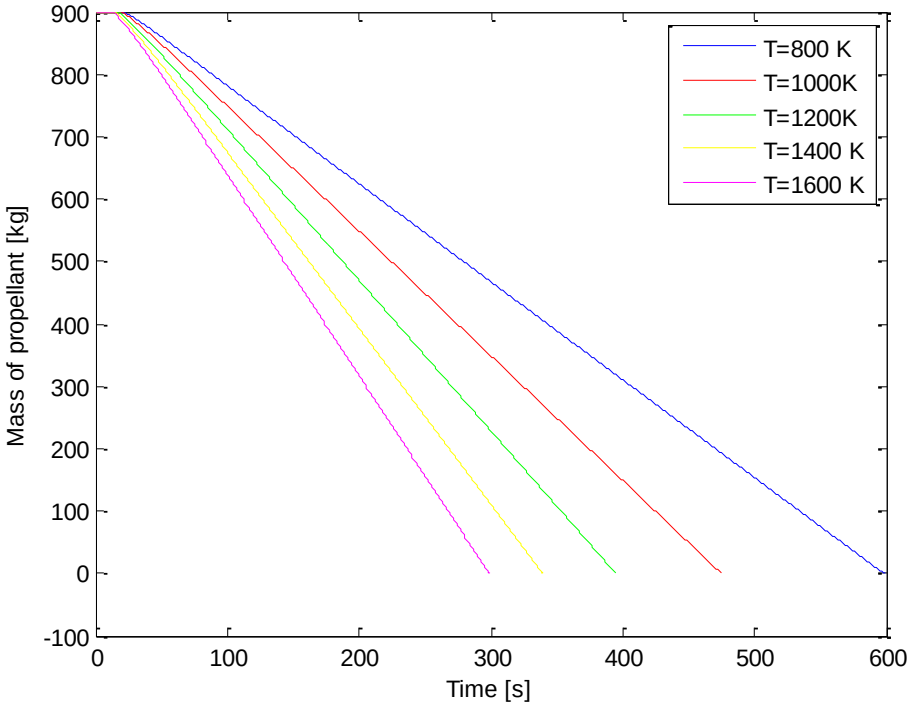

Fig. 52: Influence of the inlet temperature on the mass of propellant

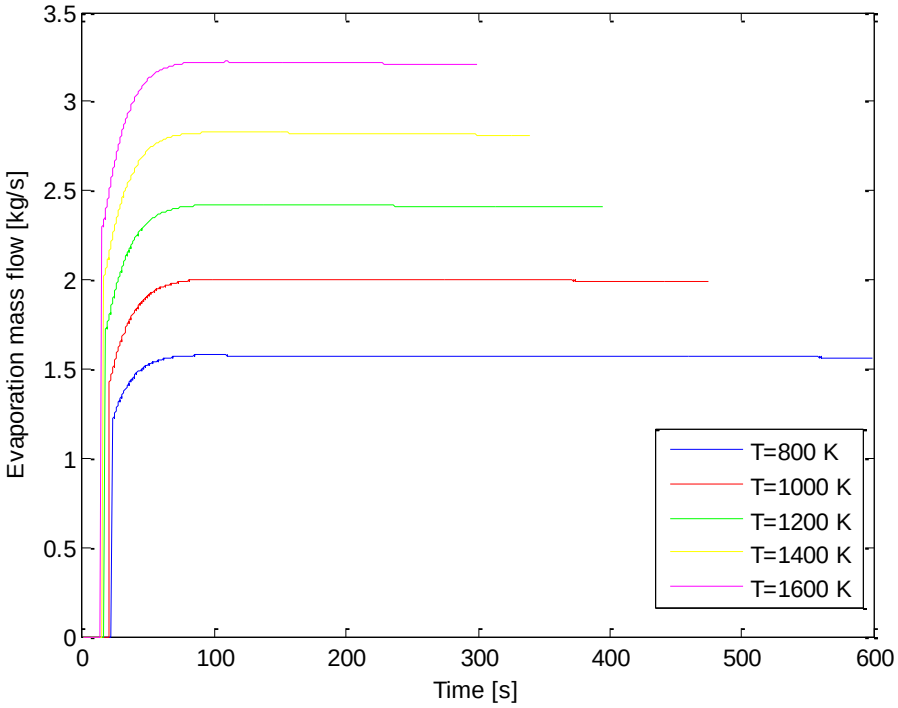

Fig. 53: Influence of the inlet temperature in the evaporation mass flow

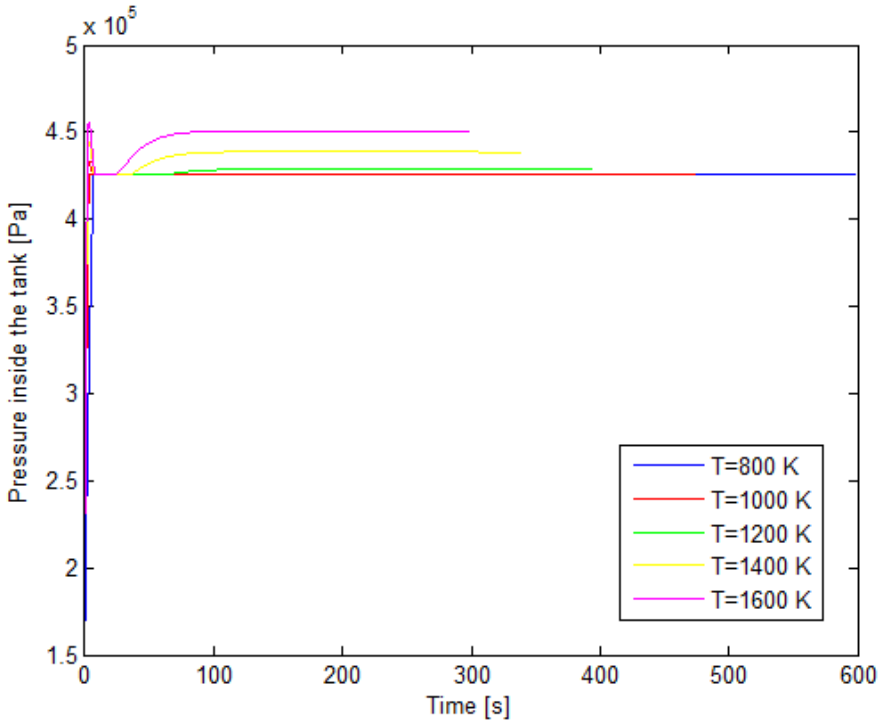

Fig.54: Influence of the inlet temperature in tank pressure

6.1.1.2 Influence of the mass flow in

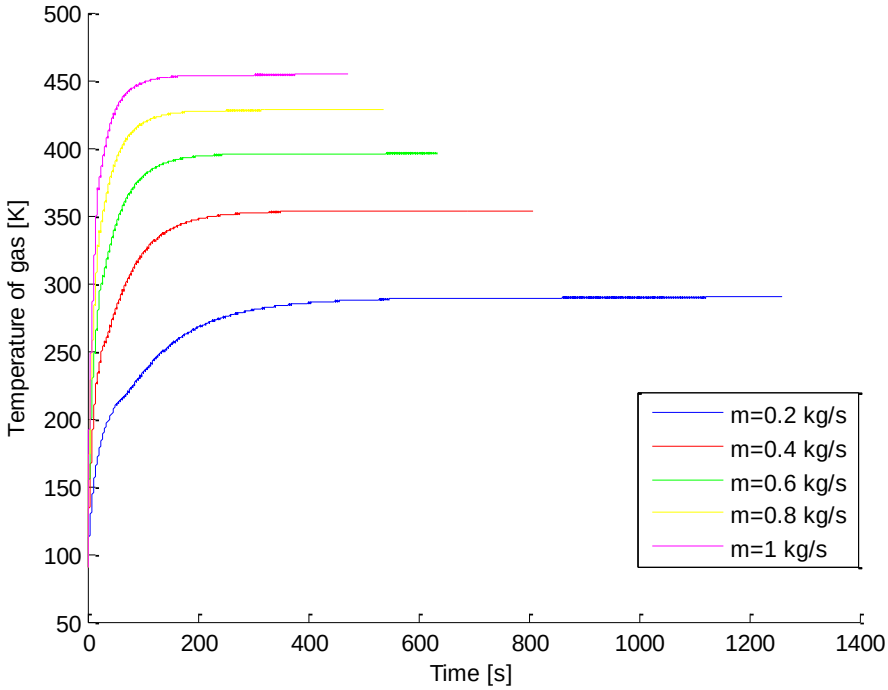

Fig. 55: Influence on inlet mass flow on tank pressure

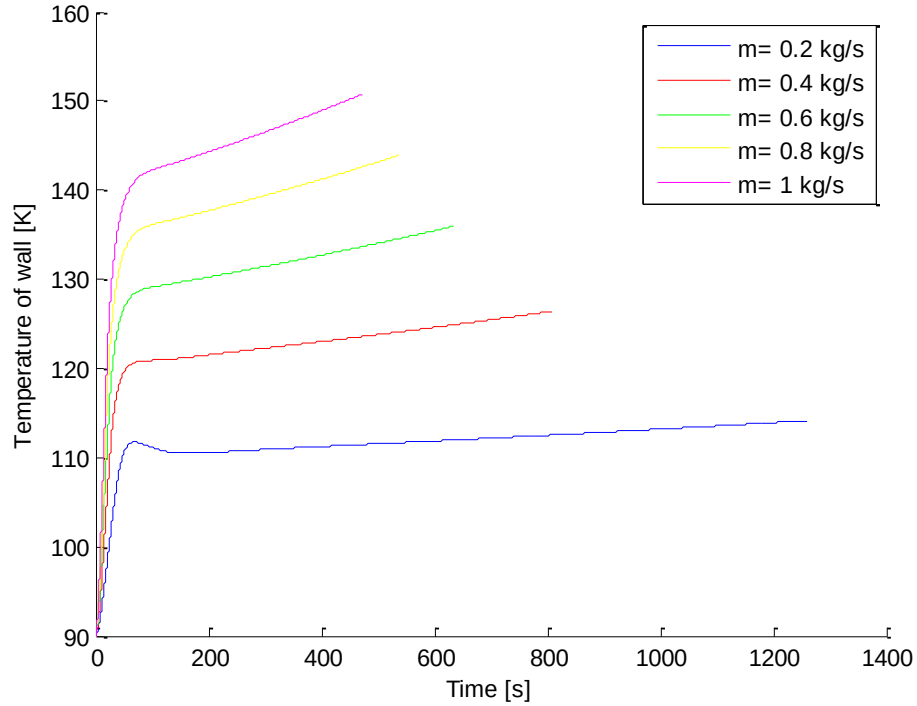

Fig. 56: Influence of inlet mass flow on wall temperature

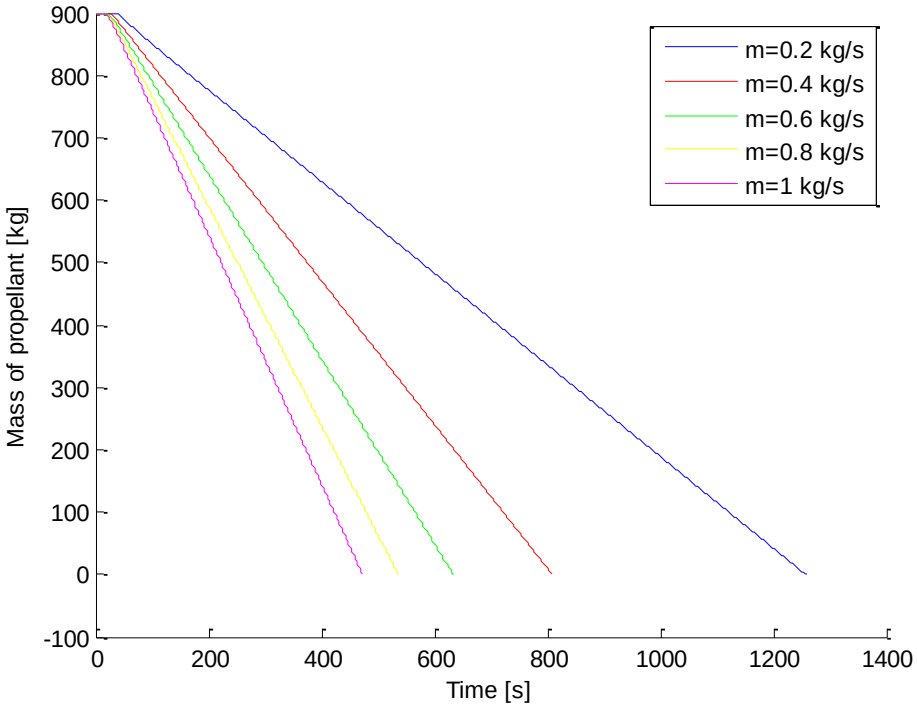

Fig. 57: Influence of inlet mass flow on mass of propellant

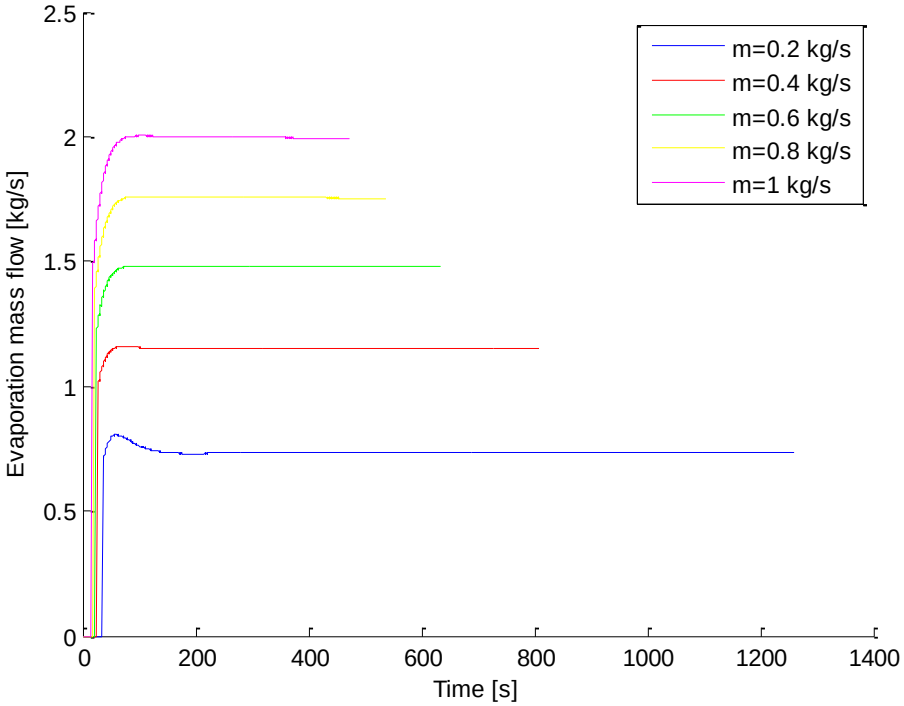

Fig. 58: Influence of inlet mass flow on evaporation mass flow rate

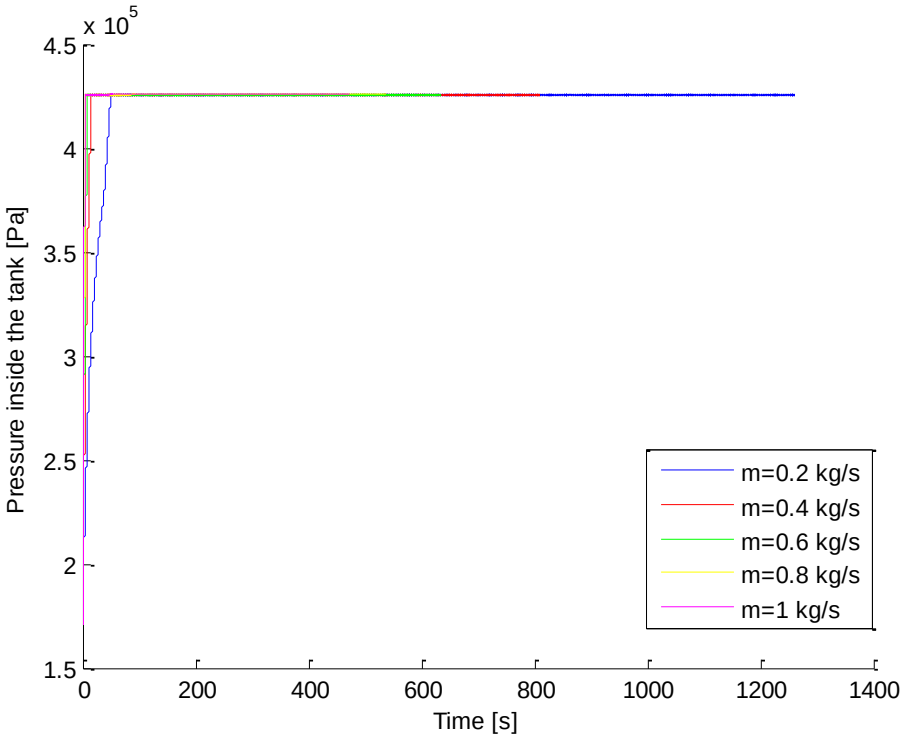

Fig. 59: Influence of inlet mass flow on tank pressure

6.1.2 Liquid in the bottom of the tank with real surface

	T=800 K	T=1000 K	T=1200 K	T=1400 K	T=1600 K
0.1 kg/s	3270.11	2662.03	2260.67	1974.75	1759.96
0.2 kg/s	2168.32	1759.96	1495.79	1306.63	1164.7
0.4 kg/s	1491.15	1206.12	1020.53	889.32	791.17
0.6 kg/s	1220.38	982.45	828.41	719.92	638.96
0.8 kg/s	1068.25	856.26	719.65	623.73	552.32
1 kg/s	968.72	773.42	648.05	560.28	495.1
1.2 kg/s	897.64	714.08	596.65	514.67	453.89

Table 18: Time for gasification (s) versus inlet temperature and mass flow

As we can see, in this case the time required for gasification will be much higher, as well the energy will be. We can understand this better if we give a look the evaporation mass flow representation:

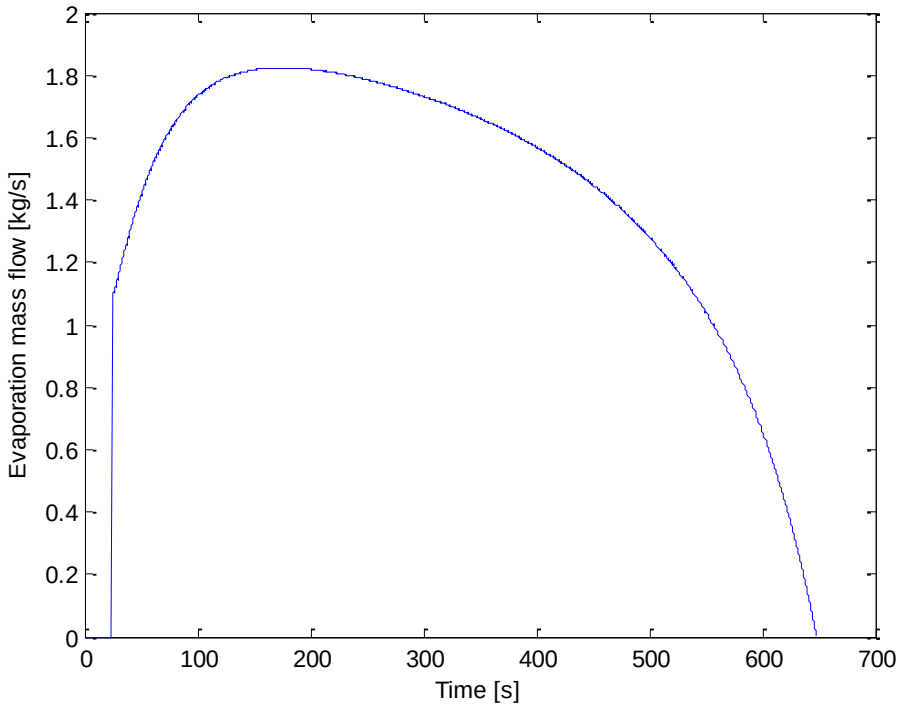

Fig. 60: Evaporation mass flow for real bottom surface

This difference of behavior lies on the different shape considered for the bottom. In the plain surface case (OmSTU's experimental case), the exchange surface keeps constant, so it allows a good heat exchange during the entire process. In the other hand, the spherical cap considered in the real case makes the exchange surface to decrease during the process, so the net heat added to the liquid will also decrease. We can see it better in the following figure:

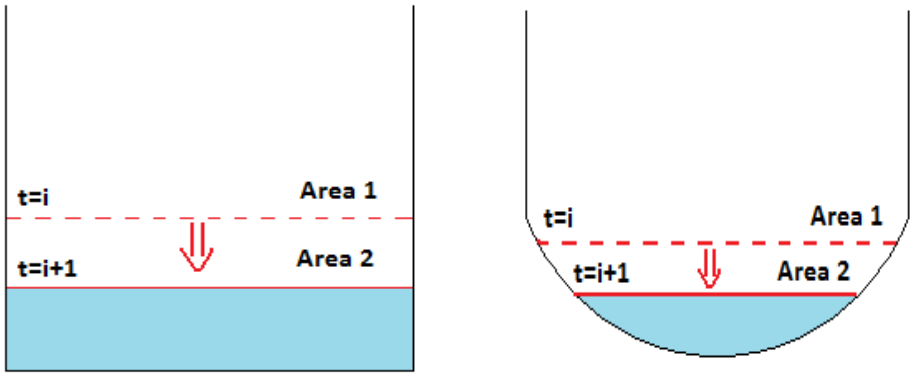

Fig. 61: Comparison between plain surface and real surface

As a result of the augmentation of the time of gasification, the mass required for gasification and the energy will increase.

	T=800 K	T=1000 K	T=1200 K	T=1400 K	T=1600
0.1 kg/s	327.011	266.203	226.067	197.475	175.996
0.2 kg/s	433.664	351.992	299.158	261.326	232.94
0.4 kg/s	596.46	482.448	408.212	355.728	316.468
0.6 kg/s	732.228	589.47	497.046	431.952	383.376
0.8 kg/s	854.6	685.008	575.72	498.984	441.856
1 kg/s	968.72	773.42	648.05	560.28	495.1
1.2 kg/s	1077.168	856.896	715.98	617.604	544.668

Table 19: Mass required for gasification (kg) versus inlet temperature and mass flow

The evolution of the parameters with temperature and mass flow in will be similar to the one seen in the precedent case. However, the shape of the curves will be slightly different as a result of the new boundary conditions. We are not going to see them, because we will do it later for the kerosene, taking into consideration the same condition (real surface in the bottom of the tank).

6.1.3 Liquid floating in the tank forming one big droplet

We are going to consider that the liquid constitutes a big drop placed in the center of the tank, levitating due to the effect of weightlessness. As we can imagine, this case will be similar to the precedent one, as the surface of the liquid will also change in time, reducing the heat exchange fluxes.

	T=800 K	T=1000 K	T=1200 K	T=1400 K	T=1600 K
0.1 kg/s	8449.36	6574.26	5394.54	4582.46	3988.14
0.2 kg/s	5932.31	4501.4	3627.96	3039.89	2616.83
0.4 kg/s	4332.33	3184.1	2506.72	2062.61	1749.84
0.6 kg/s	3687.18	2650.82	2052.28	1666.65	1399
0.8 kg/s	3326.21	2351.04	1796.25	1443.46	1201.35
1 kg/s	3091.79	2155.44	1628.85	1297.4	1071.99
1.2 kg/s	2925.77	2016.34	1509.5	1193.16	979.64

Table 20: Time for gasification (s) versus inlet temperature and mass flow

In this case, times of gasification are even larger than in the real surface case. This is because the volume versus area rate is bigger in this case than in the precedent one that is, the surface is shorter for the same mass in the case of the spherical drop. Once again, we can obtain a picture of the evaporation rate evolution from the simulations:

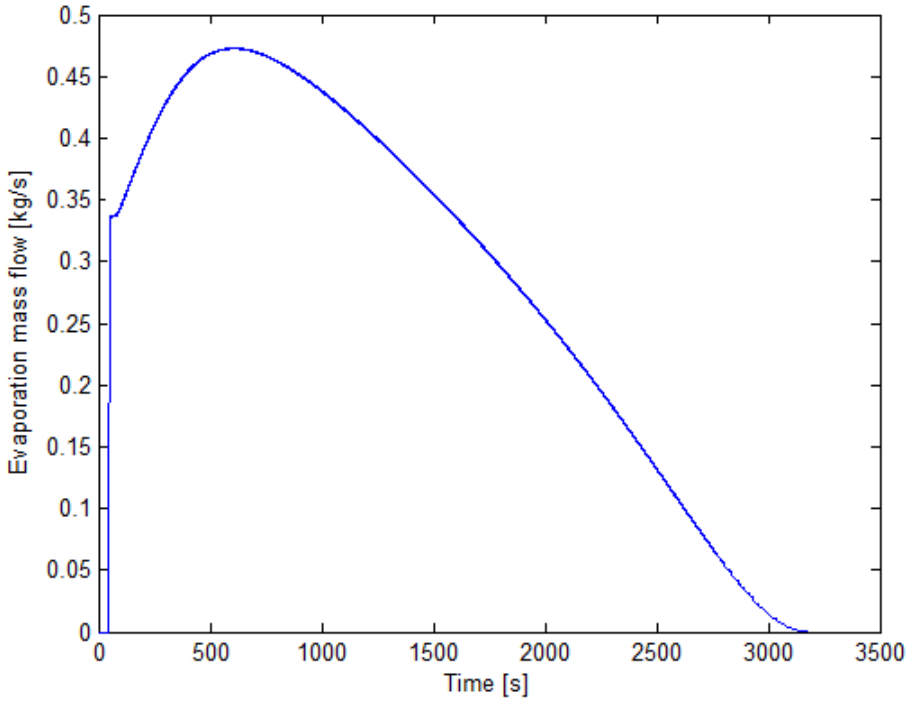

Fig. 62: Evaporation mass flow for one droplet

	T=800 K	T=1000 K	T=1200 K	T=1400 K	T=1600 K
0.1 kg/s	8449.36	6574.26	5394.54	4582.46	3988.14
0.2 kg/s	5932.31	4501.4	3627.96	3039.89	2616.83
0.4 kg/s	4332.33	3184.1	2506.72	2062.61	1749.84
0.6 kg/s	3687.18	2650.82	2052.28	1666.65	1399
0.8 kg/s	3326.21	2351.04	1796.25	1443.46	1201.35
1 kg/s	3091.79	2155.44	1628.85	1297.4	1071.99
1.2 kg/s	2925.77	2016.34	1509.5	1193.16	979.64

Table 21: Mass required for gasification (kg) versus inlet temperature and mass flow

In the next figure, we are going to see a representation of the influence of the number of droplets in the time of gasification. This simulation has been done assuming that the total mass doesn't change, but in every case fuel mass is distributed in a diverse number of equally sized drops. As we can infer, as the number of drops increase, the heat exchange surface also grows, increasing the exchange and decreasing the time for the whole process and the energy.

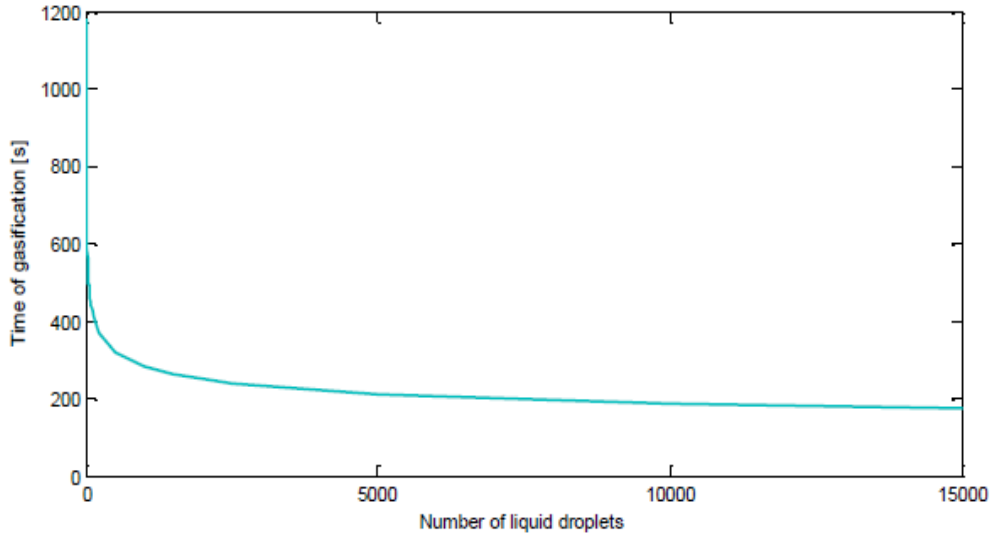

Fig. 63: Time for gasification versus number of droplets

For this simulation, we have simplified the model, not considering the radiation heat exchange for droplets (it would have been and impossible labor and out of the aim of this job). Anyway, the important message we can get from the figure is clear: we have to avoid the formation of big drops inside the tank. After the presentation of these results, some solutions were discussed. The most promising of them, now under study in the OmSTU, is using ultrasounds to break the drop's surface and make the exchange surface wider [64][65].

6.2 Fuel tank

In the case of oxidizer tank, we considered three boundary conditions: plain surface, real surface and liquid drop. To avoid repetition and giving too many data, in the case of RP-1, we are just going to consider two configurations: real tanks and spherical drop in the center of the tank.

6.2.1 Liquid in the bottom of the tank

	T=800 K	T=1000 K	T=1200 K	T=1400 K	T=1600 K
0.1 kg/s	1700.39	1355.34	1136.14	983.64	871
0.2 kg/s	948.21	766.05	649.45	567.86	507.31
0.4 kg/s	558.51	456.88	391.55	345.55	311.2
0.6 kg/s	420.26	345.75	297.74	263.85	238.45
0.8 kg/s	347.11	286.35	247.18	219.48	198.68
1 kg/s	300.94	248.57	214.79	190.91	172.95
1.2 kg/s	268.74	222.02	191.94	170.69	154.75

Table 22: Time for gasification (s) versus inlet temperature and mass flow

	T=800 K	T=1000 K	T=1200 K	T=1400 K	T=1600 K
0.1 kg/s	170.039	135.534	113.614	98.364	87.1
0.2 kg/s	189.642	153.21	129.89	113.572	101.462
0.4 kg/s	223.404	182.752	156.62	138.22	124.48
0.6 kg/s	252.156	207.45	178.644	158.31	143.07
0.8 kg/s	277.688	229.08	197.744	175.584	158.944
1 kg/s	300.94	248.57	214.79	190.91	172.95
1.2 kg/s	322.488	266.424	230.328	204.828	185.7

Table 23: Mass required for gasification (kg) versus inlet temperature and mass flow

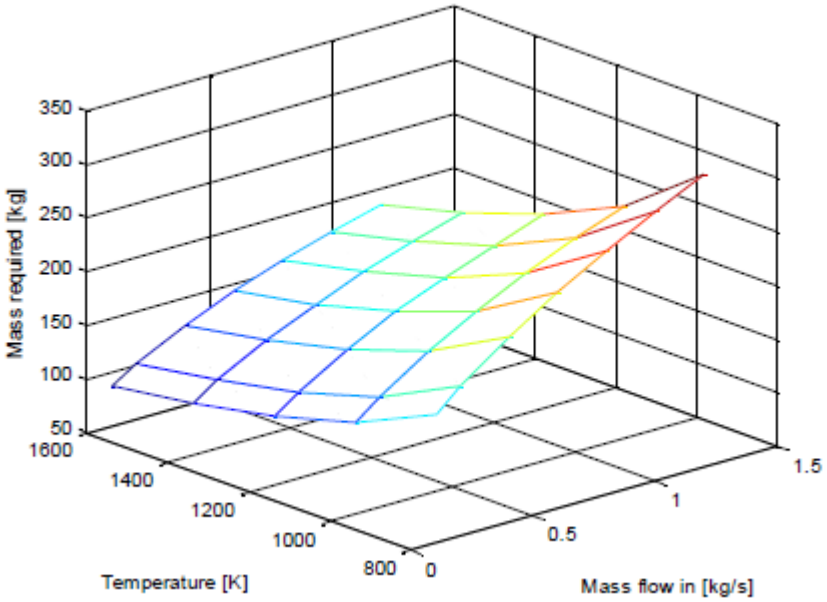

Fig. 64: Mass required for gasification (kg) versus inlet temperature and mass flow

	T=800	T=1000	T=1200	T=1400	T=1600
0.1 kg/s	2.72E+08	2.72E+08	2.73E+08	2.75E+08	2.79E+08
0.2 kg/s	3.03E+08	3.06E+08	3.12E+08	3.18E+08	3.25E+08
0.4 kg/s	3.57E+08	3.66E+08	3.76E+08	3.87E+08	3.98E+08
0.6 kg/s	4.03E+08	4.15E+08	4.29E+08	4.43E+08	4.58E+08
0.8 kg/s	4.44E+08	4.58E+08	4.75E+08	4.92E+08	5.09E+08
1 kg/s	4.82E+08	4.97E+08	5.16E+08	5.35E+08	5.53E+08
1.2 kg/s	5.16E+08	5.33E+08	5.53E+08	5.74E+08	5.94E+08

Table 24: Total energy required (J) versus inlet temperature and mass flow

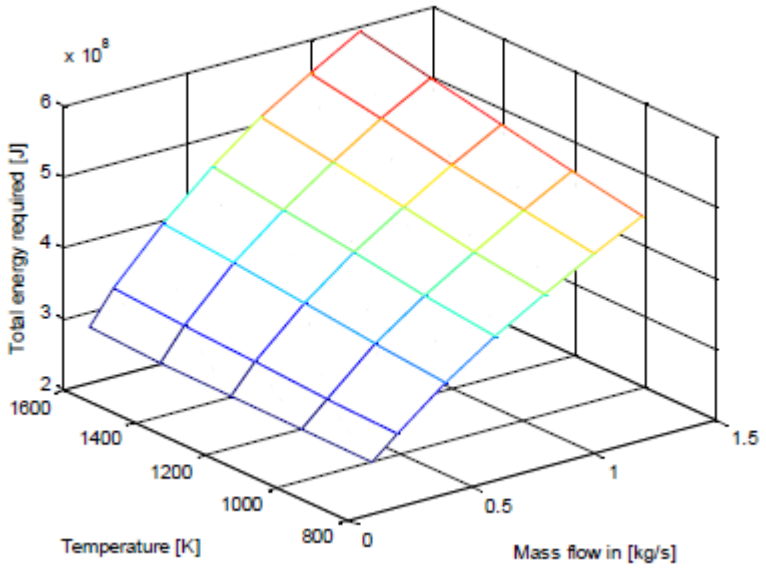

Fig. 65: Total energy required (J) versus inlet temperature and mass flow

	T=800 K	T=1000 K	T=1200 K	T=1400 K	T=1600 K
0.1 kg/s	5.94E+06	4.73E+06	3.97E+06	3.44E+06	3.04E+06
0.2 kg/s	3.31E+06	2.68E+06	2.27E+06	1.98E+06	1.77E+06
0.4 kg/s	1.95E+06	1.60E+06	1.37E+06	1.21E+06	1.09E+06
0.6 kg/s	1.47E+06	1.21E+06	1.04E+06	9.22E+05	8.33E+05
0.8 kg/s	1.21E+06	1.00E+06	8.63E+05	7.67E+05	6.94E+05
1 kg/s	1.05E+06	8.68E+05	7.50E+05	6.67E+05	6.04E+05
1.2 kg/s	9.39E+05	7.75E+05	6.70E+05	5.96E+05	5.40E+05

Table 25: Energy absorbed from space (J) versus inlet temperature and mass flow

6.2.1.1 Influence of inlet temperature

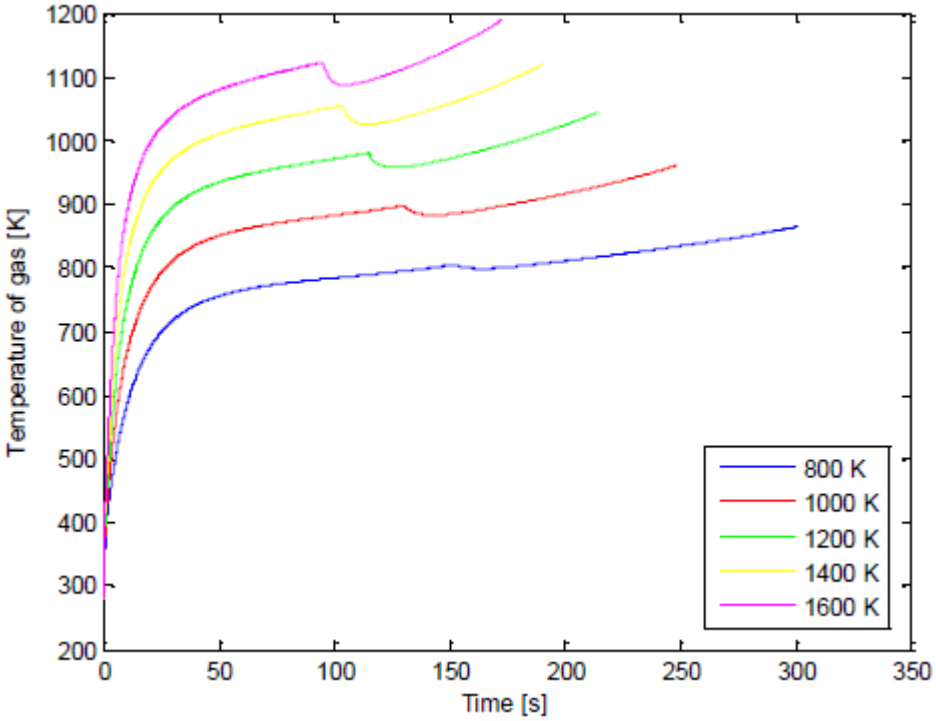

Fig. 66: Influence of the inlet temperature in the temperature of gas

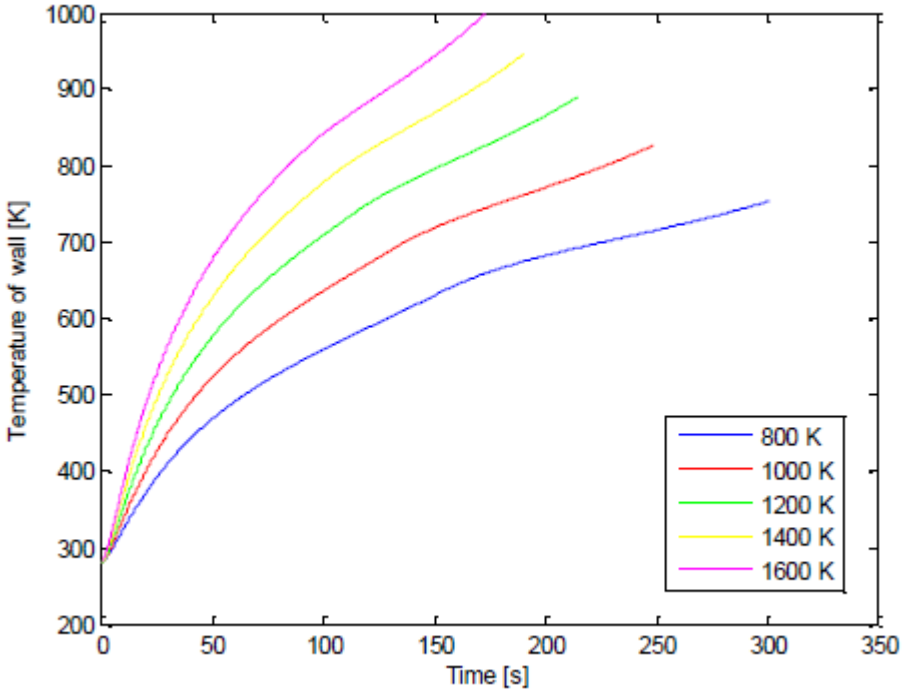

Fig 67: Influence of inlet temperature on wall temperature

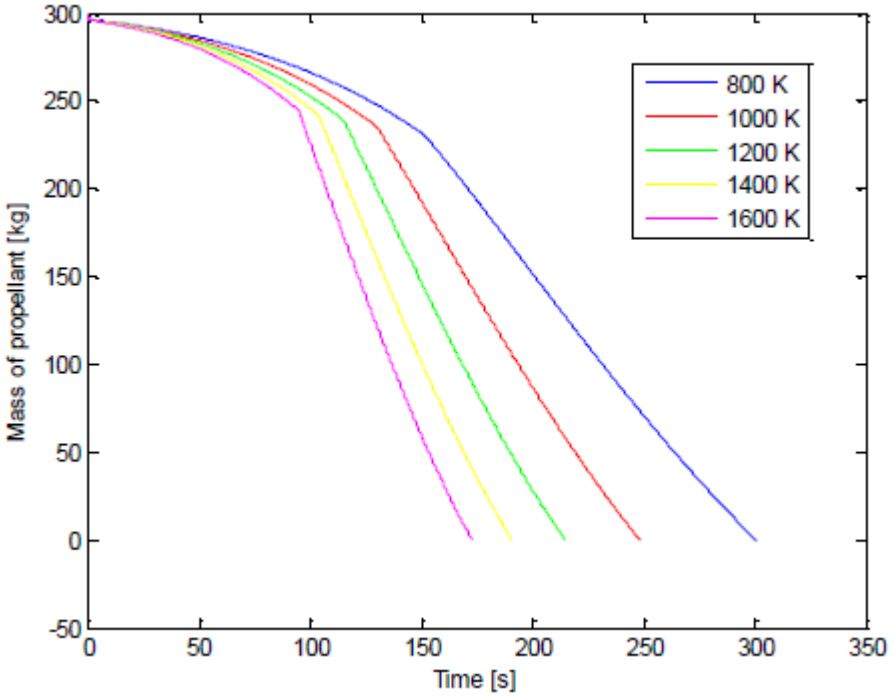

Fig. 68: Influence of inlet temperature on mass of propellant

6.2.1.2 Inlet mass flow influence

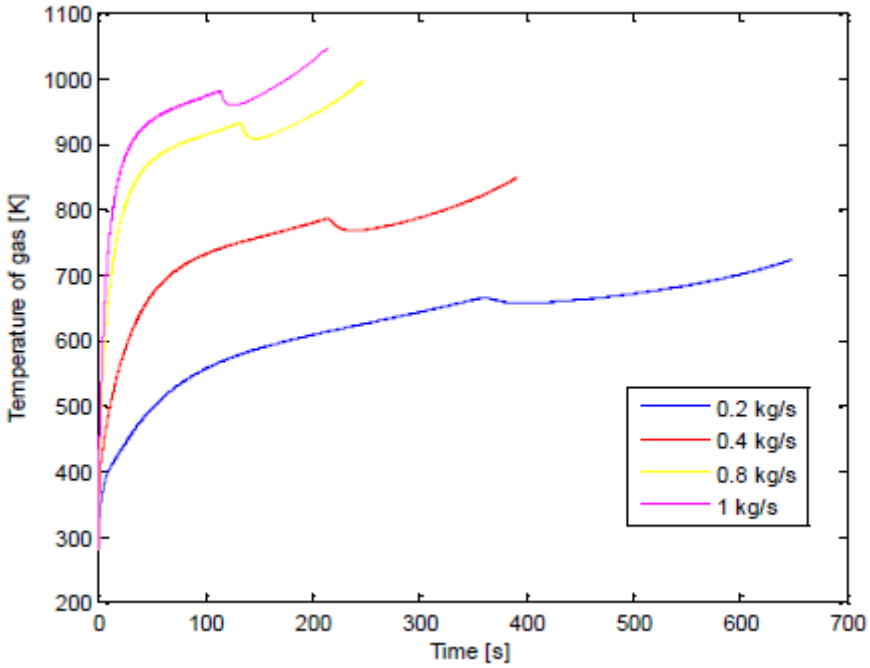

Fig. 69: Influence of inlet mass flow on the temperature of gas

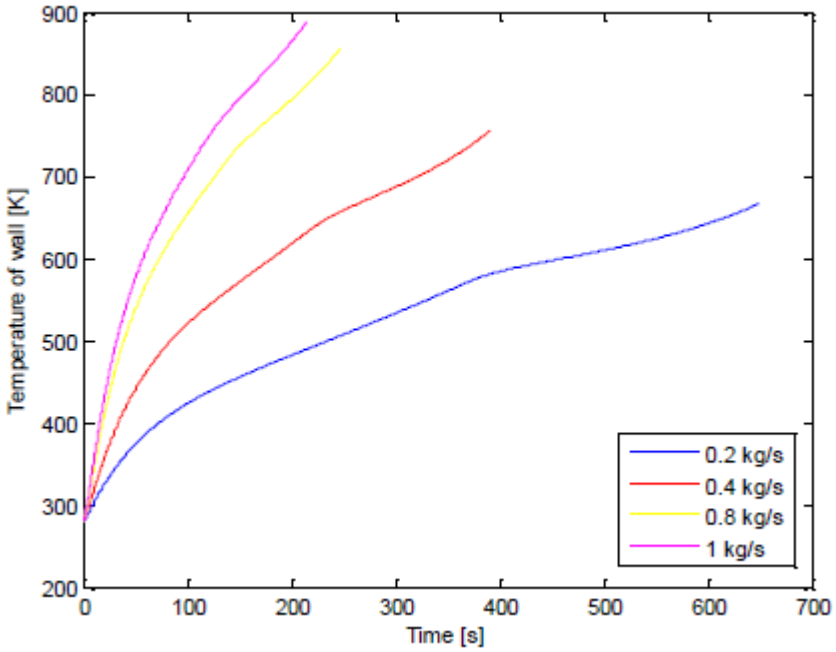

Fig. 70: Influence of inlet mass flow on the temperature of wall

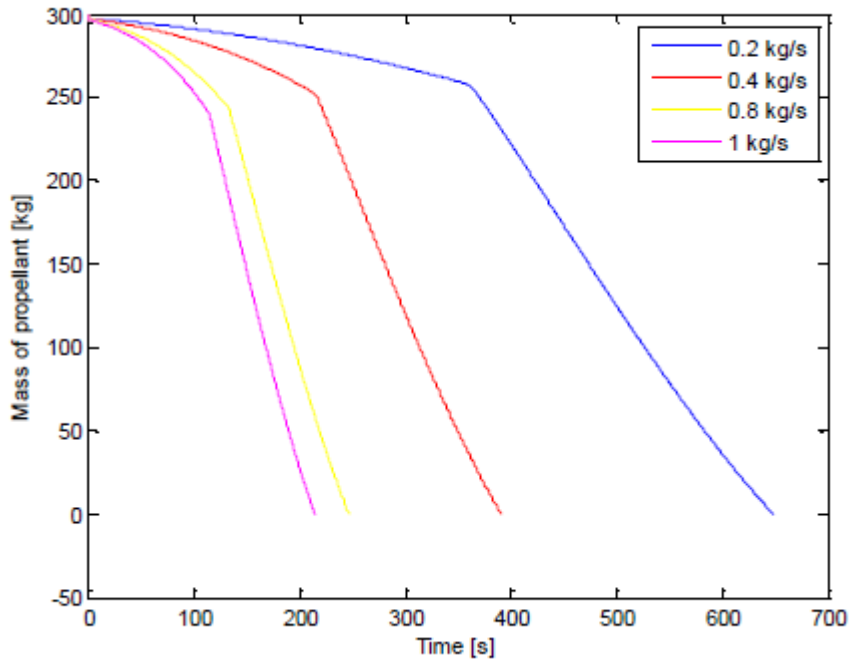

Fig. 71: Influence of inlet mass flow on mass of propellant level

As we can see, the influence of temperature and mass flow is similar to the precedent case. Nevertheless, in this case the transition to boiling is stronger, as we can see in the figures. This is due to the fact that, when the liquid starts boiling, the conditions inside the tank made the evaporation flux to be higher.

6.2.2 Spherical droplet

	T=800 K	T=1000 K	T=1200 K	T=1400 K	T=1600 K
0.1 kg/s	2878.46	2358.06	2018.62	1777.86	1597.21
0.2 kg/s	1732.15	1433.91	1236.42	1094.9	987.77
0.4 kg/s	1056.31	880.51	762.4	676.86	611.65
0.6 kg/s	789.43	660.27	572.6	508.72	459.82
0.8 kg/s	639.79	536.48	465.76	413.99	374.23
1 kg/s	542.01	455.53	395.88	352	318.28
1.2 kg/s	472.42	398.31	346.84	308.82	279.43

Table 26: Time for gasification (s) versus inlet temperature and mass flow

	T=800 K	T=1000 K	T=1200 K	T=1400 K	T=1600 K
0.1 kg/s	287.846	235.806	201.862	177.786	159.721
0.2 kg/s	346.43	286.782	247.284	218.98	197.554
0.4 kg/s	422.524	352.204	304.96	270.744	244.66
0.6 kg/s	473.658	396.162	343.56	305.232	275.892
0.8 kg/s	511.832	429.184	372.608	331.192	299.384
1 kg/s	542.01	455.53	395.88	352	318.28
1.2 kg/s	566.904	477.972	416.208	370.584	335.316

Table 27: Mass required for gasification (kg) versus inlet temperature and mass flow

6.4 Comments

After we have collected all the data from the simulations, we have to choose the best working conditions for the gas generator. When we do the trade-off among all the different options, as we pointed, the parameters of interest are:

- Time required for gasification: It should be as low as possible, necessarily less than 500 seconds for the whole process.
- Mass budget of the overall gasification system: that is, the weight of the propellant plus the tank where it is stored. The lower the better.

- Volume for the tanks: the gasification system should be as reduced as possible, so high density propellants are more suitable.
- There are other considerations, like the temperature or pressure inside the tanks. We assume that the pressure cannot reach any value over 5 atm. As we can see, there is no problem in this field.

6.3.1 Time balance

About the times, we can see that the acceptable region is very narrow, being unacceptable in many cases, especially when the liquid is found forming a big droplet. If we consider the case with the real Soyuz 2.1b tank configuration we can see that to be close to the requirements, high inlet mass flow (more than 1 kg) and Temperatures (more than 1400 K) are required. This can be unacceptable due to tank conditions or mass budget.

For the fuel tank, the region where the time is less than 500 seconds is wider: the times are right even with mass

6.3.2 Mass budget

Once we have a region of possible combinations, we will seek for the lowest mass budget.

- For the oxidizer, as we have no many options, we consider for example1 kg/s and 1600 K as the best option. So the mass required will be:

$$m_{H_2O_2} = 495.1\ kg$$

- In the case of the kerosene tank, as we have considered a time for gasification of around 500 seconds for the oxygen tank, we look the lightest option within this time. One possibility can be to choose 0.2 kg/s and 1600 K. In this case, the propellant mass required will be:

$$m_{prop} = 101.46\ kg$$

But we have a bipropellant mixture, so as we are burning with a oxidizer to fuel ratio equal to 2.35 we will finally have:

$$m_{RP-1} = 30.29\ kg$$
$$m_{Lox} = 71.17\ kg$$

To calculate the volume occupied by the propellant, we just need to divide the total mass of propellant by its density, so it is easy to obtain:

- For the oxidizer tank:

$$V_{H_2O_2} = 0.341\ m^3$$

- For the fuel tank:

$$V_{RP-1} = 0.036\ m^3$$

$$V_{Lox} = 0.062\ m^3$$

We will assume that the tanks are spherical and made from an aluminum alloy. As we already know the density of aluminum we can make some simple calculations, assuming that the thickness is 2 mm:

- For the oxidizer tank

$$m_{tank_{H_2O_2}} = 12.75\ kg$$

- For the fuel tank:

$$m_{tank_{RP-1}} = 2.85\ kg$$

$$m_{tank_{Lox}} = 4.01\ \ kg$$

So we can already calculate the weight of the combination tank plus propellant for the gasification system.

- For the oxidizer tank:

$$m_{system_{H_2O_2}} = 114.21\ kg$$

- For the fuel tank:

$$m_{system_{RP-1}} = 33.14\ kg$$

$$m_{system_{Lox}} = 75.18\ kg$$

6.3.3 Energy balance

About the total energy added to the system, we can split the contribution of the space radiation and the contribution of the energy added through the gas generator (that is, the internal energy of the mixture injected into the tanks:

- Energy absorbed from space≈ 0.2-2%
- Energy added from the gas generator≈ 98-99.8%

The energy used for the heat up and gasification of the liquid is around 20% of the energy added to the tank .The radiation losses to space will be no higher than 5 %.

6.3.4 Sources of error

This thesis is aimed to provide a methodology for futures studies and become a basis for OmSTU's future researches. Many simplifications have been made in order to make calculations as simple as possible:

We considered a zero-dimensional model. The reality is there will be difference of temperatures inside each subsystem (gas phase will be hotter in the vicinity on the injectors, liquid on the surface and walls in the parts in contact with hot gases).

We also assumed that the liquid was in a simplified state. We don't already know the state of the propellant; we have explained that there are solutions applied to these cases (see *3.2.2.4 Ariane 5 ME, the next European SLV*). Unfortunately, these solutions are not for application in our case, as the amount of propellant we have is very small.

We have also considered that the gas behaves as an ideal gas. As explained in the chapter 5, this can lead to some error especially due to the low temperatures considered for the oxidizer tank.

Another source of error can be the simplification of the radiation models. As we discussed when the assumption was made, the gas radiation effect will be very small when compared with the convection and mass transfer contributions. We also considered liquid and solid bodies diffuse and opaque. Anyway, the whole process is mainly driven by the convection heat fluxes, as radiation values are lower.

There is one last aspect to consider: the effect of microgravity in the process. Heat and mass transfer mechanisms are affected by gravity, so the results of our problem will change when the gravitational conditions change. Unfortunately, there is no great knowledge of these mechanisms under microgravity, so we can only have a general idea of how our system will behave [66]. Radiation and conduction is not governed by gravity forces, but convection can be affected, as usually the heat transfer coefficients in microgravity are lower than predicted in normal gravity conditions. In the other hand evaporation processes under low gravity are not well understood and experiments about boiling are contradictory. In the end, we can assume that the system will probably behave a bit worse (time, mass and energy required, will increase), but we don't have the tools to know how important will be this oscillation.

6.5 Current state of the OmSTU studies

OmSTU's rocket building department is in the lead of Russian investigations on space debris mitigation and remediation techniques. The gasification of remaining propellant and its use to deorbit, or to turn the upper stage into a chaser, is its main target now. They are dedicating a lot of effort during years to achieve the expected success.

Professor Valery I .Trushlyakov and Professor Victor V. Shalaj are directing a very talented group of young students, each of them focusing in a part of the problem: gas engine, gasification device, grabbing system and docking process, propellants for gas generator, tanks and experimental installations.

The studies are now in the first stages of experimental simulations, using the OmSTU's laboratory installations. The gasification process has begun to be tested in the chamber depicted in figures *Fig.72, Fig. 73*. As we have already explained, the chamber uses a container, with a plain surface on its bottom, where the liquid for evaporation is placed. After that, the injectors fill the chamber with hot gases until the mixture is vaporized, having one valve to leave the gas mixture to exit from the chamber.

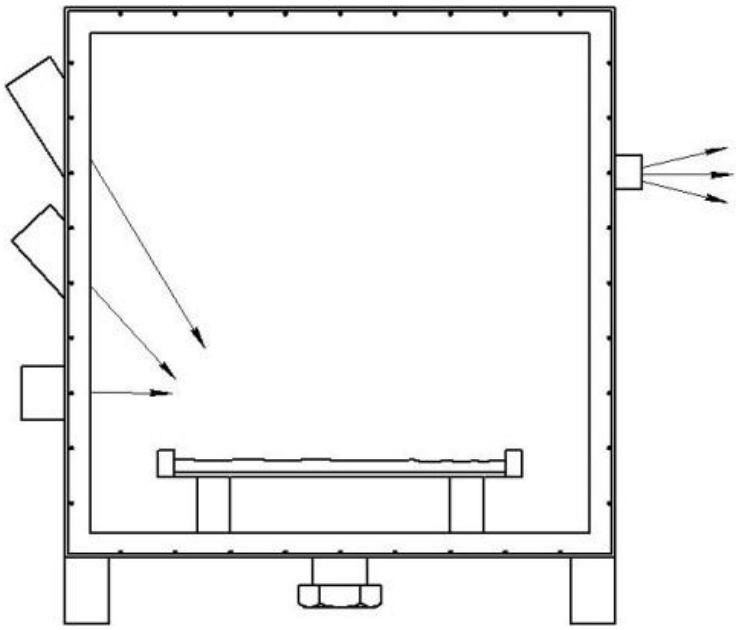

Fig. 72: Experimental installation scheme

Fig. 73: Experimental installation

Fig. 74: Experimental installation's Injectors

The next steps are programmed: (like experimental researches or the study of the ultrasounds emission system), multiple solutions are being considered (like the use of a membrane to separate gas and liquid, different propellants), and a great effort and hard work is being put on this project, and the rest of them.

Appendix 1: Soyuz 2.1b

The Soyuz family is acknowledged to be the most frequently rockets launched in the world [1]. Vehicles of this family, that launched both the first satellite (Sputnik, 1957) and the first man (Yuri Gagarin, 1961) into space, have been credited with more than 1700 launches to date.

The three-stage version known as Soyuz, first introduced in 1966, has been launched more than 850 times. Due to their close technical similarity (same lower three stages), the Molniya and Soyuz vehicles are commonly combined together for reliability calculations. In the last 25 years they have completed a success rate of 98.1% over more than 950 launches. As the primary manned launch vehicle in Russia and the former Soviet Union, and as today one of the primary transport to the International Space Station, the Soyuz has benefited from these standards in both reliability and robustness.

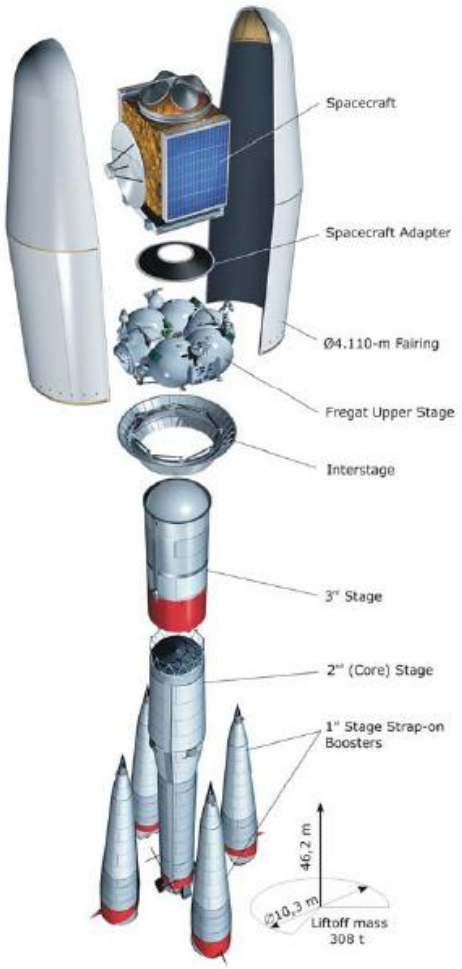

Fig. 75: Soyuz 2 LV

The addition of the flexible, restartable Fregat upper stage in 2000 allows the Soyuz launch vehicle to perform a full range of missions (LEO, SSO, MEO, GTO, GEO, and escape).

The Soyuz 2, also called Soyuz-ST, is the name for the new generation of Russian Launchers. Soyuz-2 family includes 2.1a, 2.1b and 2.1v. Soyuz 2.1b, like Soyuz 2.1a, is a variation of the U version that adds an upgraded engine (RD-0124) with improved performance to the second stage. The first launch, from Guiana, was a success (21 October 2011), for the first two Galileo IOV satellites.

A special ignition propellant is used to activate the combustion of the engine and pyrotechnic devices used to control the engine's work. Each of four combustion chambers can gimbal along a single axis to steer the vehicle.

The RD-0124 engine

The 30-ton-thrust RD-0124 is the substitute for the veteran RD-0110 in third stage (Block I) for the new versions of Soyuz rocket. It has roughly same dimensions (height: 2,327 millimeters, diameter: 1,470 millimeters) and the basic design than its predecessor. The main difference would be the introduction of the so-called closed-cycle system, where oxidizer gas used to drive the engine's pumps, would be then directed into the combustion chamber, where it would burn with the rest of the propellant, rather than being dumped overboard. Such upgrade would increase the performance of the engine and, as the result, the payload of the. A version of RD-0124 was also intended for the Angara rocket.

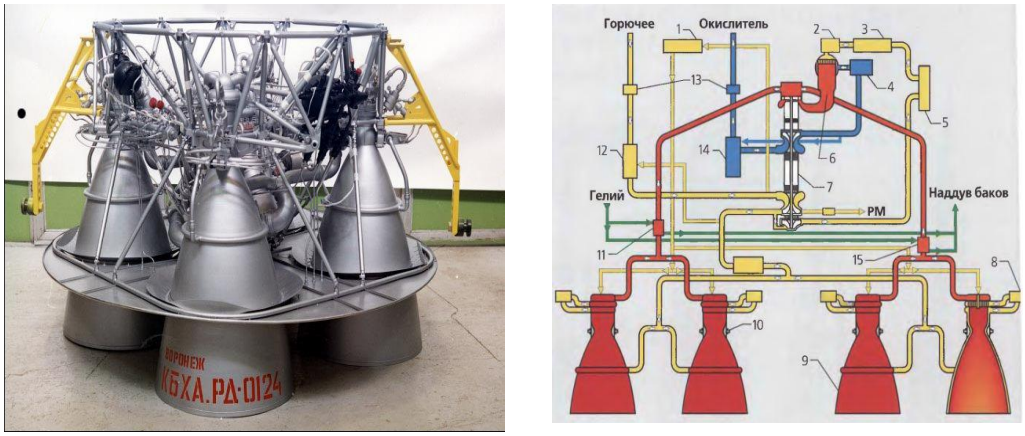

Fig. 76: The RD-0124 engine

In the following set of tables we can see the main properties of the Soyuz family stages:

PAYLOAD FAIRINGS	
Fairing	**ST**
Diameter:	4.110 m
Length:	11.433 m
Mass:	1700 kg
Structure:	Two-half-shell carbon-fiber reinforced plastic
Separation	Mechanical locks/ pneumatic jack/pushers
Interstage	
Mass:	400 kg
Structure:	aluminum skin-stringer

PAYLOAD ADAPTERS	
Off-the-shelf devices:	
	1194SF (110 kg);
	937SF (45 kg);
	1666SF (100 kg)

Table 28: Soyuz payload fairing

.	1st STAGE (FOUR BOOSTERS)
Size:	2.68-m diameter × 19.60-m length
Gross/Dry mass:	44 413 kg / 3 784 kg
Propellant:	27 900-kg LOX 11 260-kg Kerosene
Subsystems:	
Structure	Pressure stabilized aluminium alloy tanks with intertanks skin structure
Propulsion	RD-107A 4-chambers engine,
- Thrust	838.5 kN – SL; 1021.3 kN –Vac
- Isp	262 s – SL; 319 s –Vac
- Feed system	pump-fed by hydrogen peroxide (H_2O_2) gas generator
- Pressurization	Liquid nitrogen (N_2)vaporization
- Burn time / Restart	118 s / No – two level thrust throttling
Attitude Control	Two 35-kN vernier thrusters and one aerofin
Avionics	Input/Output units, TM, power
Stage separation:	Pyronuts/pushers/reaction nozzle

Table 29: Soyuz family first stage

.	2nd STAGE (CORE)
Size:	2.95-m diameter × 27.10-m length
Gross/Dry mass:	99 765 kg / 6 545 kg
Propellant:	63 800-kg LOX 26 300-kg Kerosene
Subsystems:	
Structure	Pressure stabilized aluminum alloy tanks with intertanks skin structure
Propulsion	RD-108A 4-chambers engine,
- Thrust	792.5 kN – SL; 990.2 kN –Vac
- Isp	255 s – SL; 319 s –Vac
- Feed system	pump-fed by hydrogen peroxide (H_2O_2) gas generator
- Pressurization	Liquid nitrogen (N_2) vaporization
- Burn time / Restart	286 s / No – one level thrust throttling
Attitude Control	Four 35-kN vernier thrusters
Avionics	Input/Output units, TM, power
Stage separation:	Pyronuts and 3rd stage engine ignition

Table 30: Soyuz family second stage

3rd STAGE		
Size:	2.66-m diameter x 6.70-m length	
Gross/Dry mass:	27 755 kg / 2 355 kg	
Propellant:	17 800-kg LOX 7 600 kg Kerosene	
Subsystems:		
Structure	Pressure stabilized aluminum alloy tanks with intertanks and rear skin structure	
Propulsion	RD-0110 4-chamber engine (Soyuz 2-1a)	RD-0124 4-chamber engine (Soyuz 2-1b)
- Thrust	297.9 kN (Vac)	297.9 kN (Vac)
- Isp	325 s -Vac	359 s (Vac)
- Feed system	Pump-fed gas generator, generator's gas blow down through verniers	Multi-stage pump-fed close cycle gas generator
- Pressurization	Oxygen vaporization/generator gases	Helium vaporization
- Burn time / Restar	250 s / No	270 s / No
Attitude Control	Four 6-kN vernier thrusters	Each chambers gimbaling in one axis
Avionics	Centralized control system: inertial 3-axis platform, on-board computer, TM & RF system, power	
Stage separation:		

Table 31: Soyuz family third stage

FREGAT UPPER STAGE	
Size:	3.35-m diameter x 1.50-m height
Inert mass:	950 kg
Propellant:	5350-kg N_2O_4/UDMH
Subsystems:	
Structure:	Structurally stable aluminum alloy 6 spherical tanks/8 cross rods
Propulsion	S5.92
- Thrust	Two mode thrust 19.85/14.00 kN - Vac
- Isp	Two mode thrust 331/316 s - Vac
- Feed system	Pump-fed, open cycle gas generator
- Pressurization	Ghe vaporization
- Burn time / Restart	Up to 900 s / up to 20 controled or depletion burn
Attitude Control	
- pitch, yaw	Main engine translation or eight 50-N hydrazine thrusters
- roll	Four 50-N hydrazine thrusters
Avionics	Inertial 3-axis platform, on-board computer, TM & RF systems, Power
Stage separation:	gas pressure locks/pushers

Table 32: Fregat upper stage

References

[1] Donald J. Kessler, Nicholas L. Johnson, J.-C. Liou, Mark Matney. *The Kessler Syndrome: Implications to Future Space operations*. 33rd Annual AAS Guidance and Control Conference. February 10, 2010

[2] Ben Greene. *Laser Tracking of Space Debris*.

[3] http://orbitaldebris.jsc.nasa.gov/.

[4] NASA. *The Threat of Orbital Debris and Protecting NASA Space Assets from Satellite Collisions.* 28 April 2009.

[5] T.S. Kelso. *Analysis of the 2007 Chinese ASAT Test and the Impact of its Debris on the Space Environment*.

[6] *NASA Orbital Debris Quarterly News*. Volume 15, Issue 3. July 2011.

[7] J.-C. Liou. *An Assessment of the Current LEO Debris Environment and the Need for Active Debris Remova*. NASA Orbital Debris Program Office; ISTC Space Debris Mitigation Workshop, Moscow, April 2010

[8] *Orbital Debris, a Technical Assessment*. Committee on Space Debris. National Research Council. 1995

[9] *IADC Space Debris Mitigation Guidelines*. Revision 1, September 2007.

[10] Xavier Clerc, Ingo Retat. *Astrium Vision on Space Debris Removal*. 63rd International Astronautical Congress, Naples, Italy.

[11] L.T. De Luca, F. Bernelli, F. Maggi, P. Tadini, C. Pardini, L. Anselmo, M. Grassi, D. Pavarin, A. Francesconi, F. Branz, S. Chiesa, N. Viola, C. Bonnal, V. Trushlyakov, I. Belokonov. *Active space debris removal by hybrid engine module*.

[12] J.-C. Liou, *The Top 10 Questions for Active Debris Removal*. European Workshop on Active Debris Removal. 22 June 2010. Paris, France

[13] Christophe Bonnal, *Active Debris Removal: Current status of activities in CNES. P²ROTECT Workshop Ankara, 21 March 2012*

[14] Christophe Bonnal, Pascal Bultel. *High Level Requirements for an Operational Space Debris Deorbiter*. International Orbital Debris Removal Conference, USA. December 9, 2009

[15] Christophe Bonnal. *Active Debris Removal: Current status of activities in CNES*. P²ROTECT Workshop Ankara, 21 March 2012

[16] Didier Alary. *Astrium's views on OOS & ADR*. October 30, 2012. Brussels, Belgium.

[17] Duncan Smith. *RObotic GEostationary orbit Restorer (ROGER) Executive Summary ESA/ESTEC Contract No. 15678/01/NL/WK.* September 2003

[18] M. Andrenucci, P. Pergola, A. Ruggiero. *Active Removal of Space Debris: Expanding foam application for active debris removal.* 2011

[19] Satomi Kawamoto, Yasushi Ohkawa, Hiroki Nakanishi, Yasuhiro Katayama, Heihachiro Kamimura, Shoji Kitamura, Seishiro Kibe. *Active Debris Removal by a Small Satellite*. IAC 12, Naples, Italy.

[20] *Report on Space Debris Related Activities in Japan*. UNCOPUOS/STSC February, 2010.

[21] M.L. Cosmo, E.C. Lorenzini. *Tethers in space handbook.*

[22] Jan Stupl, James Mason, William Mashall, Creon Levit. *Debris-debris collision avoidance using medium power grund-based lasers*. 2010, NASA

[23] www.boeing.com/

[24] www.spaceflightnow.com/

[25] RL10B-2 Brochure, Pratt & Whitney.

[25] R. P. Patera, K. R. Bohman, M. A. Landa, C. Pao, R. T. Urbano, M. A. Weaver, Capt. D. C. White; Controlled Deorbit of the Delta IV Upper Stage for the DMSP-17 Mission. Proceedings of the 2nd IAASS Conference "Space Safety in a Global World" 14-16 May 2007, Chicago, USA (ESA SP-645, July 2007)

[26] *Ariane 5: Data relating to Flight 205*. Astrium

[27] cs.astrium.eads.net

[28] Aestus Brochure, Astrium.

[29] Carine Leveau, Isabelle Rongier, Alain Gaillard; A5ES-ATV: Challenges and results of the first European controlled deorbitation for the upper composite of a launcher. 3rd IAASS Conference

[30] Hugues Lanteri. *Ariane 5: Data relating to Flight 200*. Astrium

[31] www.esa.int/

[32] Martin Sippel, Etienne Dumont, Ingrid Dietlein. *Investigations of Future Expendable Launcher Options*. IAC 11, Cape Town, South Africa.

[33] P. Alliot, E. Dalbies, A. Pacros. J.-M. Ruault. *Overview of the Development Progress of the Ariane 5 Upper Stage VINCI Engine.* IAC 02, Houston, Texas, United States.

[34] Anne Pacros, Jérémy Follet, Snecma Moteurs, Bruno Vieille. *Microgravity activities for the VINCI engine re-ignition capability*. Proceedings of the Microgravity Transport Processes in Fluid, Thermal, Biological and Materials Sciences III. Davos, Switzerland. September 2003.

[35] Kazuo Tasake, Masanori Tsuboi, Shigeru Mori, Kiyoshi Kobayashi; *Successful Demonstration for Upper Stage Controlled Re-entry Experiment by H-IIB Launch Vehicle*. Mitsubishi Heavy Industries Technical Review Vol. 48 No. 4 (December 2011)

[36] Japan Aerospace Exploration Agency (JAXA), Mitsubishi Heavy Industries, Ltd. (MHI); *H-IIB Launch Vehicle No. 3 (H-IIB F3) Overview*.

[37] Martin Sippel, Armin Herbertz, Chiara Manfletti, Holger Burkhardt, Takayuki Imoto, Dietrich Haeseler, Andreas Götz; *Studies on Expander Bleed Cycle Engines for Launchers*

[38] William Sack, Koichi Okita, Akihide Kurosu, Akira Ogawara, Kimito Yoshikawa, Masahiro Atsumi, Kenji Kishimoto, Kevin Lunde; *Excellence of the Japanese Expander-Bleed Cycle Rocket Engine and Enhancements for Future Engine Applications*.

[39] Kazuo Tasake, Masanori Tsuboi, Shigeru Mori; *Upper Stage Controlled Re-entry Experiment by H-IIB Launch Vehicle*.

[40] *Successful Execution of Controlled Re-entry of Launch Vehicle Upper Stage*, JAXA Today No. 6, August 2012

[41] Makarov Yu., Raykunov G., Shatrov Ya., Oleinikov I., Yakovlev M., Baranov A., Trushlyakov V. *Development of autonomous onboard active systems for debris removal.* 2nd European Workshop on Active Debris Removal, CNES Paris, France 18 - 19 June ,2012.

[42] George P. Sutton, Oscar Biblarz. *Rocket Propulsion Elements, Seventh edition.* John Whiley and Sons, 2001.

[43] http://www.chem.ucla.edu

[44] Angelo Cervone, Lucio Torre, Luca d'Agostino, Antony J. Musker, Graham T. Roberts, Cristina Bramanti, Giorgio Saccoccia. *Development of Hydrogen Peroxide Monopropellant Rockets.*

[45] Однажды и навсегда. Документы и люди о создателе ракетных двигателей и космических систем академике В.П.Глушко.

[46] http://www.astronautix.com

[47] V. A. Volodin, Construction and design of rocket engines

[48] L. Meyer, J. Nichols, J. M. Jones, *Integrated Powerhead Demonstrator (booster hydrogen oxygen rocket engines)*. AIAA, Space Programs and Technologies Conference, Huntsville, AL, Sept. 24-26, 1996

[49] www.nasa.gov

[50] Stephen G. Hanna, *Integrated Powerhead Demonstration (IPD), IHPRPT Phase I Cryoboost Demo*, Nov 2004`

[51] L.T. .Kayser. *Investigations on a bipropellant hot gas rocket engine for orbit and attitude control.* National Aeronautics and Space Administration. July, 1971.

[52] Казаков А.Ю. *Меоретические и экспериментальные исследования рабочих процессов в газовом ракетном двигател.*

[53] Frank P. Incropera, David DeWitt, Theodore L. Bergman, Adrienne S. Lavine, *Fundamentals of Heat and Mass Transfer, 7th Edition*. 2011

[54] John H. Lienhard IV, John H. Lienhard V. *A Heat Transfer Textbook, 3rd Edition*.

[55] Michael J. Moran, Howard N. Saphiro. *Fundamentals of Engineering Thermodynamics, 6th Edition*. John Whiley and Sons, 2008.

[56] Hans Dieter Baehr, Karl Stephan, *Heat and Mass Transfer*.

[57] R. Siegel, J.R. Howell. Thermal Radiation Heat Transfer. Taylor and Francis. Hemisphere, 4th edition, 2001.

[58] H. C. Hottel, A.F. Sarofim. Radiattive Transfer. Mcgraw-Hill, New York, 1967.

[59] Payam Rahimi, Charles A. Ward. *Kinetics of Evaporation: Statistical Rate Theory Approach.*

[60] Z.-J. Wang, M. Chen and Z.-Y. Guo. *A nonequilibrium molecular dynamics simulation of evaporation*. International Conference "Passive and Low Energy Cooling 543 for the Built Environment", May 2005, Santorini, Greece.

[61] A.P. Kryukov, V.Yu. Levashov, S.S. Sazhin. *Evaporation of diesel fuel droplets: kinetic versus hydrodynamic models*. International Journal of Heat and Mass Transfer.

[62] Peter Fortescue, John Stark, Graham Swinerd. *Spacecraft systems engineering*, Third Edition. John Wiley and Sons, 2003.

[63] Nicolas Spycher, Karsten Pruess, Jonathan Ennis-King. *CO_2-H_2O mixtures in the geological sequestration of CO_2. I. Assessment and calculation of mutual solubilities from 12 to 100°C and up to 600 bar.* Geochimica et Cosmochimica Acta. Volume 67, Issue 16, 15 August 2003, Pages 3015–3031

[64] A.L. Yarin, D.A. Weiss, G. Brenn, D. Rensink. *Acoustically levitated drops: drop oscillation and break-up driven by ultrasound modulation.* International Journal of Multiphase Flow 28 (2002) 887–910

[65] T.K. Jagannathana, R. Nagarajana, K. Ramamurthib. *Effect of ultrasound on bubble breakup within the mixing chamber of an effervescent atomizer.* Chemical Engineering and Processing 50 (2011).

[66] *Microgravity Science on the ISS, a primer for new researchers.* Nasa.gov

[67] *Soyuz User's Manual*. Arianespace, 2006.